
Unterschrift des Betreuers



TECHNISCHE
UNIVERSITÄT
WIEN
Vienna | Austria

DIPLOMARBEIT

**COMPARISON OF ACTIVE AND PASSIVE OPTICAL METHODS
FOR MAPPING RIVER BATHYMETRY**

Ausgeführt am Department für

Geodäsie und Geoinformation

Forschungsgruppe Photogrammetrie

der Technischen Universität Wien

Unter der Anleitung von:

Univ. Prof. DI Dr. techn. Norbert Pfeifer

DI Dr. techn. Gottfried Mandlbürger

DI Dr. techn. Camillo Ressler

Durch

Michael Wimmer

Favoritenstraße 106, 1100 Wien

10. Mai 2016

Unterschrift (Student)

Abstract

Optical methods for high resolution shallow water depth estimation are currently in a phase of rapid development driven by technical progress and growing interest in several scientific fields. Throughout the last years a diversity of potential applications has driven the creation of evolved methods and sensors. However, this trend primarily concerns Airborne Laser Bathymetry (ALB) while passive methods, particularly two-media photogrammetry, lack comparable advancements. A possible reason for the lesser amount of interest could be the limited spatial resolution when working with feature-based image matching. On account of this restraint, two-media photogrammetric methods concentrated on the reconstruction of individual points so far.

Adopting the relatively new technique of dense image matching, this thesis takes a different approach and aims at a high-resolution description of the river bed as seen from aerial images through the water column. The effect of light refraction at the boundary between the two media, air and water, is theoretically investigated under varying conditions. Based on these findings, a practical refraction correction procedure is derived, implemented and embedded into the photogrammetric workflow.

For evaluation under realistic conditions, the enhanced photogrammetric processing chain is applied to a set of aerial images of the pre-Alpine Pielach River in Lower Austria. Reference data are provided by a simultaneous ALB campaign. With both methods, digital terrain models (DTMs) including the river course and water depth models are derived, enabling direct comparison of the respective characteristics and quality assessment of the introduced photogrammetric procedure. Under favorable conditions, differences between the two methods rarely exceed 10-20 cm, but obstacles like overhanging trees or effects like sun glint are responsible for larger deviations. In the study area, a mean absolute difference between photogrammetric and ALB depth models of about 15 cm is achieved.

Despite revealing some shortcomings in the demanding study area, the general capability of two-media photogrammetry to map shallow water bodies can be approved. Running through the procedure provides important insights into the possibilities and necessities of adapting the processing pipeline of commercial photogrammetric software packages to the peculiarities of the two-media problem. Besides, flights for data acquisition have to be planned carefully as well in order to restrict effects like sun glint or overexposure of bright objects while at the same time ideally resolving river bed texture.

One of the most critical steps for active as well as passive methods is the extraction of the water surface which is needed for refraction correction. In addition to qualitative considerations, mainly the achievable degree of automatization is a question of particular importance since it decisively influences the practical applicability of a certain method for more extensive surveys.

Acknowledgements

I would like to gratefully thank everyone supporting the development of this thesis. First of all, this concerns my supervisors

Univ. Prof. DI Dr. Norbert Pfeifer

DI Dr. Gottfried Mandlbürger and

DI Dr. Camillo Ressler.

Their active and competent support contributed a great deal to the successful completion of the thesis and the preceding practical work. In this context I would also like to mention the scientific and organizational personnel of the research group Photogrammetry at TU Wien in appreciation for providing ideal conditions of work in a familiar atmosphere.

Particularly in the context of this thesis, gratitude is furthermore owed to DI Philipp Glira for his contribution to ALB strip adjustment and to *Riegl Laser Measurement Systems GmbH* for providing state-of-the-art ALB data along with simultaneously acquired aerial images.

Table of Contents

1	Introduction.....	6
1.1	The importance of surveying water bodies.....	6
1.2	Legal commitments (Europe)	7
1.3	Motivation of optical Remote Sensing	7
2	History and State of the art	10
2.1	Spectral Regression and Classification	10
2.2	Two-Media Photogrammetry.....	13
2.3	Airborne Laser Bathymetry (ALB).....	14
3	Study area and data acquisition for practical work.....	18
4	ALB workflow	22
4.1	Quality control and strip adjustment	22
4.2	Digital Surface Model (DSM)	23
4.3	Amplitude Mapping.....	23
4.4	Water surface determination.....	24
4.5	Refraction error estimation and correction	26
4.6	Digital Terrain Model interpolation including submerged areas	28
5	Photogrammetric Workflow.....	29
5.1	Image Orientation	29
5.2	Image Matching.....	31
5.2.1	SURE	31
5.2.2	Match-T	33
5.3	Refraction effect on photogrammetric measurements	34
5.4	Refraction correction procedure.....	38
5.5	Interpolation and combination of height models	40
6	Results and discussion.....	43
6.1	Topographic mapping quality.....	43
6.2	Water Surface Model (DWM).....	47
6.3	Refraction correction.....	51

6.4	Water Depth Model	52
6.4.1	Sector East	52
6.4.2	Sector West	55
6.5	Evaluation and direct comparison.....	56
7	Conclusions.....	63
8	Outlook	65
	List of abbreviations	67
	References	68
	Web References	72

1 Introduction

1.1 The importance of surveying water bodies

Rivers and shallow waters in general are often subject to particular interest – for scientists of various disciplines as well as for political decision-makers, public administration and private companies (Mandlbürger et al., 2011; Mandlbürger et al., 2012; Westaway et al., 2001; Legleiter et al., 2013; Fryer, 1983). The reasons for such a multitude of concerns touching a land cover type of comparably small extent are manifold:

The maybe most obvious one is that rivers and water reservoirs are sources of fresh water and therefore vital for any human population (Mandlbürger et al., 2011; Mandlbürger et al., 2012; Pfennigbauer et al., 2010; Steinbacher et al., 2010; EU, 2000b). For a government, it is an essential task to ensure water supply for all citizens. This task necessitates measures such as monitoring, regulation or renaturation of water bodies.

However, the social benefits of riverine landscapes are not limited to the provision of drinking water. Another aspect is the recreational value that shouldn't be underestimated (Westaway et al., 2001). The way how water enriches and models landscapes on different scales creates potential touristic attractions which have to be made accessible and at the same time have to be protected and preserved.

Coming to commercial use of water bodies, the number of potential profiteers is limited to state-owned or private companies. The associated value is nonetheless huge. Rivers and tidal forces are fundamental sources of energy. Well-suited coast lines are used to build and extend harbors for global trading and waterways can be lifelines for entire regions (Fryer, 1983).

Besides all these positive effects for humans, rivers can as well be a source of danger. Floods threatening homes, possessions and even lives of people require accurate risk analysis and effective measures for prevention or at least limitation of damage (Mandlbürger et al., 2015a). Another slow-acting hazard arises from the dynamics water imposes on its environment (Delai et al., 2014). Ongoing erosion has the potential of destroying buildings or infrastructure in the immediate vicinity and even though the time horizon is typically much longer than for flood management, well-considered actions such as riverbed regulation or prohibition on building in endangered areas may be inevitable.

A last major point is the role of water as an irreplaceable ecosystem sustaining countless organisms and species (Legleiter et al., 2013) some of which obviously play important roles for humankind – for example fish as a source of food. Others contribute to the quality of the ecosystem in ways which might be invisible to the observer. However, numerous inhabitants of these unique, vulnerable environments need protection against destruction of their habitat and against anthropogenic changes in the ecosystem structure.

1.2 Legal commitments (Europe)

In addition to these factual arguments for an accurate surveying of shallow water, there also is a legal compulsion in some areas. For example, regarding the relevant legislation of the European Union, currently three Directives can be named:

The chronologically first one was the “*Directive on the conservation of natural habitats and of wild fauna and flora*”, also called the *Fauna-Flora-Habitat Directive (FFH)*, which was adopted in 1992 (EU, 1992). The general purpose of the Directive is to “*promote the maintenance of biodiversity, taking account of economic, social, cultural and regional requirements*” [I]. More than 1000 species and 200 habitat types are enumerated demanding different levels of conservation ranging from mere protection to active measures ensuring the continuing functionality of the habitat. The Member States are compelled to “*draw up a report on the implementation of the measures taken under this Directive*” (EU, 1992) every six years including description but also impact assessment of the taken measures. This is where the surveying of water bodies comes into play again being an irreplaceable source of information for the requested reporting – especially since a considerable portion of the concerned habitats are aquatic habitats (Mandlbürger et al., 2015a; Mandlbürger et al., 2015b).

Similarly, also the *EU Water Framework Directive (WFD)* (EU, 2000a; EU, 2000b) demands repeated surveys for providing river basin management plans reviewed every six years. The aim is “*a holistic approach to protecting the whole body of water, its source, tributaries and river mouth*” (EU, 2000b) with focus on improving water quality for human use, most notably as drinking water. Quality is defined as good chemical status and good ecological status, the latter including among others “*the quality of the biological community*” [II] with parallels to the *FFH Directive* and “*Morphological features, such as quantity, water flow, water depths and structures of the river beds*” (EU, 2000b).

Most recently, namely in 2007, the “*Directive on the assessment and management of flood risks*” (*EU Floods Directive*: EU, 2007) became effective. By requiring the Member States to provide flood risk assessment, flood hazard and flood risk maps as well as flood risk management plans, a common platform for the coordinated implementation for active measures is created. The focus is on finding the best way of reducing and managing “*the risks that floods pose to human health, the environment, cultural heritage and economic activity*” [III] across national borders. Like in the other two Directives, there exists a six years monitoring cycle requiring repeated survey and modelling of water courses and coast lines along with the surrounding topography.

1.3 Motivation of optical Remote Sensing

The various obligations and potential applications described in Sections 1.1 and 1.2 show the necessity of tasks like flood simulation, risk analysis, sediment transport modeling, change monitoring or habitat mapping (Mandlbürger et al., 2011; Marcus et al., 2003; Moretto et al., 2014; Legleiter, 2012). Morphological change in the highly dynamic environment of a river, e.g. through sediment transport, can amongst other possibilities be detected based on repeated surveys resulting in a Digital Terrain Model (DTM) of the submerged area from which the morphodynamics changes can be derived via a Digital Elevation Model of Differences (Mandlbürger et al., 2015b). Shallow sea

bed DTMs can be used for applications like Archeology locating shipwrecks or sunken foundation walls along coastlines (Mandlbürger et al., 2012).

Flood simulation but also habitat mapping just as many other tasks requiring information on variable water depth and/or flow velocity are based on 1D or 2D hydrodynamic-numeric simulation (Mandlbürger et al., 2015b; Feurer et al., 2008; Williams et al., 2013). However, 1D approaches based on river cross sections are not state of the art any more since they are not capable of sufficiently resolving the flow patterns in natural rivers (Legleiter, 2012). Advanced 2D methods need adequate, high-resolution terrain representation of the watercourse and the relevant surrounding area (Mandlbürger et al., 2011; Hilldale and Raff, 2007).

The first and still very popular method (McKean et al., 2009) of determining shallow water depths is field wading survey. For single measurements this is a very precise method, but, however, it is subject to some critical restrictions, especially when talking about coverage of large areas. In spite of modern instruments like Robotic Total Stations, the method remains extremely time- and personnel-intensive since every single point in the river has to be accessed. Therefore, everything going beyond the measurement of single river cross sections or sparse point grids is unreasonably expensive, disabling ground-based measurements to create high resolution models covering larger sections or the whole course of a river (Mandlbürger et al., 2013b; Feurer et al., 2008; Westaway et al., 2001). Furthermore, the slowness of terrestrial work makes it difficult to react to the natural dynamics of a river environment (Mandlbürger et al., 2015b; Delai et al., 2014), even during one campaign of a few days, flow conditions can change significantly. One last major limitation is the question of accessibility: Places that cannot be entered safely by the operator (e.g. because of currents or steep river banks) or which must not be entered for protection reasons (e.g. swamps or meadows) consequently cannot be surveyed.

A second important group of techniques includes waterborne methods like multi-beam echo sounding or acoustic Doppler measurements (e.g. Renard and Allenou, 1979; Parsons et al., 2005). These are particularly beneficial for deep and turbid water where light is unable to penetrate the water column. But as soon as the water body becomes very shallow or currents hinder navigating, waterborne techniques are inherently incapable of measuring depths for reasons of pulse length and again accessibility (Mandlbürger et al., 2011; Doneus et al., 2012; Mandlbürger et al., 2013b; McKean et al., 2009); furthermore, the equipment is rather expensive, even compared with active optical sensors (Guenther et al., 2000).

To sum it up, there is interest in techniques providing detailed information on submerged terrain and offering the possibility to cover large areas in a short time period to avoid temporal decorrelation. Speed and mobility are also key properties of a system enabling situational data acquisition following sudden events like floods (Guenther et al., 2000; Williams et al., 2013, Westaway et al., 2001). Ideally, one sensor covers the river bed as well as the terrain around it in order to receive consistent data with a good relative accuracy which is absolutely vital for the hydrological workflow (Mandlbürger et al., 2015b; Guenther et al., 2000; Williams et al., 2013). If in practice, the use of one sensor is not

feasible, it is at least desirable to have sufficiently overlapping datasets for quality-checking (Mandlbürger et al., 2011).

Airborne optical techniques can possibly cope with most of these requirements since flying platforms ensure faster and more extensive surveys than ground-based or waterborne ones. Thereby, nowadays sub-meter resolutions can be achieved. If working reliably in shallow water, they can be ideal for shallow rivers and additionally complement other techniques near water-land-boundaries. The next chapter outlines the most important optical methods based on the respective literature.

2 History and State of the art

During the last years and decades, a growing number of articles have been published concerning airborne optical methods to determine water depth. The presented techniques can generally be divided into active and passive ones. Three different categories are discriminated, namely Regression/Classification based on spectral properties and Two-Media Photogrammetry as passive techniques and Airborne Laser Bathymetry (ALB) which is an active technique. In the following, basic principles and the development of the different approaches are summarized.

2.1 Spectral Regression and Classification

Working with aerial images, it can be recognized that water bodies change their color and look darker where the water is deeper (Figure 1). Consequently, this depth-color relationship can be used to gain information about the water and/or the submerged terrain from greyscale, RGB and multispectral imagery.



Figure 1: Section of an aerial image from the study area (Section 3). Without further quantitative evaluation, the tendency of and darker, green-blue appearance of deeper water can be perceived.

For acquiring water depth D , a common approach is to train a regression model relating water depth and spectral properties with linear coefficients. For example, in (Delai et al., 2014) simply the spectral bands are combined up to third order:

$$D = \alpha + \beta_0 R + \beta_1 G + \beta_2 B + \beta_7 R^2 + \beta_8 G^2 + \beta_9 B^2 + \beta_{10} R^3 + \beta_{11} G^3 + \beta_{12} B^3 + \beta_3 RB + \beta_4 RG + \beta_5 GB + \beta_6 RGB \quad (\text{Eq. 1})$$

α and β_i hereby stand for the 14 parameters and R, G, B for the red, green and blue color band. In the course of model calibration using in situ depth measurements, the parameters are estimated. In order to reduce their unnecessary high number, many of them are subsequently eliminated based on their significance.

Although comparably good results have been reported for this and similar regression models (Feurer et al., 2008; Moretto et al., 2014), they merely stand on an empirical basis and lack physical derivation. Therefore, the results may strongly depend on influences like substrate reflectivity, the light transmissibility of water and the sun illumination conditions. Whereas these values are probably only subject to slight variations within a limited study area, applying the trained model a few kilometers downstream or on a completely different river where no training data are available may result in useless outcomes.

A very profound discussion is provided by (Stumpf et al., 2003) and (Legleiter et al., 2009). Reconsidering the physical background of radiative transfer, it is argued that a certain degree of independence from bottom reflectance and water clarity can be achieved by forming band ratios. This way it is possible to make use of the wavelength-dependent degree of light absorption in the water [XX]. The numerator of the band ratios should be a wavelength where scattering in the water column is the dominant effect (e.g. green or blue) whereas the denominator should be mainly affected by absorption in the medium water (red). Eq. 2 shows the model used amongst others by (Legleiter, 2012) and (Legleiter et al., 2013) corresponding to these findings:

$$D = \alpha + \beta \cdot \log\left(\frac{G}{R}\right) \quad (\text{Eq. 2})$$

(Williams et al., 2013) favor a blue numerator instead of green. Again, α and β refer to the parameters and R, G, B to the color bands. The logarithm is responsible for a linear relation between the band ratio and the depth.

Another physically justified approach is to use a simplified absorption model (Eq. 3) of light passing through a transparent medium (Lane et al., 2010; Carbonneau et al., 2006):

$$I_{out} = I_{in} \cdot e^{-cx} \quad (\text{Eq. 3})$$

I_{in} and I_{out} stand for the ingoing and outgoing intensity, c is the absorption rate and x the thickness of the medium water. By finding the unknown parameters I_{in} using unsubmerged riverbed and c using training data, the water depth can be calculated based on the measured intensity I_{out} . This method has the advantage of only needing one band and therefore is applicable to greyscale images. Apart from that, there are some major disadvantages: First, the assumption of one value for I_{in} doesn't account for illumination and bottom reflectivity differences in any way and second, also the absorption rate is set constant. This limits the validity of the calibrated model to the area where training data are available; an application in other sections of the same river is not promising. This problem of inflexibility is mitigated by histogram matching and strong spatial averaging (Carbonneau et al., 2006).

Some other more particular features usually derived from water depth can be acquired by classification of multi- or hyperspectral data (Marcus and Fonstad, 2008; Marcus et al., 2003; Legleiter and Goodchild, 2014). Beneath the detection of algae and woody debris, the differentiation of different habitat types is a very interesting application. Using a supervised classification, (Marcus et al., 2003) differentiate between pools, glides runs, riffles and standing water. Subsequently, the results are used to determine separate regression parameters for the water depth of different habitat types. Since for the transitional areas between habitat types, the assignment is not always unambiguous, a generalization is made in (Legleiter and Goodchild, 2014): Using Fuzzy Logic, each pixel gets a certain “*grade of membership*” in a class.

The limitation due to sun glint which is omnipresent for passive methods is overcome using different filters: Median filtering (Legleiter, 2012), adaptive Wiener Filter (Legleiter et al., 2013) or down sampling of the original images (Moretto et al., 2014) – obviously with negative effects on spatial resolution. Therefore, another approach is to set any smoothing aside and to eliminate single pixels depending on their respective intensity (Williams et al., 2013). If a Near Infrared channel is available, a possible way of “deglinting” (i.e. the pixel value reconstruction by eliminating the specular portion of the reflected light) of the image using a regression between NIR and Visible bands is presented in (Hochberg et al., 2003) and (Hedley et al., 2005).

An advantage of these spectral methods is the relatively easy data processing based on standard aerial imagery not necessitating expensive equipment. There also is the possibility to resort to publicly available images (Legleiter et al., 2013; Stumpf et al., 2003) though in this case the synchronization with the field campaign is more difficult.

Inherently, regression and classification approaches have in common that they only work for submerged areas. Therefore, a delineation of the riverbed is necessary. In the literature, this is often done manually or by using point density and intensity of Airborne Laser Scanning (ALS) data collected at the same time as the aerial images (Legleiter, 2012). The limited area of application (only submerged areas) generally is a clear drawback with respect to other optical techniques since it requires combination with other methods like Near Infrared (NIR) topographic ALS as soon as height information of dry terrain is needed. Apart from reduced cost effectiveness, the combination with other techniques also poses the problem of consistency since the datasets are typically not overlapping.

Another issue is the dependence on field data for calibration. As discussed in Section 1.3, terrestrial surveys are afflicted with some major limitations, including high time and cost efforts. A possible way out is the use of feature-based photogrammetry for calibration (Lane et al., 2010), but in this case, it seems more convenient to use photogrammetry alone (like it was done in this thesis) instead of propagating the error through two methods. This is particularly true since the result of the spectral regression is no 3D point but a depth value. To acquire a DTM of the water course, the depth value is subtracted from a of the water surface height model (DWM), whereby an error in the DWM

translates 1:1 into a DTM error. In the photogrammetric correction procedure, the same error makes an impact corresponding to less than 1/3 of its magnitude (c.f. next sections).

2.2 Two-Media Photogrammetry

The idea of using photogrammetry through the boundary of media with different optical depths goes back many decades (Tewinkel, 1963; Rinner, 1969). In the beginning, the main interest was concentrated on marine coastal waters. The possibility of comparably cost effective mapping repeatable in short time intervals was very beneficial for engineering projects, for example around harbors, as well as for matters of biological resource monitoring or archeology. Throughout the years, all thinkable aerial platforms such as kites, balloons or unmanned aircraft were employed (Fryer and Kniest, 1985). For close-range images, simple floating platforms were developed with transparent trays to avoid water surface waves (Fryer, 1983).

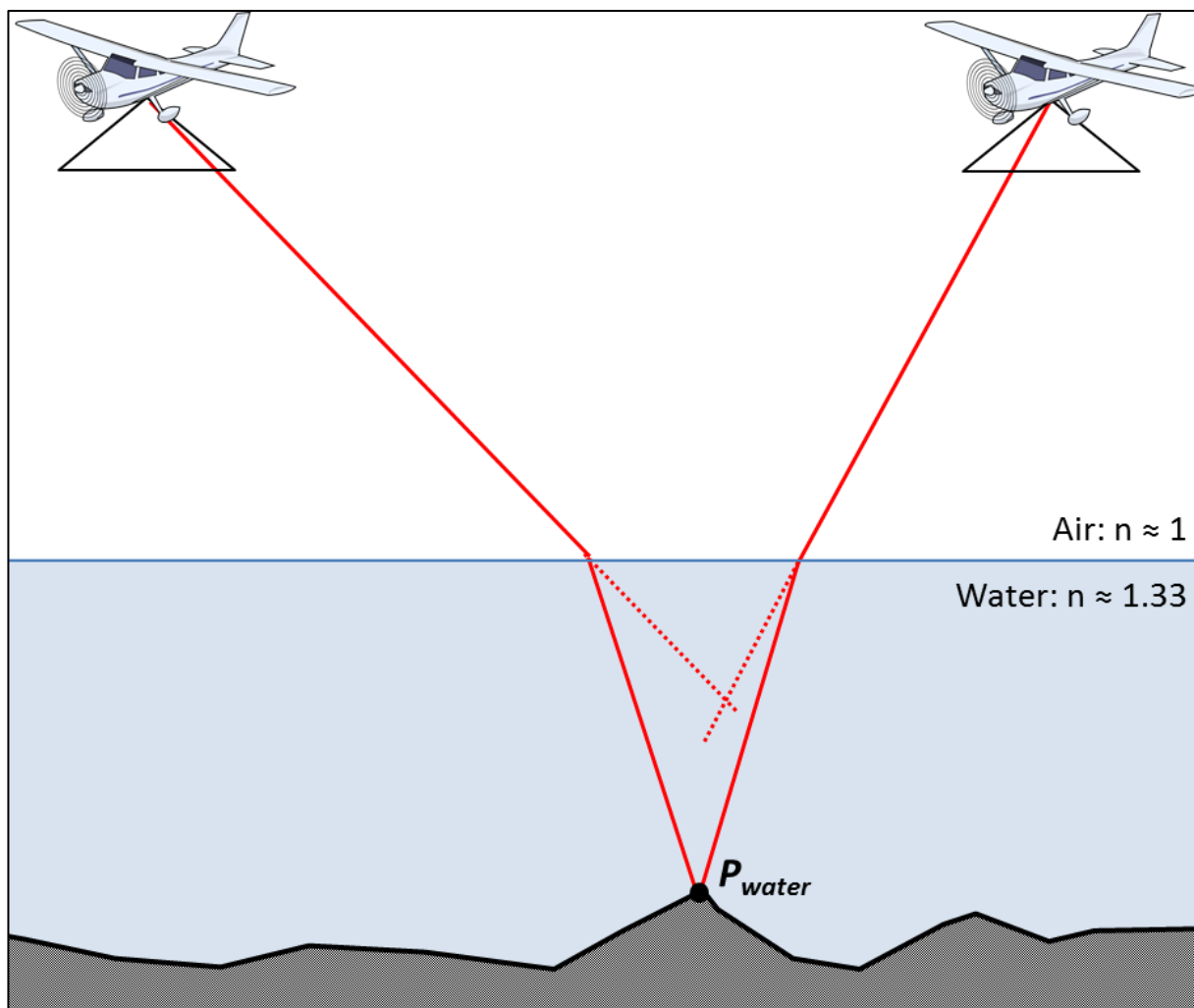


Figure 2: Basic characteristics of two-media-photogrammetry. Observing an underwater point from two different image positions, the light rays follow different paths (solid red lines) than the photogrammetric model assumes (dotted red lines).

With the new possibilities of digital photogrammetry, through-water applications started to arouse interest for morphological change monitoring in fluvial environments (Pyle et al., 1997). While the first studies had the main focus on high-resolution mapping of river banks and channel delineation,

the need for terrain models also including the submerged parts of the river bed motivated the development of a refraction correction procedure for automatic matching results. Approximations of such a procedure were realized by multiplying the apparent depth of a point by the refraction index of water (Westaway et al., 2000). However, this approach completely ignores the dominating geometric effect of light refraction which is different for every image ray. Therefore, the presented method is subject to systematic errors growing with depth and was soon replaced by a more geometry-related one (Westaway et al., 2001). Some assumptions made about the rigorous solvability of the problem were later relativized, yet with small impact on the practical solution (Murase et al., 2008).

The feature-based matching algorithms used in most of the studies (e.g. Westaway et al., 2001) still have shortcomings concerning point density in submerged areas. In order to get area-wide models, methods like Kriging or Triangulation are used (Westaway et al., 2001) or the most reliable photogrammetric points are extracted to train a depth-color regression (Lane et al., 2010). Recently, the advent of dense image matching offers the facility of a considerable data densification (Hirschmüller, 2005; Hirschmüller, 2011) possibly enabling through-water photogrammetry at sub-meter resolutions. Another critical issue is the determination of the water surface where the light is refracted. Since no static objects floating on that surface can be identified in images, the representation is realized by interpolating points on the water-land boundaries (Westaway et al., 2001). However, as stated before, the effect of errors in the water surface models is not as strong as for Spectral Regression.

A tremendous advantage of photogrammetric methods is the potential of mapping submerged and dry terrain from a single data source. Even though additional ALS data might be necessary in vegetated areas, the overlapping photogrammetric and ALS datasets facilitate relative orientation and quality checking. From the economical point of view, photogrammetry requires less cost intensive field work than spectral methods due to the fact that except for a few ground control points per image block no additional field measurements are needed (c.f. Section 2.1). Photogrammetry therefore also allows the analysis of archival and greyscale images with modern methods as long as the texture elements from the river bottom can be identified.

The principle of two-media photogrammetry is illustrated in Figure 2. A more detailed discussion of the refraction effect can be found in Section 5.3.

2.3 Airborne Laser Bathymetry (ALB)

The second method capable of covering complete riverine landscapes within a single campaign is Airborne Laser Bathymetry (ALB). Having the first origins in the 1960's shortly after invention of the Laser itself makes this technique or at least the basic principle a rather old one as well. The primary purpose of Laser Bathymetry during the first years was military reconnaissance (Mandlbürger et al., 2011; Guenther et al., 2000). Systems were developed for the detection of submarines in coastal waters. Thus, it is not very surprising that the U.S. Navy and the NASA were pioneers in that context.

Numerous systems were developed in the following decades – a detailed historical overview is given in (Guenther et al., 2000).

In principle, ALB systems work in a similar way like Airborne Laser Scanning (ALS) systems for mapping topography. By combining direction and distance measurement with trajectory and attitude information, directly georeferenced point clouds representing terrain and objects above are obtained. However, the conventional ALS systems typically operating in the near infrared (NIR) range (e.g. $\lambda=1064$ nm) cannot penetrate noteworthy into water due to the strong absorption in their spectral range [XX].

To overcome this inherent limitation, ALB systems use a laser operating in the green domain of the spectrum (e.g. $\lambda=532$ nm) which altogether has the best capabilities to penetrate water bodies (Doneus et al., 2012). An additional necessity when working in the visible parts of the spectrum is to ensure eye safety either by widening up the laser beam or by working with reduced pulse energy.

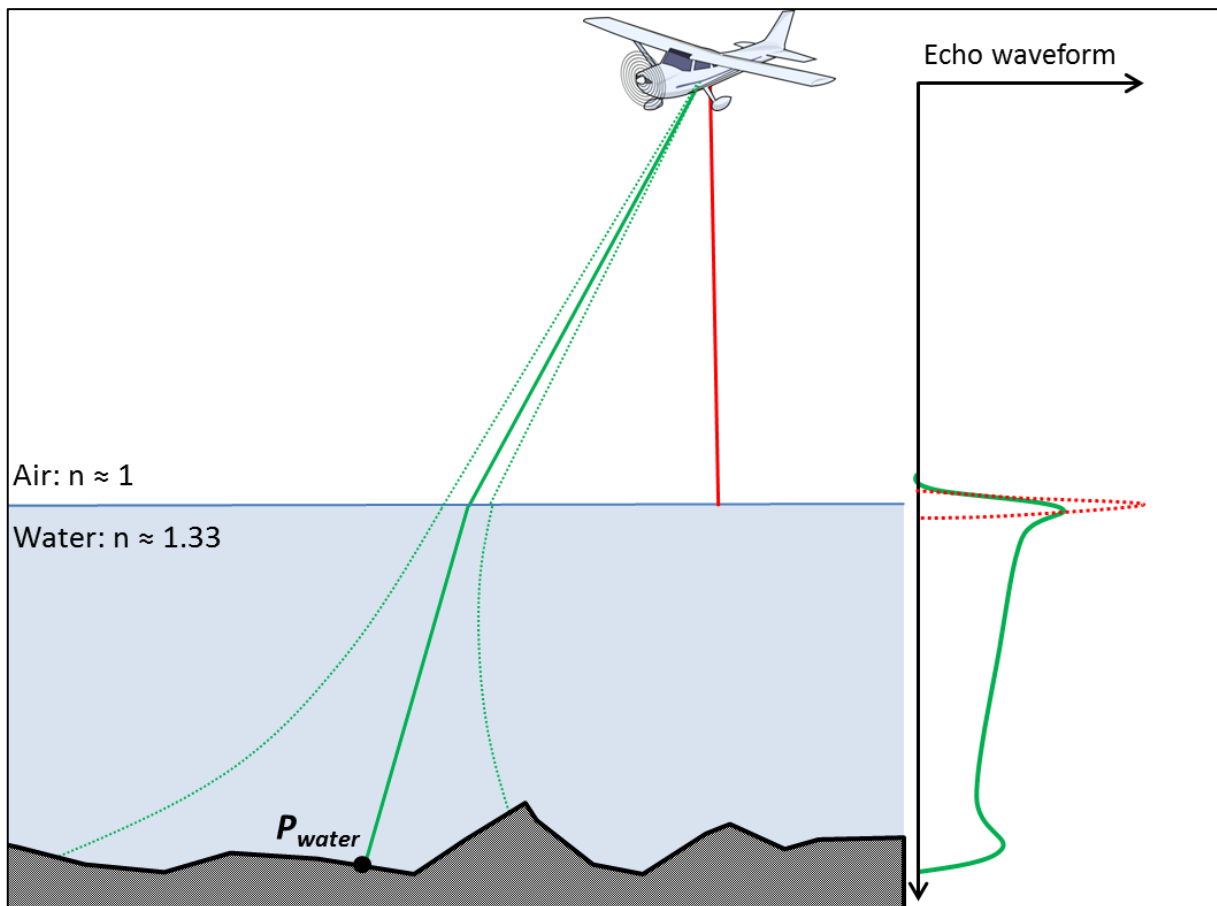


Figure 3: Ideal case of ALB data acquisition. The red line denotes the Infrared laser which does not penetrate into the water only resulting in one echo from the water surface (right). The green laser beam reaches the ground and ideally gives one local maximum from the water surface and one from the bottom which can be discriminated from volume scattering in the water column. In practice, neither the clear surface echo nor the clear bottom echo is guaranteed. The dotted green lines indicate the widening of the beam, because of the higher beam divergence as well as because of volume scattering under water.

The main difference between ALS and ALB data is again the effect of light refraction when passing through media of different optical depth exhibiting different propagation speed and propagation

direction (Figure 3). In contrast to two-media photogrammetry, where only the geometrical effect is relevant, ALB measurements also have to be corrected for runtime differences associated with the slower velocity of light in water:

$$\frac{c_{Water}}{c_{Air}} = \frac{n_{Air}}{n_{Water}} \xrightarrow{n_{Water} \approx 1.33} c_{Water} = c_{Air} \cdot \frac{n_{Air}}{n_{Water}} \approx 0.75 \cdot c_{Air} \quad (\text{Eq. 4})$$

Again, an accurate estimation of the water surface is needed for correction of the refraction bias. Historical systems, but also a couple of modern systems therefore use an additional infrared laser scanner delivering comparably reliable echoes from the water surface. This is especially state of the art for systems with wide point spacing since the variable reflection properties of water surfaces for green light can cause large gaps in the water surface data.

A second approach which came up more recently is to reduce systems to a stand-alone green laser and to rely on the sufficient occurrence of water surface reflections. Additionally, green light is scattered when interacting with sediment particles or molecules in the water body. Besides further widening of the beam under water (Mandlbürger et al., 2012), this effect also enables estimating the water surface as an upper hull of volume scattering (Mandlbürger et al., 2013a). Though water surfaces derived from green laser are less accurate than from infrared, the associated impact on the refraction correction possibly lies below the laser ranging precision (Mandlbürger et al., 2015c).

Coming to operable ALB systems, different categories can be distinguished based on how spatial resolution and penetration depth are traded off against each other. Applications for the surveying of marine environments, navigation channels etc. are usually designed to achieve best possible penetration depth. For example, the *Scanning Hydrographic Operational Airborne Lidar Survey (SHOALS)* system (Guenther et al., 2000; Hilldale and Raff, 2007) uses high-energy pulses (5 mJ). Consequently the necessary beam divergence to ensure eye safety results in a beam diameter on the ground of several meters. Along with a comparably small measurement rate in the range of 1000 Hz [XII] this reduces spatial resolution and disables the sensor to detect smaller objects. On the other hand, depths up to 50 m can be measured under favorable conditions, making this system a valuable complement to waterborne techniques in coastal waters (Guenther et al., 2000). A further example for systems with similar characteristics is the *Fugro Laser Airborne Depth Sounder (LADS) Mk3* [XIII] again having a wide point spacing of 4 m on the ground at a flying altitude of about 300 m.

Other instruments rather focus on spatial resolution and accuracy than on penetration depth. One of the first systems going in that direction was the *NASA Experimental Advanced Airborne Research LIDAR (EAARL)* – Nayegandhi et al., 2009) developed for mapping very shallow coastal areas and coral reefs. With small pulse energy of 70 µJ, it is possible to use a narrow beam resulting in a spot diameter on the ground of only 20 cm when flying at 300 m. Furthermore, the short pulse length of 1.2 nsec offers significantly better vertical accuracy (McKean et al., 2009). However, the mentioned improvements come at the price of lower penetration depth - namely about 25 m under best conditions.

Nevertheless, the favorable features of the system for mapping shallow waters at high accuracies also motivated the application of ALB systems for riverine environments (Kinzel et al., 2007; Kinzel et

al., 2006) and the suitability of the method to deliver adequate input data for hydraulic modeling could be confirmed (McKean et al., 2009). The remaining drawback of *EAARL* is the still relatively low measurement rate of about 5 kHz resulting in a point spacing of 2 m for the nominal flying height of 300 m.

Latest Laser technologies have allowed a significant step forward in this respect (Pfennigbauer et al., 2010; Steinbacher et al., 2010). The *Riegl VQ-820-G* [XV] system released in 2011 and designed particularly for rivers with depths at the order of a few meters, has a measurement rate of 200 kHz. The follow-up system, *Riegl VQ-880-G* [V], which was used in this study, even offers up to 550 kHz achieving a dense coverage of >10-20 points per m². Consequently, there already exists a considerable amount of literature concerning applications of these sensors. Starting from basic river mapping (Mandlbürger et al., 2011; Mandlbürger et al., 2012), more evolved tasks like monitoring of morphodynamics (Mandlbürger et al., 2015a), archeological sites (Doneus et al., 2012) or instream habitats (Mandlbürger et al., 2013b; Mandlbürger et al., 2015b) are reported.

Finally, there also exist sensors trying to combine the advantages of systems optimized for deep water and those focused on high resolution and accuracy. For example, the *Leica AHAB HawkEye III* [XIV] is equipped with one Near Infrared (NIR) and two green lasers: One for deep water bathymetry and the other one ensuring precise, high-resolution measurements in shallow water. A comparison of bathymetric LiDAR systems available in 2013 can be found at [XVI].

3 Study area and data acquisition for practical work

Practical assessment of the methods introduced in Section 2.2 (two-media photogrammetry) and Section 2.3 (ALB) was done with data covering a section of the Pielach River between Loosdorf and Melk in Lower Austria. Throughout the study area “Neubacher Au”, the river flows in a gravel bed partly surrounded by alluvial forest. Except for a few pools, water depth rarely exceeds 2 meters. Due to the good suitability of providing habitat especially for numerous bird and fish species, the whole stream course is protected as Fauna Flora Habitat protection area “Pielachtal” within Natura 2000 conservation area “Niederösterreichische Alpenvorlandflüsse” [IV]. Further detailed description of the study can be found in the related literature (Mandlbürger et al., 2013a; Mandlbürger et al., 2013b; Mandlbürger et al., 2015b; Mandlbürger et al., 2015c).

The data acquisition flight took place on April 14th, 2015. Four parallel strips and two cross strips were scanned with the *Riegl VQ-880-G Topo-Hydrographic Airborne Laser Scanning System* [V] with a green laser scanner only. The scan pattern is circular (Palmer scanner) ensuring a roughly constant incidence angle of about 20° in case of horizontal terrain. Using a flying height of 600 m, the footprint diameter amounts to approximately 60 cm. One additional strip was scanned in descent in the western part of the study area in order to achieve an incidence angle of around 0° enabling the sensor to detect specular reflections for an accurate water surface determination.

In five of the strips (4 parallel and 1 crosswise), additional aerial RGB images were captured with an *Allied Vision Prosilica GT6600* 28.8 Megapixel Camera [VI]. The pixel size of 5.5 µm corresponds to about 6.5 cm on the ground therefore operating at a significantly smaller ground sampling distance than the ALS system. With 50-60% in flight direction and <50% between two strips, the overlap is rather modest but sufficient. The study area is depicted in Figure 4 with the stars denoting the positions of image projection centers.

For further investigations, two smaller Areas of Interest were focused on. The first one is the meandering part close to the village Neubach which will henceforth be denoted as “Sector East” (Figure 4b). The second one is the adjacent straighter part of the river course called “Sector West” (Figure 4a). Whereas Sector East is a hydrologically more diversified area, Sector West was chosen due to the availability of specular water surface reflections offering most accurate surface determination. However, in this sector, large parts of the river are occluded by overhanging trees hampering depth estimation via two-media photogrammetry for large parts of the channel.

The practical workflow is depicted in Figure 5. More detailed descriptions follow in Section 4 for ALB and in section 5 for two-media photogrammetry separately. In Section 6, the results are compared and discussed.

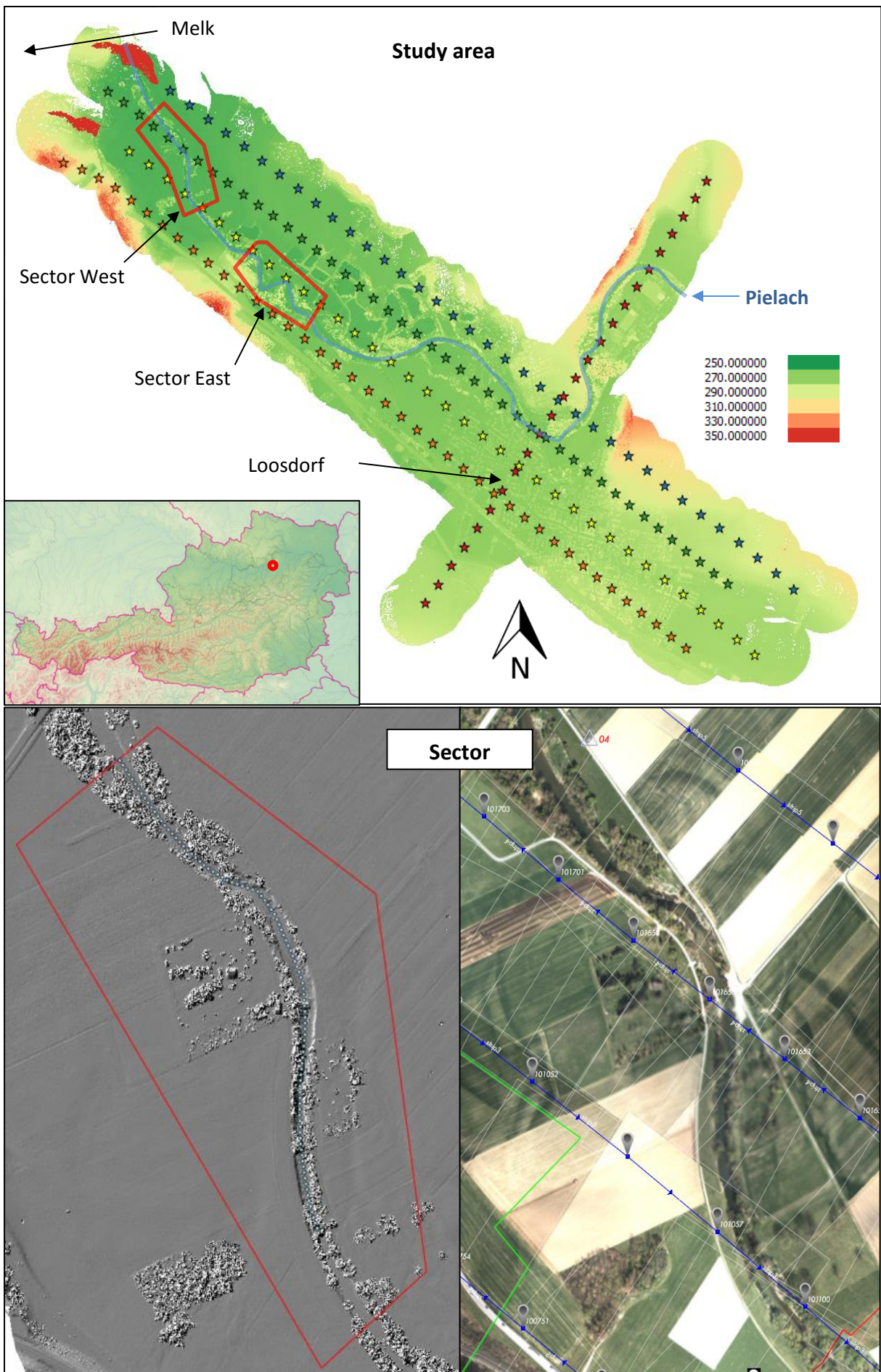


Figure 4a: Overview of the study area and Sector West (ALB DSM and aerial image overview). The small location map of Austria was adapted from SRTM and GATM (www.gatm.org) data.

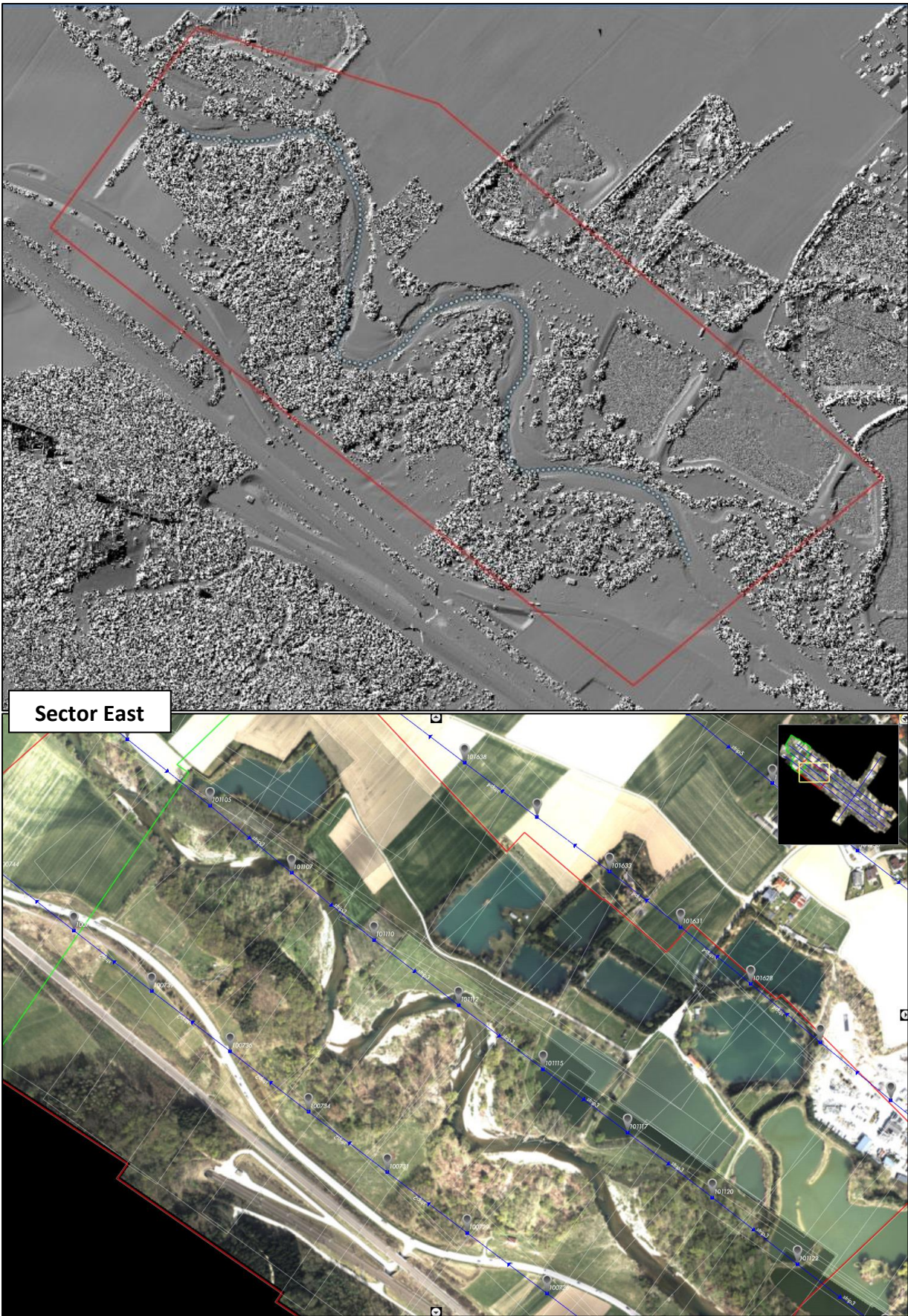


Figure 4b: Enlarged maps of the area of Interest "Sector East". A DSM derived from ALB data is compared to an image overview created in the Trimble Inpho Software. The river axis is described by the blue dotted line.

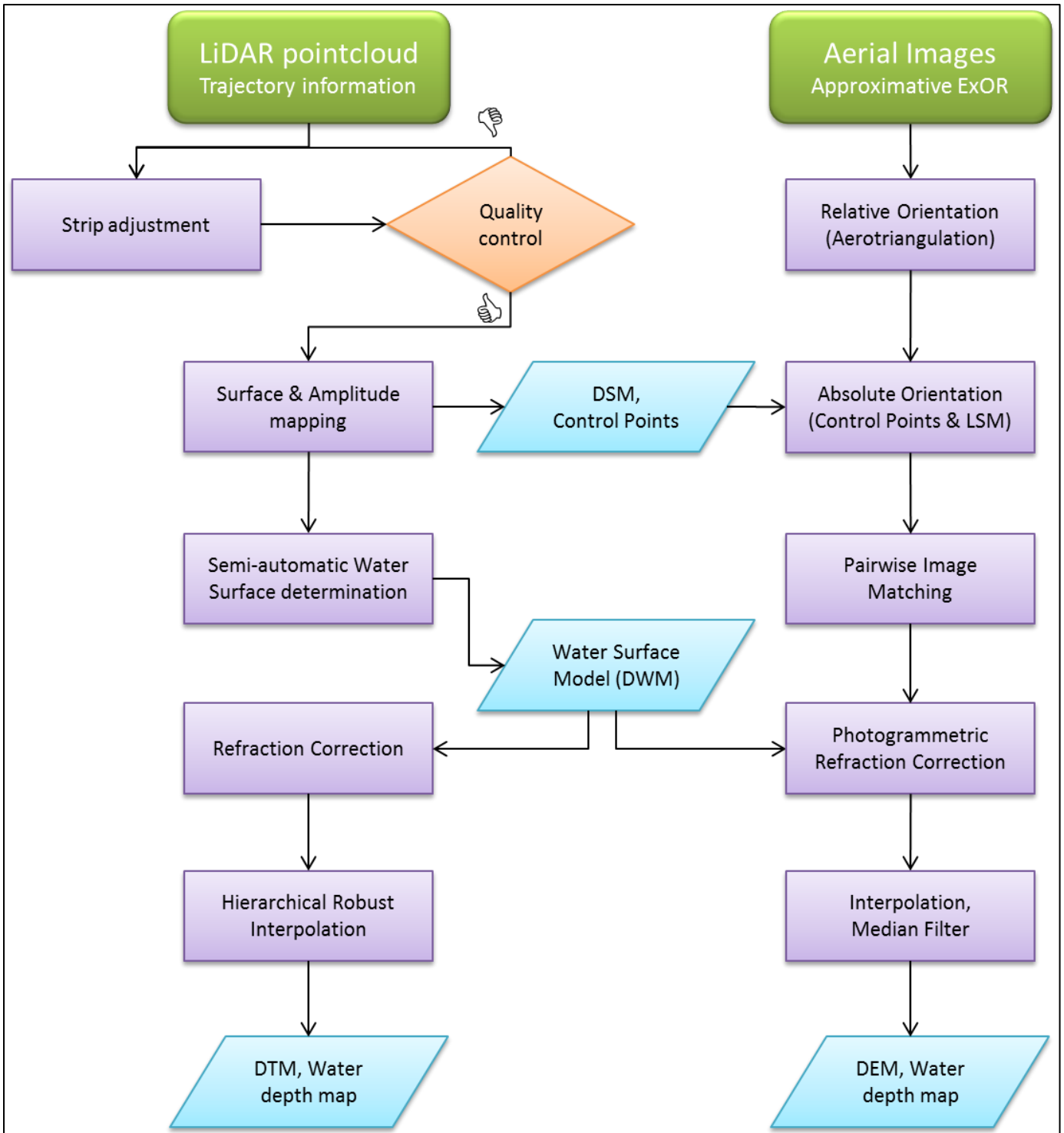


Figure 5: Overview of the major practical steps. ALB (left) and Photogrammetry (right) have nearly separate workflows except for the water surface model where the same one is used for both techniques.

4 ALB workflow

In the following section, the processing steps for ALB data are outlined with emphasis on the differences compared to the topographic ALS workflow. Furthermore, a short theoretical estimation of the refraction induced bias is done.

Most of the steps were accomplished using the program system *OPALS – Orientation and Processing of Laser Scanning Data* (Pfeifer et al., 2014) [XI] developed at *TU Wien*.

4.1 Quality control and strip adjustment

The ALB dataset was already delivered as a georeferenced LAS point clouds. Therefore, the first step is the assessment of data quality. This is basically done including two criteria: Point density (Figure 6) and pairwise differences of overlapping strips.

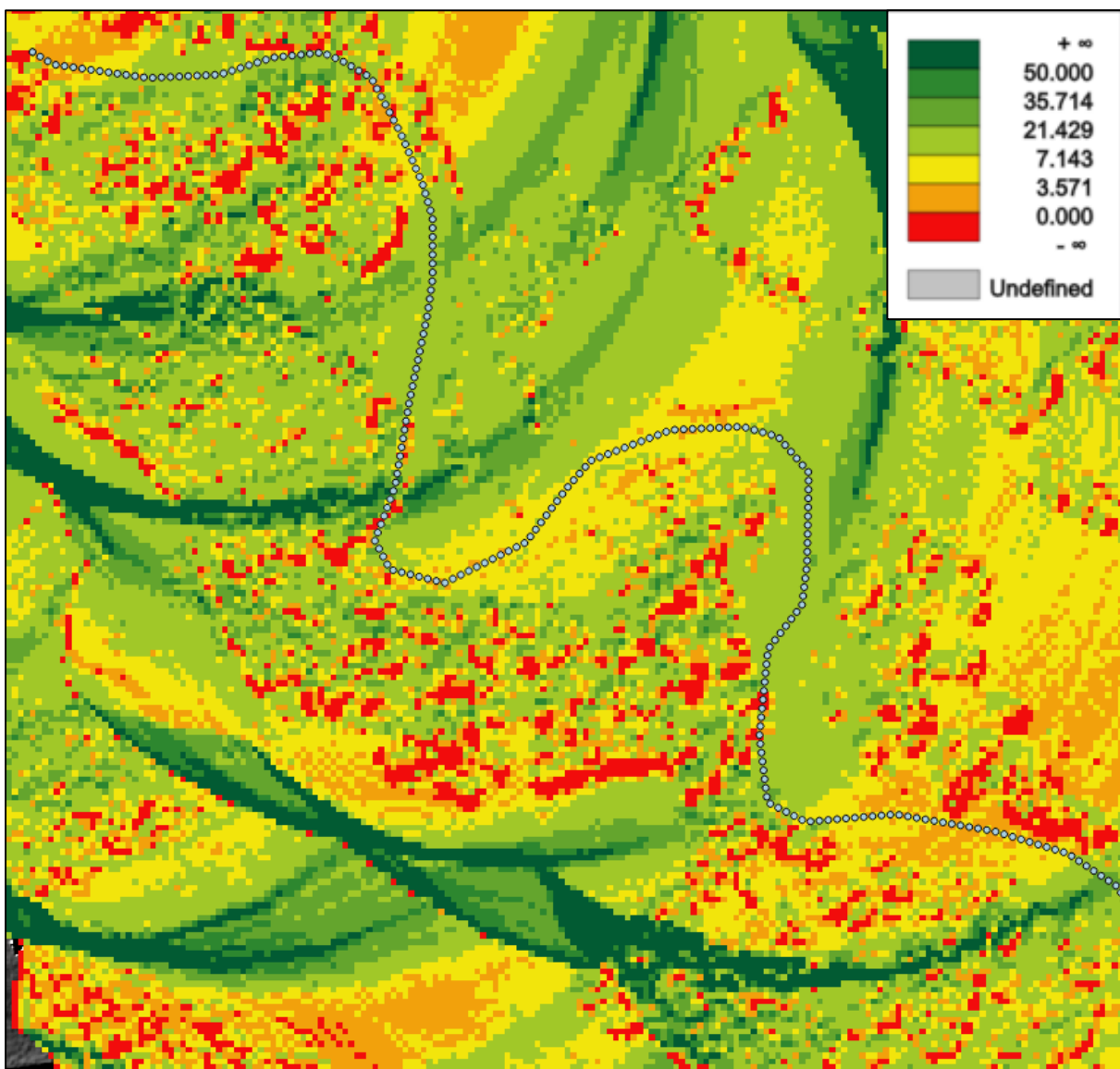


Figure 6: Point density map for one ALB strip covering Sector East. No significant differences between the river bed (the blue dotted line corresponds to the river axis) and dry terrain are visible. Only vegetation is responsible for smaller point densities.

The strip differences are computed by interpolating digital elevation models (DEMs) from the point clouds, masking out areas lacking certain smoothness (σ_z and excentricity threshold) and subtracting overlapping DEMs (Ressl et al., 2008). Using *OPALS* an automatized run through this procedure is provided in the *opalsQuality* package.

Inspection of these strip differences showed unacceptable large deviations, for several strip pairs even exceeding 10 cm. Some strips were strongly tilted w.r.t others. All in all, the revealed differences necessitated additional adjustment prior to further processing.

First of all, an adjustment without including trajectory information was tried (Ressl et al., 2009). This approach uses least-squares matching based on strip-wise DEMs to determine five transformation parameters for each strip. According to (Ressl et al., 2009), these parameters are “one 3D shift, one roll angle and one affine yaw parameter” – 3 translation and 2 rotation parameters. The adjustment is implemented in the *opalsGeoref* package. Another quality check showed improvements yet not being completely satisfying.

Therefore, the final strip adjustment was performed taking a rigorous approach (Glira et al., 2015a). In contrast to the approximate approach described above translating and rotating the point clouds, rigorous strip adjustment aims at a re-calibration of the system by eliminating errors in the original measurements (e.g. range scale and offset, scan angle scale and offset, misalignment of boresight angles etc.). This is done without interpolating a raster model but by introducing an error metric directly based on correspondences between the point clouds (Glira et al., 2015b).

4.2 Digital Surface Model (DSM)

After the successful strip adjustment, a *Digital Surface Model (DSM)* is derived from ALB data. The *DSM* is used for visualization purposes but also for control point measurements in the course of the image block orientation (Section 5.1). Furthermore, comparison and *LSM* with height models resulting from image matching need a *DSM* as a reference.

In contrast to the model interpolated during quality checking, the approach taken here combines different interpolation types depending on their ability to map surfaces of varying roughness, c.f. (Hollaus et al., 2010). Smooth surfaces are represented by a *movingPlanes* interpolation, whereas rough surfaces like vegetation etc. are better described by taking the highest z-value in each raster cell. The DSMs for the two areas of Interest are shown in Figure 4.

4.3 Amplitude Mapping

Establishing point correspondences between image and ALB data (Image Orientation: Section 5.1) is not or only roughly possible with height models alone since they contain no texture. Better comparability can be assured by extracting texture information from the LiDAR point clouds. This can be done using the *Amplitude* parameter which is stored for each point and is related to the target reflectivity.

The most meaningful maps were obtained by representing each 0.5 meter raster cell by the highest contained Amplitude value. The remaining gaps were filled by raster based techniques (mean filter based on square kernel neighborhoods).

In the resulting map, objects like houses etc. can be clearly delineated, but also boundaries between different ground cover types are visible. Partially, even road marking is perceptible. Figure 7 shows a comparison of the amplitude map and an aerial image covering the same area.



Figure 7: Comparison of an aerial RGB image (right) and an Amplitude map derived from ALB data. Though the aerial image shows a clearly better resolution, most major objects can be identified in both representations – even the lines on the soccer field can be recognized.

4.4 Water surface determination

Coming to bathymetric processing, an essential prerequisite for refraction correction is first of all finding an estimation of the interface between the media air and water, i.e. the water surface. However, the number of water surface reflections for green laser is very small in the given dataset, making a fully automatic and accurate water surface modeling apparently impossible (Guenther et al., 2000), especially in case of overhanging vegetation. Nevertheless, data contain inherent information about the water surface. Although the density of reflections from smooth water surfaces is rather poor, this smoothness enables a semi-automatic determination of a continuous surface model. In this work, the semi-automatic approach introduced in (Mandlbürger et al., 2015a) and (Mandlbürger et al., 2015b) is adopted:

First of all, the river axis is digitized manually (c.f. Figure 4) which is a simple solution for the comparably small areas of interest. If it comes to large, more complicated channel systems, an automatic extraction framework requiring clearly engraved stream valleys is proposed by (Passalacqua et al., 2010).

The further procedure relies on the assumption of an approximately horizontal water surface perpendicular to the river axis. Consequently, splitting the point cloud along the river axis in narrow

cross sections makes it possible to estimate a horizontal line through each of the slices which is a good estimation for the water surface. Densifying this information finally leads to a continuous model.

A script supporting the described procedure was developed at TU Wien. Inputs are the point cloud of the Area of Interest and a river axis in WNP format. The perpendicular cross sections are created and plotted (Figure 8) for the operator to decide, where the water surface is located or, if this cannot be reliably determined, at least the width of the river bed. In practice, it has worked out best to choose the water surface as an upper closure of the points apparently belonging to the water body since only rarely, real surface echoes are present. For this study, each cross section covered one meter of the river axis. During the manual measurements, the operator is assisted by interpolations of the water height along the river axis between already specified positions. So it is recommendable to measure only every 100th cross section in a first run to have already good approximations when going into detail. After densification along the measured lines, a point cloud is returned, which is then interpolated to obtain a water surface model (DWM).

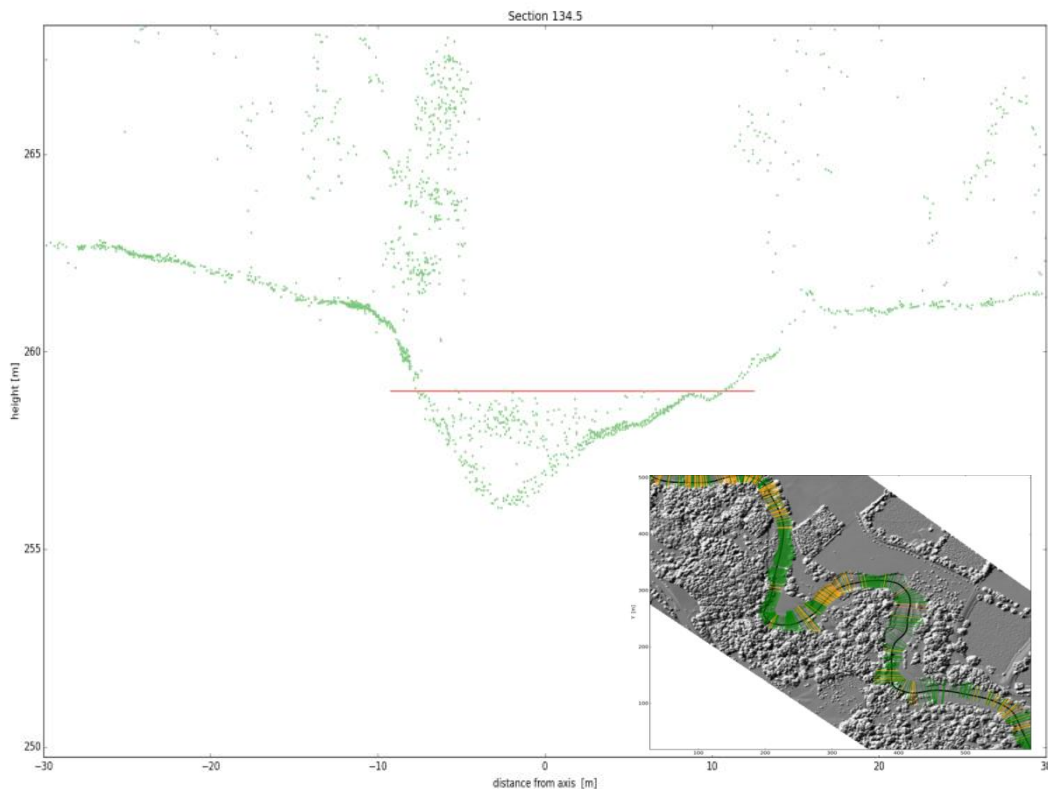


Figure 8: User interface of the “picking tool” for semiautomatic water surface detection. The red line can be adjusted to represent the water surface for the plotted cross section. The small overview image shows all measured cross sections (green) and all cross sections where only the lateral extent of the water surface could be identified (yellow). The remaining gaps in between are closed by interpolation.

In Sector West, where a descending flight strip offers the additional availability of specular surface reflections, these can be used to refine the water surface after the semi-automatic procedure. In a height range of +/- 7 cm of the estimated surface all ALB points are chosen and re-interpolated assuming that they belong to the water surface. This is approvable because typically most echoes

near nadir are from specular reflections and there hardly exists any volume scattering from the water body below. The high point density on the surface enables much higher resolution mapping (grid size 25 cm instead of 1 m) and allows rough, non-horizontal water surfaces as well.

4.5 Refraction error estimation and correction

As mentioned before, light refraction at the water surface has two relevant effects for airborne laser bathymetry. These effects are illustrated in Figure 9.

A laser pulse emitted from P_0 hits the point P_w in the river bed; the beam widening shown in Figure 3 is neglected during the following calculations. Furthermore, for this simulation, a horizontal water surface is assumed. Crossing the water surface the light is refracted. Thereby propagation direction and propagation speed are altered.

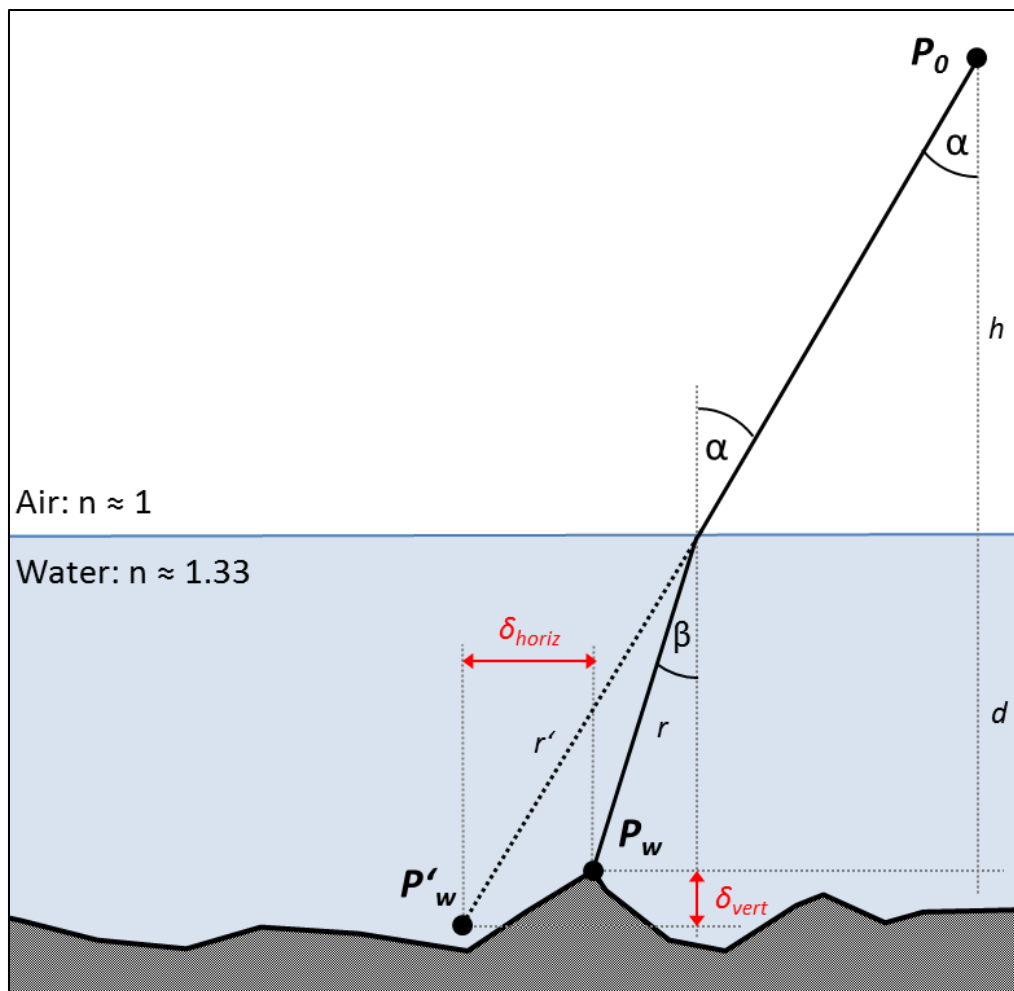


Figure 9: Sketch of the vertical and horizontal bias introduced to ALB measurements by refraction: The slower speed of light in water is responsible for the length difference between r and r' , the directional effect is manifest through the different angles α and β .

First regarding the propagation direction, light is refracted towards the plumb line when entering the optical thicker medium water. Depending on the refraction indices of air and water, n_{air} and n_{water} , Snell's law formulates the following relationship between incoming and outgoing angle:

$$n_{air} \cdot \sin \alpha = n_{water} \cdot \sin \beta \quad (\text{Eq. 5})$$

With $n_{Air} \approx 1$ we can simplify and solve the equation for β in dependence of α :

$$\beta = \text{asin} \left(\frac{\sin \alpha}{n_{water}} \right) \quad (\text{Eq. 6})$$

Propagation speed of light in a medium c_{medium} can also be expressed as a function of the respective refraction index n_{medium} and the speed of light in vacuum c :

$$c_{medium} = \frac{c}{n_{medium}} \quad (\text{Eq. 7})$$

According to Eq. 7, the speed of light in the media air and water, c_{air} and c_{water} , can be related:

$$\frac{c_{water}}{c_{air}} = \frac{n_{air}}{n_{water}} \quad (\text{Eq. 8})$$

To get a rough estimate of the horizontal and vertical deviation caused by refraction, P_w is compared to the apparent terrain point P'_w which results from the measurements if the effects described above are not considered. Due to the slower speed of light in water, the distance from the water surface is overestimated if wrongly assuming the speed of light in air:

$$r' = c_{air} \cdot \Delta t \quad r = c_{water} \cdot \Delta t \quad (\text{Eq. 9})$$

Substituting Eq. 8 yields:

$$r' = \frac{n_{water}}{n_{air}} \cdot r \quad \text{with} \quad r = \frac{d}{\cos \beta} \quad (\text{Eq. 10})$$

Now the horizontal and vertical error caused by refraction can be determined:

$$\delta_{horiz} = r' \cdot \sin \alpha - r \cdot \sin \beta \quad (\text{Eq. 11})$$

$$\delta_{vert} = r' \cdot \cos \alpha - r \cdot \cos \beta \quad (\text{Eq. 12})$$

To get numeric values, some typical values are assumed. For α , 20° is adopted which is the nominal incidence angle of the *VQ-880-G* scanner (c.f. chapter 3). According to Eq. 6, β then equals 14.9° . The refraction indices are $n_{Air} \approx 1$ and $n_{Water} \approx 1.33$. So for example, a water depth $d = 1 \text{ m}$ leads to a horizontal displacement $\delta_{horiz} \approx 20 \text{ cm}$ and $\delta_{vert} \approx 29 \text{ cm}$ in vertical direction. Both errors grow linear with depth.

In practice, the refraction correction for ALB data is implemented in *OPALS Module Snellius*. Mandatory inputs are a raster *water surface model (DWM)* and the point cloud to be corrected. For the point cloud, the beam vectors, i.e. the direction from the instrument to the target, already have to be contained as attributes. This can be done with *Module Import* when specifying the trajectory file of the ALB flight. As a result of the correction procedure, the input point cloud is not changed geometrically, but attributes corresponding to the corrections for all three coordinates are added which can be used to compute a corrected point cloud separately.

4.6 Digital Terrain Model interpolation including submerged areas

Digital Terrain Models (DTMs) of the river course and the surrounding floodplain are a valuable input for many applications described in Section 1.1. Therefore, it is the most important final product of bathymetric mapping per se.

The final DTM was computed using hierarchical robust interpolation (Pfeifer et al., 2001; Briese et al., 2002) as implemented in the terrain data management software *SCOP++* [XVII]. This method introduces a weighting to reduce the influence of points above terrain on the interpolation. Thereby, buildings are removed from the model as well as trees and also water volume scattering under the prerequisite that a ground echo is available in the proximity.

The result and further evaluations follow in Section 6.1.

5 Photogrammetric Workflow

In this section the full photogrammetric workflow from the aerial images to high resolution water depth models is described. This includes amongst others theoretical investigations on the effects of light refraction at the media boundary between air and water as well as the development of a practical correction procedure to eliminate the respective error.

5.1 Image Orientation

The images were provided as TIF files with an additional CSV file for each strip, holding information about the corresponding positions and attitudes of the camera. First qualitative inspections of the original exterior orientation were done by incorporating these values into world files, small external text files storing transformation parameters to georeference the respective images [VII]. Visualization in *ArcGIS* showed that the given orientations rather had the character of approximations.

For the relative orientation, an Aerotriangulation (AT) was carried out in the *Trimble Inpho Software* [VIII] using the module *Match-AT*. Due to the failure of an AT with automatically extracted tie points ($\sigma_{\text{naught}} > 2$ pixel), about 1000 tie points had to be measured manually corresponding to 3700 single point measurements (c.f. Figure 11). However, despite very careful measurements and subsequent controls, this brought only a slight improvement at the additional cost of implausible trajectory deformations (Figure 10).



Figure 10: Strip deformations resulting from a failed Aerotriangulation.

Assuming a problem in *Match-AT*, the approximate orientations and the manual measurements were exported to the photogrammetric adjustment software *ORIENT* (Kager and Waldhäusl, 1989). There, the adjustment was performed including a new estimation of the camera calibration parameters and the lever arm showing reasonable results. After correcting the indicated worst point measurements, it finally brought the expected standard deviation of manual point measurements ($\sigma_{\text{manual}} \approx 1/3$ pixel).

Without proof, the problem in *Match-AT* is likely to be associated with the handling of image distortion parameters. Therefore, the parameters from *ORIENT* were used to undistort the images enabling the further workflow using the *Trimble Inpho* software. The calibrated camera model was imported to *Match-AT* as well. This enabled a final refinement of the relative orientation with automatic tie point measurements ($\sigma_{\text{automatic}} \approx 1/10$ pixel).

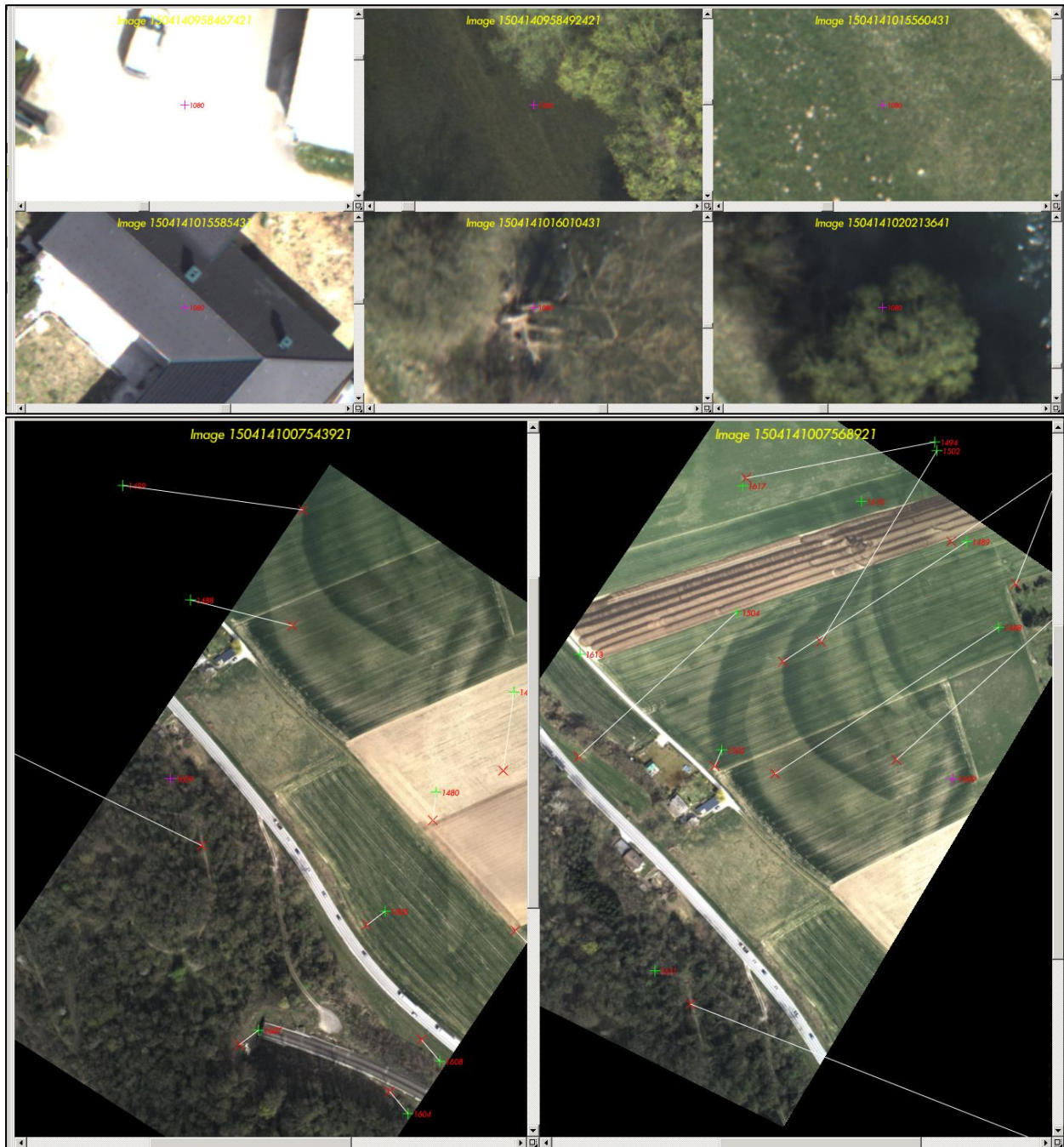


Figure 11: Screenshots from the Match-AT point measurement tool illustrating the poor initial exterior orientations. In the six windows above, the position of one and the same point is estimated in six overlapping images – obviously the resulting positions don't have much to do with each other. The two larger images show the situation after tie point measurements with large residuals between measurements (red) and estimation based on the measurement in the other image (green).

The absolute orientation was set w.r.t. the ALS block. In order to ensure comparability with the images for finding correspondences, an amplitude map was derived of the ALS data (c.f. section 4.3). The respective height of the control points was determined using a Digital Surface Model (DSM). It turned out to be more promising to extract points on relatively planar surfaces such as roads instead of sharp corners on buildings. Though the latter can be easily identified in images, their height extracted from 0.5 m resolution DSMs is not very reliable. Four control points were measured in the corners of the four parallel strips and two at the ends of the cross strip, making 6 points in total responsible for an approximate absolute orientation.

However, first DSMs derived from Image Matching still showed a bias of about 15 cm between the orientation of the image block and the orientation of the ALS block. This motivated a final refinement by Least Squares Matching (LSM) of Surface Models derived from image matching and laser scanning data respectively. The DSMs were extracted for four built-up areas distributed through the block.

5.2 Image Matching

Due to refraction at the media boundary between air and water, geometric distortions are introduced for submerged areas. This may be a challenge for image matching algorithms because of unanticipated alterations of the presumed conditions, for example the deviation from epipolar geometry.

In order to compare how different algorithms react to the new circumstances, image matching is performed using two different program environments, namely the dense image matching software *SURE* (Wenzel et al., 2013) and *Match-T DSM [IX]* which is as well part of the *Trimble Inpho* software.

Furthermore, it is intended to match all overlapping image pairs separately as this is the easiest way to know which images are responsible for one certain matched point. This knowledge is necessary for the refraction correction procedure (c.f. Section 5.4). In this section, the most important settings for image matching in both software packages are discussed.

5.2.1 SURE

Working with default settings, *SURE* produces one matched point per pixel resulting in an enormous amount of data with point densities at the order of >400 points per m^2 for bare ground. When processing large areas it is therefore essential to filter the point cloud prior to all following steps. Of the few controllable parameters, the minimal point-to-point distance is the most influential one. Small distances only make the result noisier without conserving additional information whereas large point spacings possibly eliminate existing details in the data. Values between 0.1 and 0.2 m empirically brought the best results, thus 0.2 m was chosen resulting in a smaller amount of data.

Pairwise Matching in *SURE* can be realized with batch processing: The following command starts image matching of all images contained in *imglist.txt*. Their respective exterior orientations can be found in the Inpho PRJ file *fullproject.prj*:

```
sure fullproject.prj -img imglist.txt -scenario OBLIQUE
```

Concerning scenarios, *oblique* worked out best, changes to the parameters can be made in the control-files stored in the working directory.

By automatically generating image lists where each list contains exactly one image pair, pairwise matching can easily be implemented.

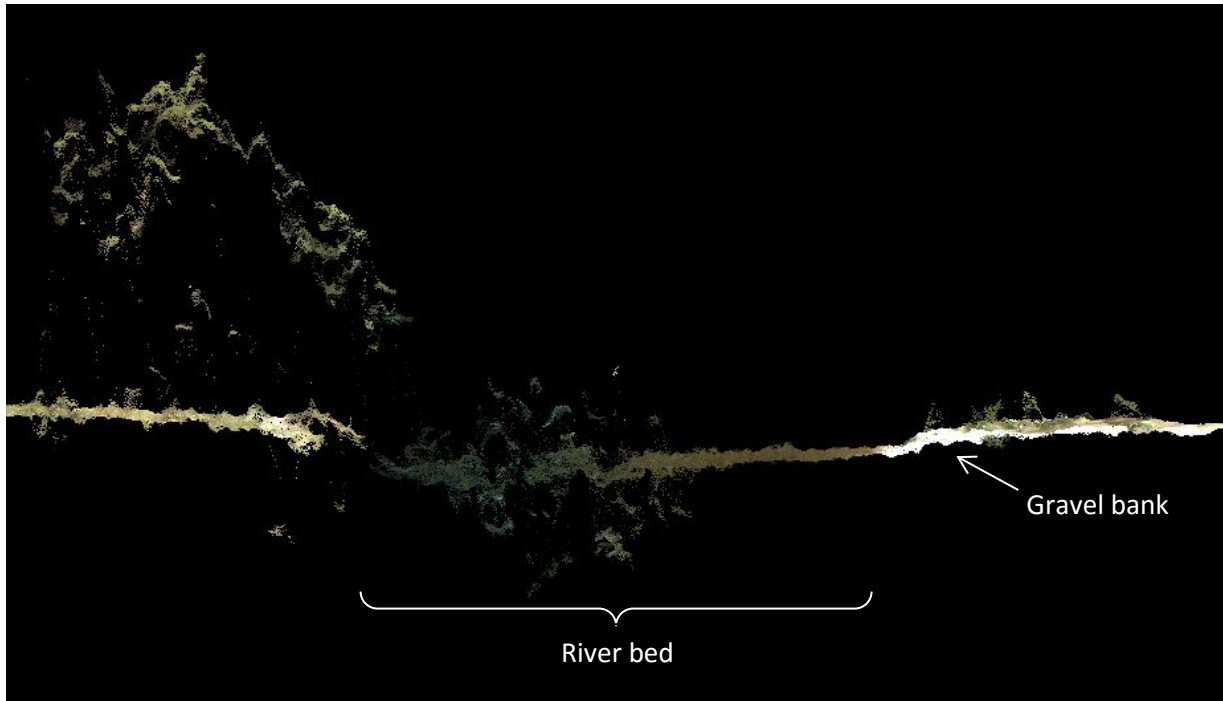


Figure 12: Cross Section through a point cloud resulting from dense image matching in SURE. With some exceptions, terrain is well represented. The scattered appearance in the river bed with deviations in positive and negative direction show the necessity of robust point filtering.

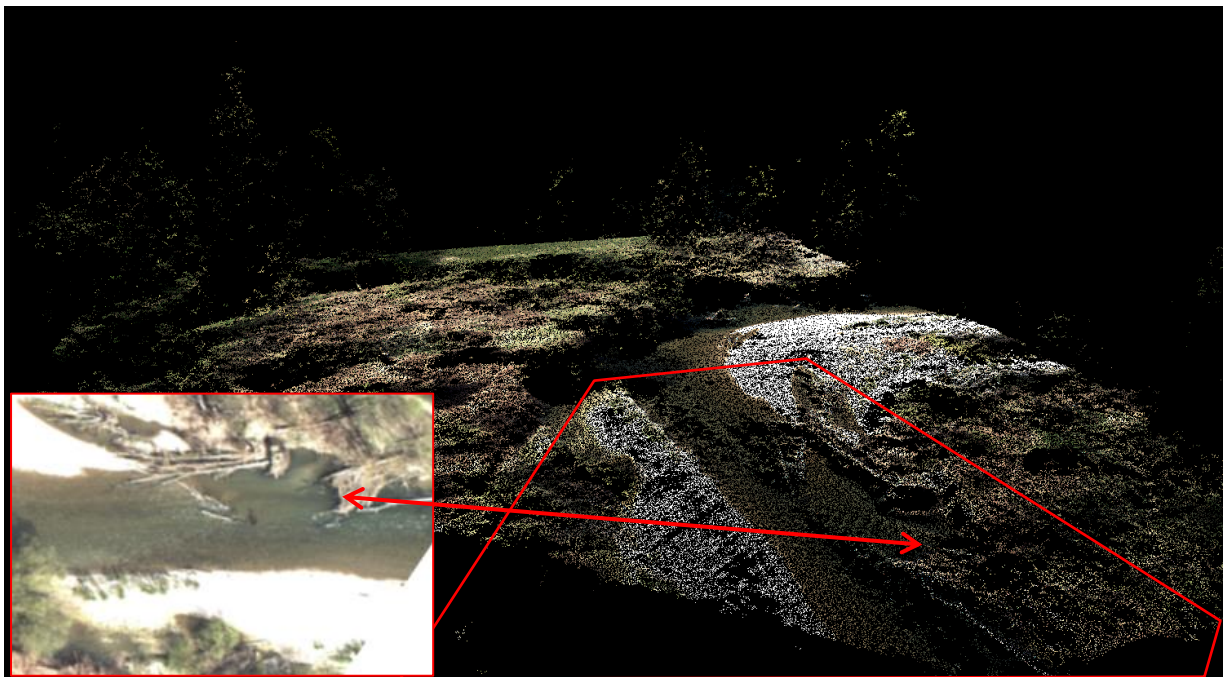


Figure 13: 3D view of another SURE point cloud. In the lower right corner, driftwood lying in the water (c.f. the red marks and the aerial image) can be identified. In the meander, the effects of overhanging trees occluding the terrain and casting shadows can be observed.

5.2.2 Match-T

In contrast to *SURE*, *Match-T* also offers the possibility of feature-based matching (FBM) in addition to the dense cost-based matching (CBM) approach – corresponding to the generation types “*Digital Terrain Model*” for FBM and “*Digital Surface Model*” for CBM. These types can be incorporated in user-defined matching strategies. Further parameters were chosen empirically by comparing the respective matching results:

For the feature density, the value “*dense*” works out best in this case study; the ideal point cloud density is 3 pixels – this significantly reduces noise without eliminating terrain features. The “*strip constraint*” allowing matching only between two images of one strip is turned off in order to reduce fringes occurring with CBM (c.f. Figure 21). The final *Optimize* parameter is set to “*Balance*”, since “*UAV*” and “*Precision*” bring no real improvement but need a disproportionately longer processing time.

In *Match-T*, pairwise matching can be assured by manipulating the *Inpho PRJ* file: After the strip definition, subblock definitions are inserted, each containing one image pair (Figure 14 left). After the image and camera references, the subblocks can be used to create matching jobs (Figure 14 right). For these definitions, the predefined matching strategies are applied. Finally, matching of all image pairs is started in the *Match-T Commander*. Actually, each image pair is matched twice – feature-based (DTM strategy) and cost-based (DSM strategy).

<pre> 69 101553 101556 101558 101601 70 101621 101623 101626 101628 71 101648 101651 101653 101656 72 strip5 127.57 15469.86 0.00 73 101933 101936 101938 101941 74 102001 102003 102006 102008 75 102028 102031 102033 102036 76 \$END_STRIPS 77 \$END 78 \$BLOCK 79 \$BLOCK_ID : 100741_101112 80 \$IMAGES : { 100741 101112 } 81 \$END 82 \$BLOCK 83 \$BLOCK_ID : 100741_101102 84 \$IMAGES : { 100741 101102 } 85 \$END 86 \$BLOCK 87 \$BLOCK_ID : 100729_100736 88 \$IMAGES : { 100729 100736 } 89 \$END 90 \$BLOCK 91 \$BLOCK_ID : 100726_100736 92 \$IMAGES : { 100726 100736 } 93 \$END </pre>	<pre> 3099 \$FOCAL_LENGTH : 31.166396 3100 \$PRINCIPAL_POINT_PPA : 0.000000 0.000000 3101 \$GPS_ANTENNA_OFFSET : 0.000000 0.000000 3102 \$CAMERA_MOUNT_ROTATION : 15469.860469 3103 \$COMMENT : 3104 ProsilicaGT6600afterOrient 3105 \$END 3106 \$END 3107 \$DTM_PAR 3108 \$DTM_PAR_ID : DTM_100729_100736 3109 \$WITHHOLD : On 3110 \$BLOCK_ID : 100729_100736 3111 \$TYPE : DTM 3112 \$START_STOP : -1 -1 3113 \$GRID_WIDTH : 1.900000 3114 \$STRIP_CONSTRAINT : Off 3115 \$GRID_OUTPUT : Off 3116 \$GRID_TPIX : Off 3117 \$ADDITIONAL_OUTPUT : On 3118 \$OUTPUT_DIRECTORY : U:\Match_T_results 3119 \$POINT_CLOUD_TPIX : Off 3120 \$USE_SURFACE_POINTS : Off 0.000000 3121 \$USE_BREAKLINES : Off 0.000000 3122 \$BREAKLINE_DENSE : Off 0.000000 3123 \$USE_EXCLUSIONS : Off 0.000000 3124 \$USE_FORMLINES : Off 0.000000 3125 \$END 3126 \$DTM_PAR 3127 \$DTM_PAR_ID : DTM_100726_100736 3128 \$WITHHOLD : On 3129 \$BLOCK_ID : 100726_100736 3130 \$TYPE : DTM 3131 \$START_STOP : -1 -1 </pre>
-------------------------------------------------------------------------------------------------------------------------------------------------------------------------------------------------------------------------------------------------------------------------------------------------------------------------------------------------------------------------------------------------------------------------------------------------------------------------------------------------------------------------------------------------------------------------------------------------------------------------------------------------------------------------------------------------------------------------------------	---------------------------------------------------------------------------------------------------------------------------------------------------------------------------------------------------------------------------------------------------------------------------------------------------------------------------------------------------------------------------------------------------------------------------------------------------------------------------------------------------------------------------------------------------------------------------------------------------------------------------------------------------------------------------------------------------------------------------------------------------------------------------------------------------------------------------------------------------------------------------------------------------------------------------------------------------------------------------------------------------------------------------------------------------------------------------------------------------------------------------------------------------------------------------

Figure 14: Subblock definitions (left) and matching instructions (right) inserted in the *Inpho PRJ* File for the image pair 100729-100736.

5.3 Refraction effect on photogrammetric measurements

As for Laser Bathymetry, refraction at the two-media-boundary also introduces a significant error to the point clouds resulting from image matching which has to be corrected. As a first step towards a practical correction procedure, the effect is theoretically assessed in this section.

In contrast to ALB where also the deceleration of the speed of light in the medium water has to be considered, for Photogrammetry only the directional effect is relevant. In the following calculations to determine the bias introduced by light refraction, a plane water surface is assumed, i.e. the water surface normal is vertical.

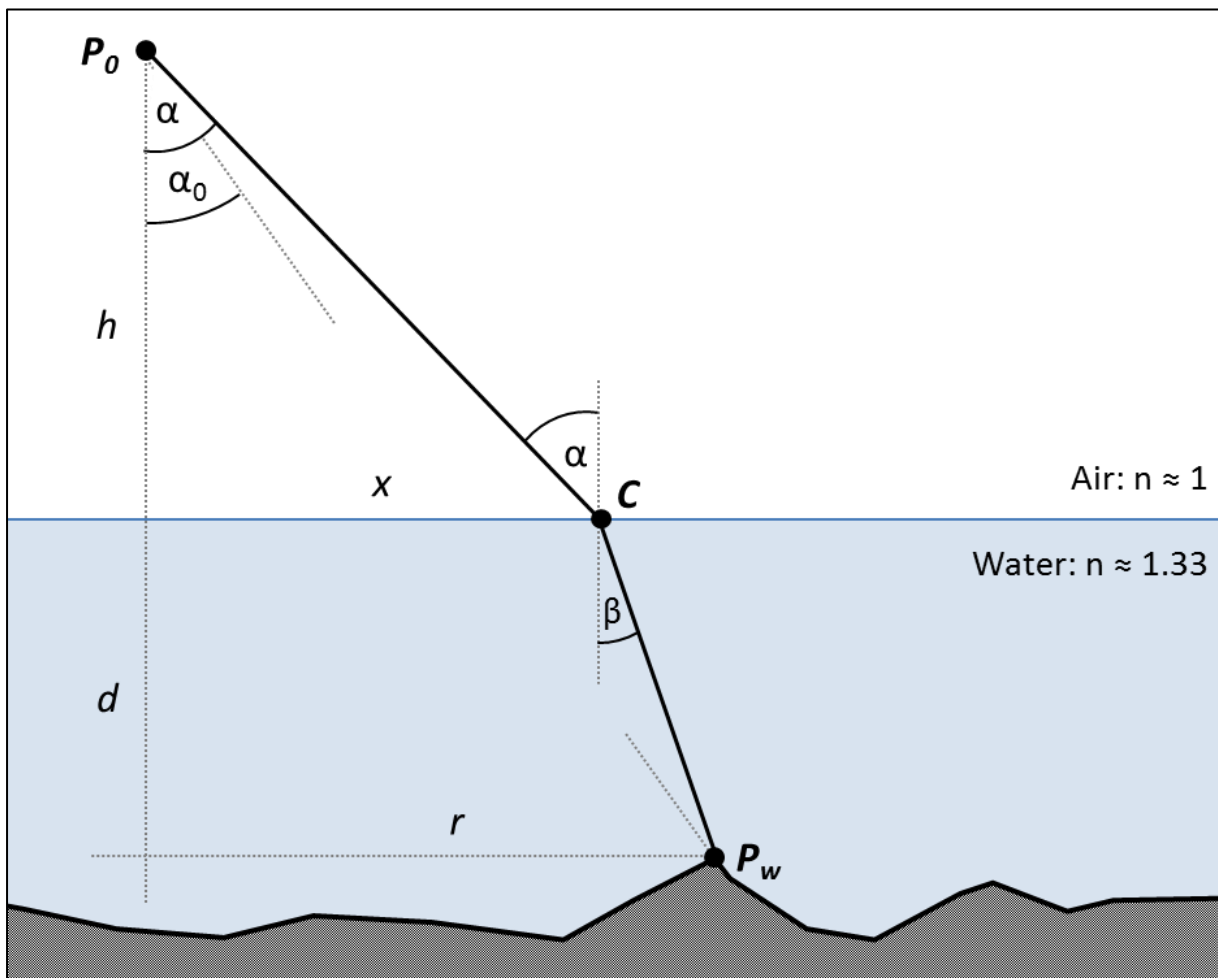


Figure 15: Geometry of a light ray passing through the interface between air and water.

An underwater point P_w is seen from a point P_0 above the water – e.g. an image projection center. Assuming that in this simulation we know water depth d , the horizontal distance r between P_w and P_0 and the height h of P_0 above the water surface we can iteratively determine the light ray from P_w to P_0 . This is accomplished by introducing another horizontal distance x between P_0 and the water intersection point C of the light ray where the refraction takes place. Using α (the angle between the water surface normal and the line $\overline{CP_0}$) and β (the angle between $\overline{P_wC}$ and the water surface normal), we can relate these angles using Snell's law (c.f. Eq. 5):

$$\alpha = \text{asin}(n_{\text{water}} \cdot \sin \beta) \quad (\text{Eq. 13})$$

$$\beta = \text{asin}\left(\frac{\sin \alpha}{n_{\text{Water}}}\right) \quad (\text{Eq. 14})$$

Another way of relating α and β is to calculate x from two different triangles, one above and one under the surface. Equalizing the two solutions we get:

$$h \cdot \tan \alpha = x = r - d \cdot \tan \beta$$

$$\tan \alpha = \frac{r}{h} - \frac{d}{h} \cdot \tan \beta$$

$$\alpha = \text{atan}\left(\frac{r}{h} - \frac{d}{h} \cdot \tan \beta\right) \quad (\text{Eq. 15})$$

Now α can be determined iteratively using Eq. 14 and Eq. 15. For aerial images, where typically $h \gg d$, a good approximation for α can be found by drawing a straight line $\overline{P_0 P_w}$:

$$\alpha_0 = \text{atan}\left(\frac{r}{h+d}\right) \quad (\text{Eq. 16})$$

Usually, the iteration converges after few steps yielding α which is the nadir angle of the apparent direction to P_w as seen from P_0 .

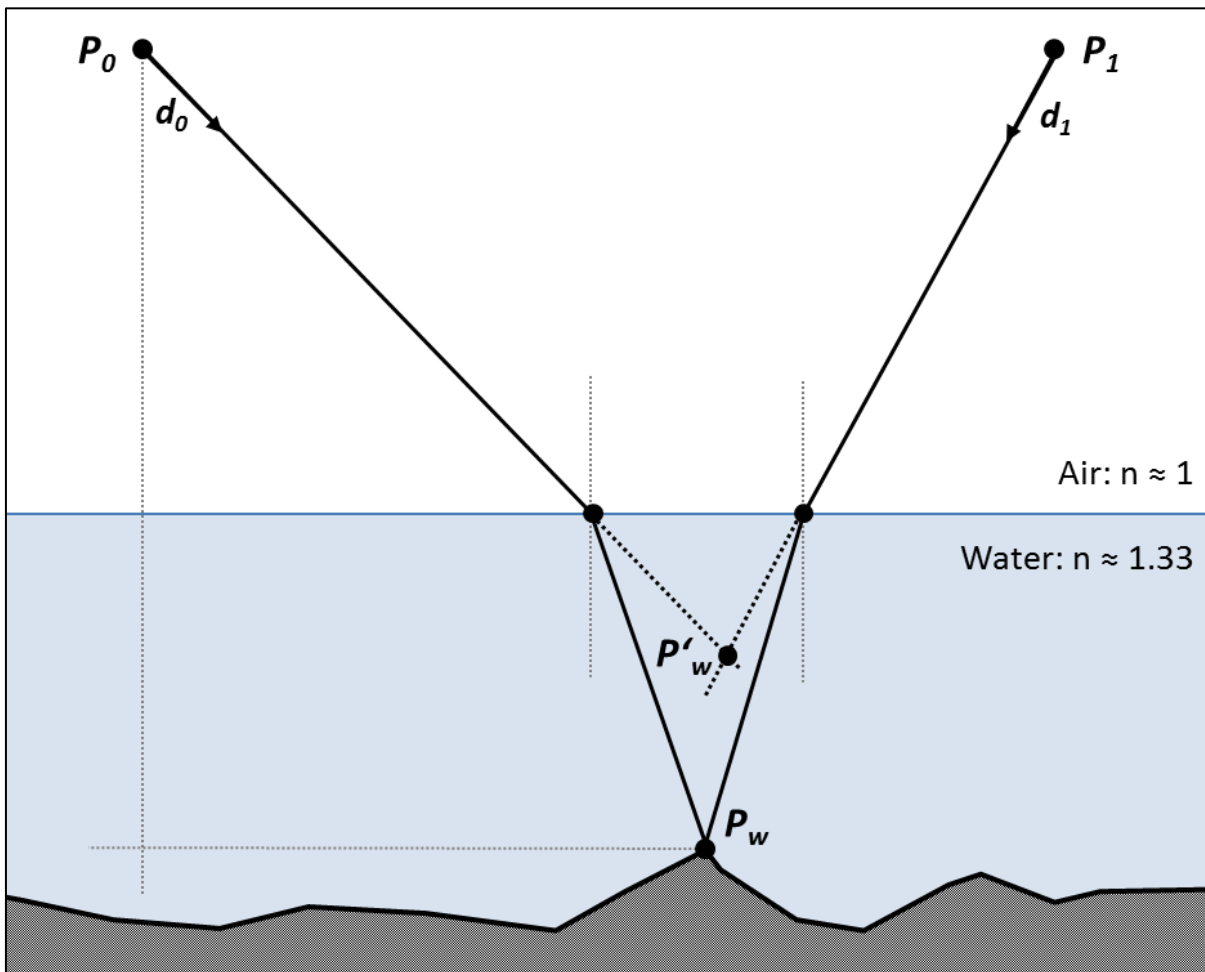


Figure 16: Effect of light refraction on photogrammetric point determination.

Under the premise of a horizontal water surface, the azimuth ϕ is not changed by refraction and can be computed using the x and y coordinates of P_w and P_0 .

$$\varphi = \text{atan2}(y_w - y_0, x_w - x_0) \quad (\text{Eq. 17})$$

By these two angles, the apparent directional vector is defined:

$$\mathbf{d}_0 = [\sin \alpha \cdot \cos \varphi, \sin \alpha \cdot \sin \varphi, -\cos \alpha]^T \quad (\text{Eq. 18})$$

Introducing a second projection center \mathbf{P}_1 above the water surface (Figure 16), the corresponding apparent directional vector \mathbf{d}_1 to \mathbf{P}_w can be found following the same procedure as for \mathbf{d}_0 . Now the apparent object point \mathbf{P}_w' can be determined by solving

$$\mathbf{P}_0 + \rho \cdot \mathbf{d}_0 = \mathbf{P}_1 + \mu \cdot \mathbf{d}_1 \quad (\text{Eq. 19})$$

with parameters ρ and μ . In general, these two lines are skew and no strict solution exists for the equation. However, the over-determination of 3 equations for the three coordinates vs. 2 parameters can be used to find a close-by solution, i.e. the point where the two lines are closest to each other:

$$\mathbf{P}_0 + \rho \cdot \mathbf{d}_0 - \mathbf{P}_1 - \mu \cdot \mathbf{d}_1 = \mathbf{0} + \mathbf{v} \quad \mathbf{v}^T \cdot \mathbf{v} \rightarrow \min \quad (\text{Eq. 20})$$

The adjusted parameters $\hat{\rho}$ and $\hat{\mu}$ indicate the points on the two lines with the smallest distance in between. The apparent object point \mathbf{P}_w' is set in the middle between them:

$$\mathbf{P}_w' = \frac{1}{2} \cdot (\mathbf{P}_0 + \hat{\rho} \cdot \mathbf{d}_0 + \mathbf{P}_1 + \hat{\mu} \cdot \mathbf{d}_1) \quad (\text{Eq. 21})$$

Comparing this point with the real object point \mathbf{P}_w which is known in the simulation, the error introduced by refraction can be found.

In order to assess the spatial distribution of this error, an overlapping area of two images is simulated in Matlab [XXI]. Assuming a certain image constellation and a certain water depth, the height deviation caused by refraction is calculated for an arbitrary number of sample points distributed over the whole overlapping area. For the following example (Figures 17 & 18), a flying height $h = 600 \text{ m}$ and a constant water depth of $d = 1 \text{ m}$ is adopted. The radius of the red circles is scaled with the height error in the respective center points. The horizontal errors are at the order of mm or rarely cm and therefore do not appear in the plot.

Obviously, the error magnitude varies throughout the area depending on the geometric constellation of the projection centers and the target points. For a better quantitative comparison of these variations, the vertical error is plotted as a function of the x-coordinates, i.e. in lines orthogonal to the basis (Figure 18). One of the lines is placed directly in the middle between the two projection centers and one at the edge of the overlapping area. The plots show the error variability growing with the distance from the basis and when moving away from between the projection centers.

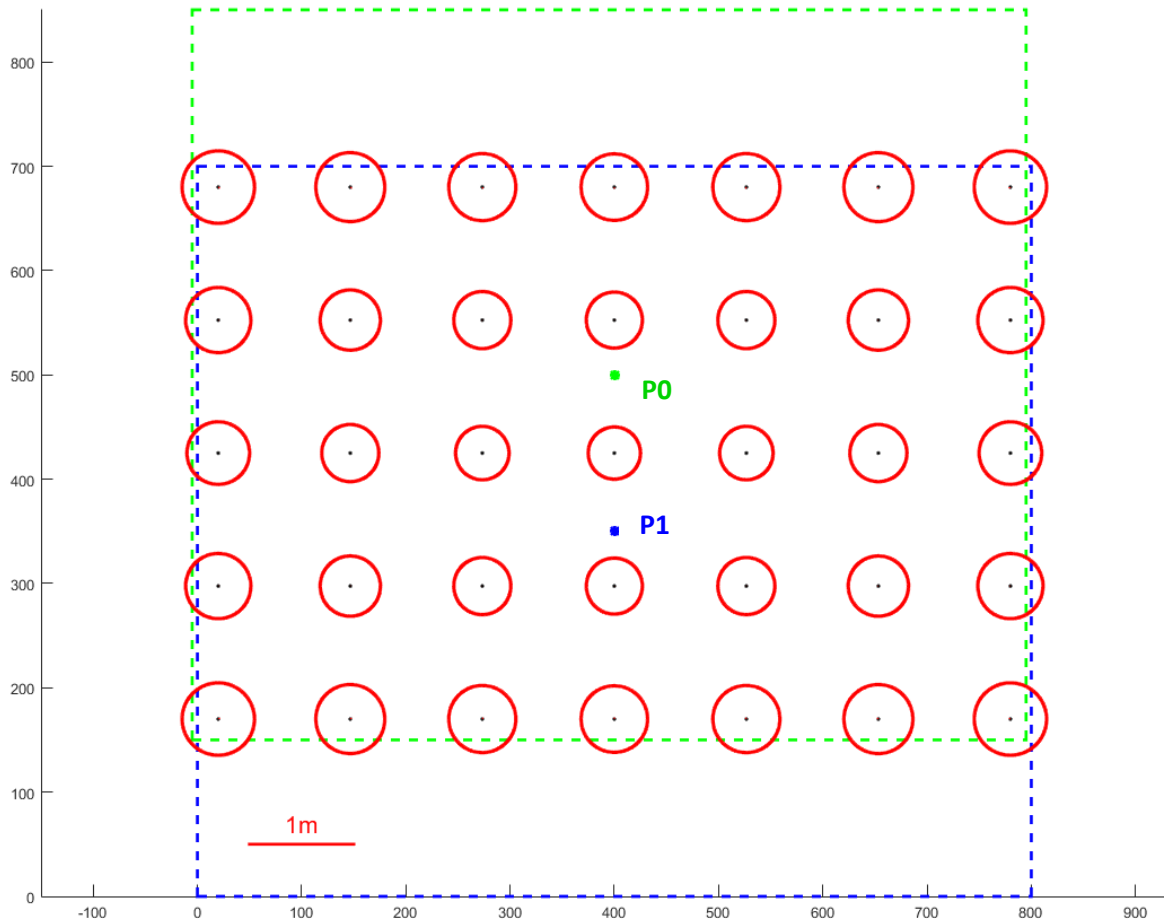


Figure 17: Plot of the refraction bias on photogrammetry as a function of image geometry. Unit is meters. In the overlapping area of two images (blue and green), the errors in point determination are plotted assuming a constant water depth of 1m. The radius of each circle corresponds to the height error determining the center point of the circle. The horizontal errors are too small to be visible in the plot.

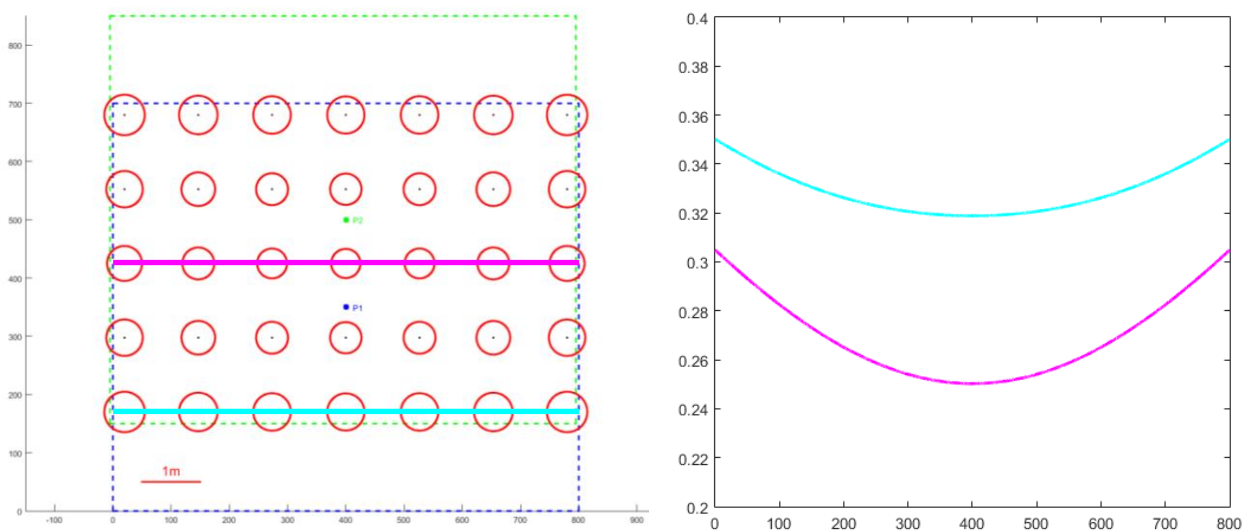


Figure 18: Height error through refraction plotted as a function of distance from the basis. The error is generally minimal in the center of the overlapping area and grows towards the edges. The unit of all axes is meters.

5.4 Refraction correction procedure

The theoretical simulations clearly show that a simple vertical scaling of the apparent depth cannot lead to satisfying results. Therefore, a correction procedure is needed which considers the geometric constellation. This was another reason why the image matching was performed pairwise as it is evident which projection centers are relevant for a particular point of the point cloud.

However, the described correction procedure is not limited to using only two different projection centers. It can handle an arbitrary number of involved images taking into account all relevant image rays. This means that image matching doesn't necessarily have to be carried out pairwise as long as there remains another way of determining which images were used for a certain point.

In the following, the correction procedure applied in the study at hand is described, i.e. assuming a point cloud resulting from pairwise image matching of images I_a and I_b with projection centers P_a and P_b . More or less, it corresponds to the workflow of theoretical error determination in reverse direction.

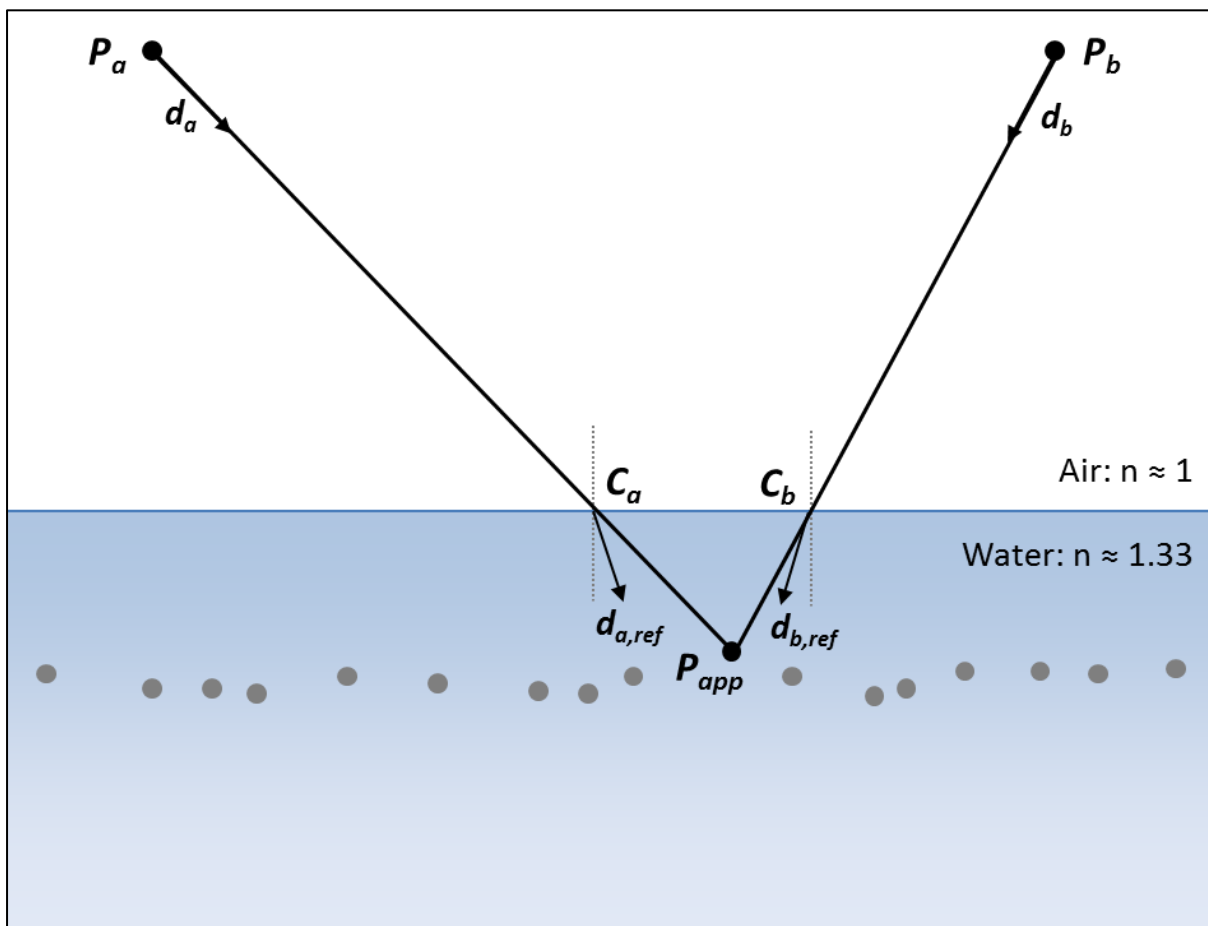


Figure 19: First part of the photogrammetric refraction correction. The uncorrected point cloud resulting from image matching is known as well as the projection centers P_a/P_b and the water surface. From the coordinates of one apparent point P_{app} , the apparent directional vectors d_a and d_b can be obtained.

The implementation was done in Matlab. The point clouds can be directly used in LAS format like they are provided by image matching software. For reading the LAS files, a tool by Teemu

Kumpumäki [X] was used. The image projection centers are directly read out of a PRJ file. Additionally, the water surface model has to be given as a TIF raster file.

Let the apparent point P_{app} be a point of the point cloud which lies under the water surface in a plausible range (apparent depth < 3 m). Since for the image matching, the two-media-problem has not been considered, simply connecting P_a and P_b to P_{app} and dividing by the length gives the apparent directional unit vectors d_a and d_b :

$$d_a = \frac{P_{app} - P_a}{|P_{app} - P_a|} \quad d_b = \frac{P_{app} - P_b}{|P_{app} - P_b|} \quad (\text{Eq. 22})$$

Intersecting the lines $P_a + \rho \cdot d_a$ and $P_b + \mu \cdot d_b$ with the water surface gives the points C_a and C_b . Based on the directional vectors d_a and d_b above the water surface, the refracted directional vectors $d_{a,ref}$ and $d_{b,ref}$ under water are derived using Snell's law (Figure 19).

Now, the apparent point P_{app} can be replaced by the corrected point P_{corr} which is obtained by "intersecting" two skew lines:

$$C_a + \rho \cdot d_{a,ref} = C_b + \mu \cdot d_{b,ref} \quad (\text{Eq. 23})$$

The best solution is again the point where the two lines are closest to each other as calculated in Eqs. 19 & 20.

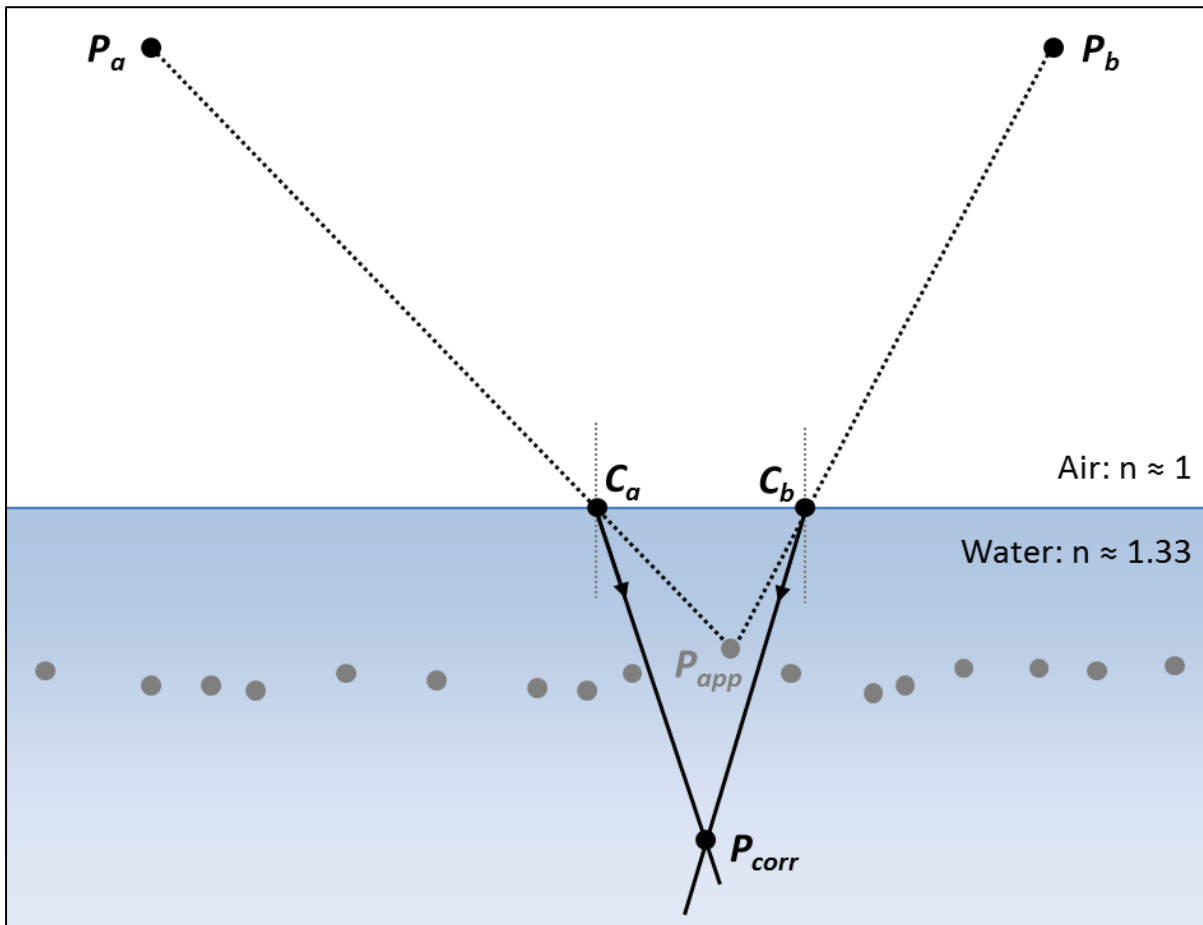


Figure 20: Second part of the correction procedure. The biased apparent terrain point P_{app} is replaced by refraction corrected terrain point P_{corr}

A short remark on the treatment of the water surface model given as a raster file: The simplest approach is to use nearest neighbor interpolation where the height for each raster cell is assumed to be constant. This is the fastest method but results in a discontinuous surface. Another possibility is to apply bi-linear interpolation within a grid cell using the four corner points to determine the parameters a , b , c and d :

$$z = a + bx + cy + dxy \quad (\text{Eq. 24})$$

However, when intersecting a line with the usually rather smooth water surface, the points resulting from the two different surface representations differ at the order of mm or smaller. This is far below the expected water surface accuracy and therefore it was decided that the much faster nearest neighbor approach is sufficient.

5.5 Interpolation and combination of height models

Once the point clouds of all image pairs are corrected for the systematic refraction effect, they can finally be recombined. Point cloud processing again was performed with the program system *OPALS*.

The first step is to interpolate a raster model for the corrected point cloud of each image pair with a minimal amount of smoothing in order not to eliminate fine structures and sharp edges. Therefore, a moving Planes interpolation as offered by *OPALS Module Grid* was used limiting the number of neighbors to 4 and selecting them quadrant-wise. With the given point density, a grid size of 0.5 m brought the best interpolation results.

Having applied both matching strategies, *Match-T* data now offer direct comparison of feature-based and cost-based matching in the river bed (Figures 21 & 22). The former looks more incomplete lacking coverage in larger areas. The covered areas show a noisy appearance but the existing data seem to be less prone to artifacts. On the other hand, cost-based matching achieves nearly full coverage except for the ponds in the north-east of the scene and around vegetation. In the slightly tilted, plain meadows north of the river, the fringes occurring with cost-based matching can be observed.

In the face of the interpolated grids, it seems reasonable to combine the different raster models in a robust way. This is accomplished by taking the Median of all overlapping rasters. For *Match-T* data, the models acquired from the two different matching strategies are used equally.

Results for both matching programs, *SURE* and *Match-T* are provided and compared in Chapter 6.

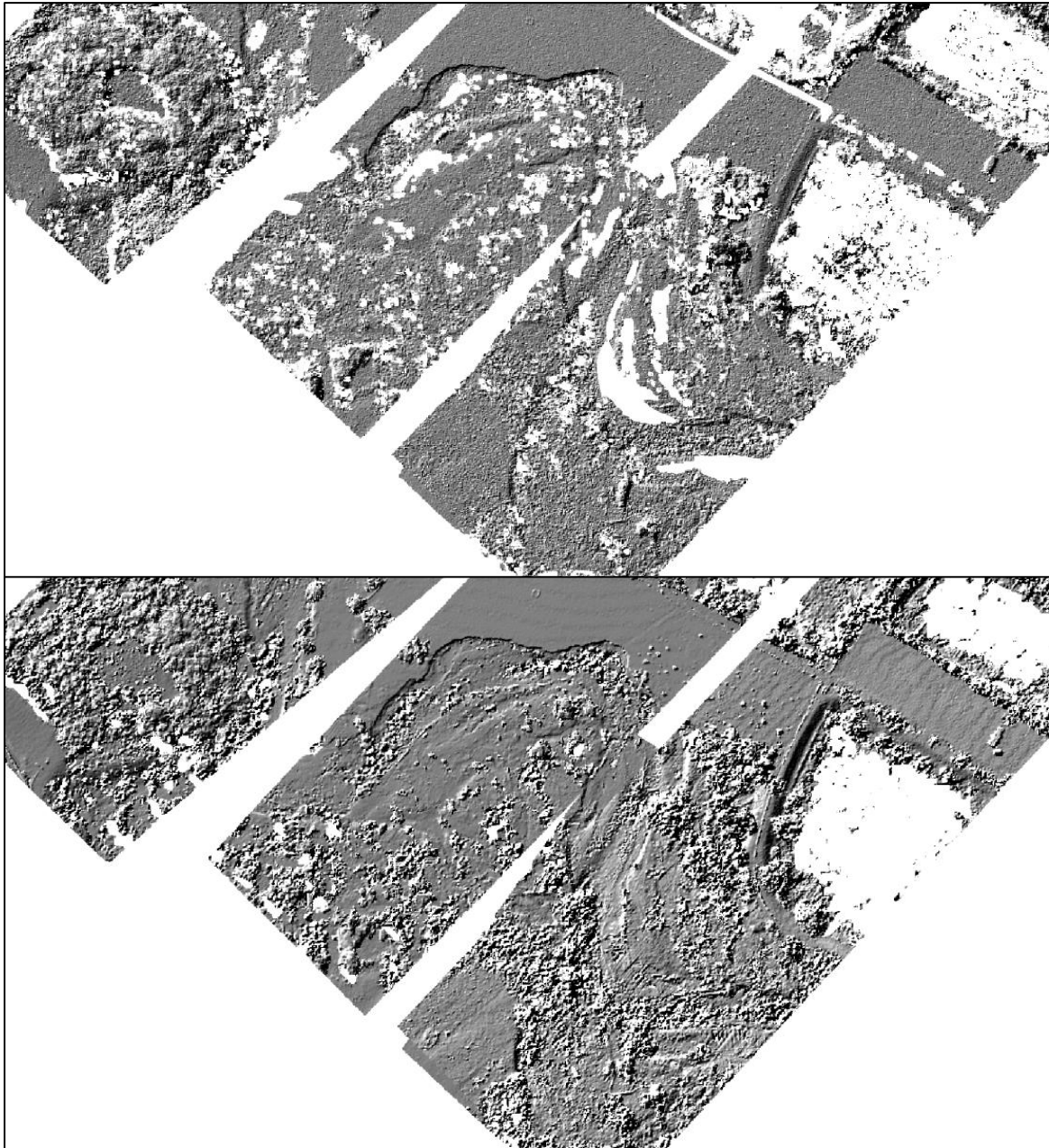


Figure 21: Pairwise interpolations of the point clouds resulting from feature-based matching (FBM, above) and cost-based matching (CBM, below).

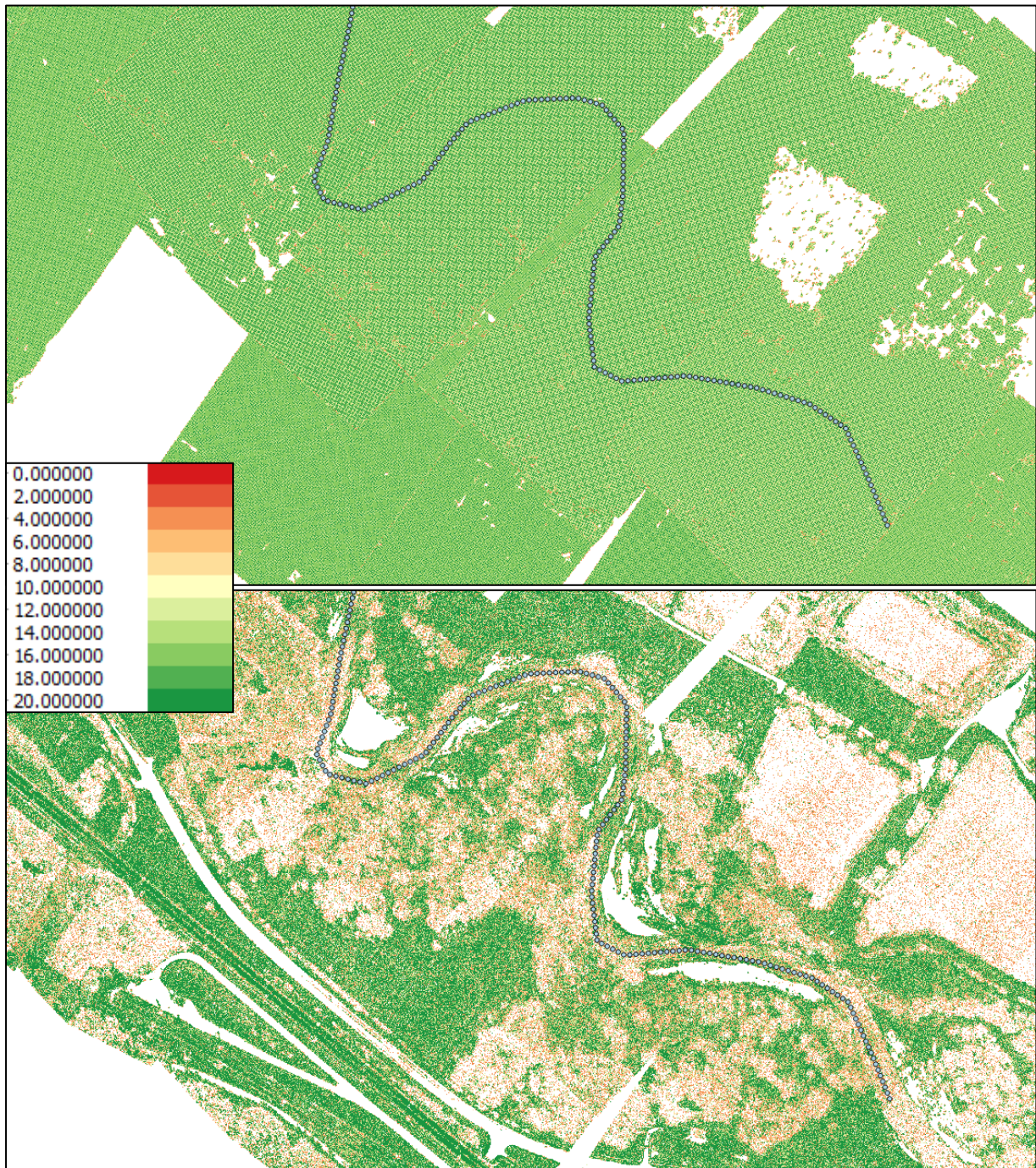


Figure 22: Comparison of the point densities resulting from CBM (above) which is nearly terrain-independent and FBM (below) showing variations associated with land cover types: Practically no matched points are present on the gravel banks around the river and on roads due to the overexposure of these bright surfaces (c.f. Figure 43). But also the river bed shows a smaller point density than the grasslands north of it.

6 Results and discussion

The result of both workflows, ALB and Photogrammetry, is a Digital Elevation Model (DEM) which is representing the terrain and the river bed in open areas. Limitations exist in the elimination of objects like vegetation or buildings. As long as no such objects obstruct the water body, this issue is not directly relevant for bathymetry, but as discussed in sections 1 and 2, one large advantage of both techniques is their ability to map submerged and dry terrain at the same time.

Therefore, the first part of the evaluation will focus on the quality of terrain mapping, before a closer look at bathymetry is taken.

6.1 Topographic mapping quality

For qualitative assessment of the terrain mapping capabilities, the final DEMs are compared to a DTM of “Sector East” obtained combining NIR Topographic Airborne Laser Scanning (ALS) and green ALB for the river course. The ALS flight took place at the end of February 2016 with a *Riegl LMS-Q1560* [XIX] scanner. A shading of the combined model is shown in Figure 23.

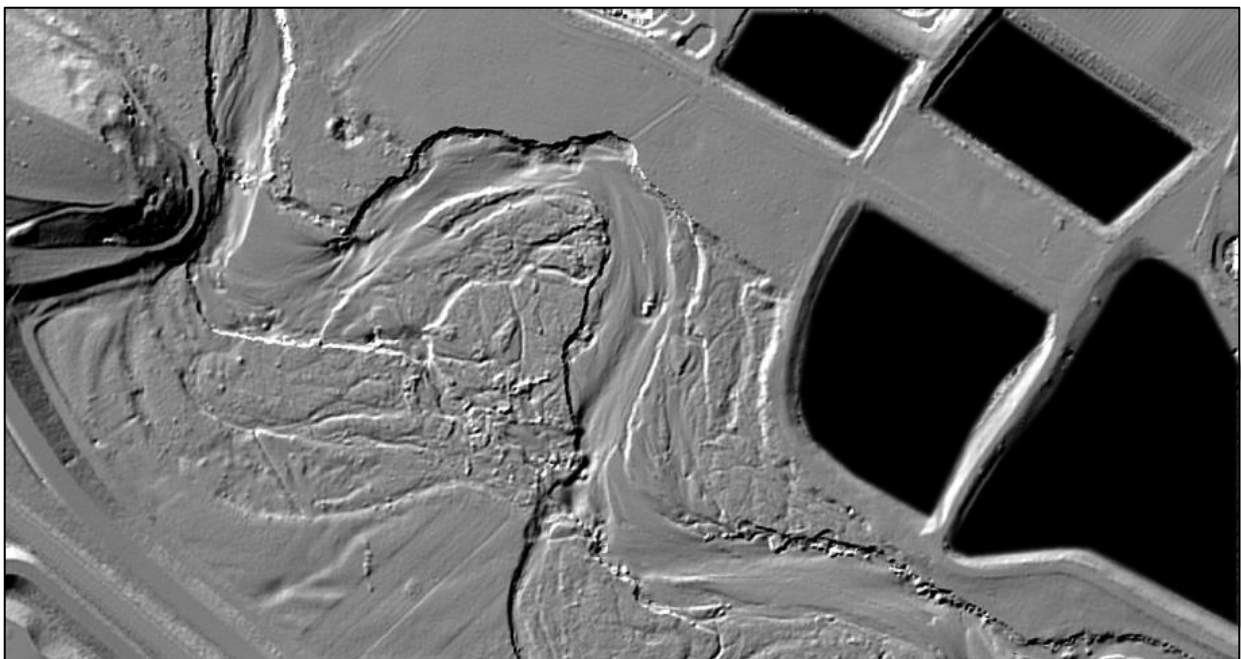


Figure 23: Digital Terrain Model (DTM) of Sector East derived from Topographic ALS and ALB. The ponds in the north-eastern part yield no meaningful height information and are therefore masked out.

Comparison to the ALB-only DTM (Figure 24) shows, that basically the two models have a similar appearance but do show differences when going into detail. Generally, a sharper representation of terrain edges is noticeable for the ALS data. A simple explanation therefore is the significantly smaller footprint of 15 cm compared to 60 cm for ALB (Mandlbürger et al., 2015c).

For the matter of completeness it is remarked that the most distinct edge (Detail *D1* in Figure 24) is not affected since it was conserved by introducing a breakline manually during DTM generation.

Another reason for the sharper edges of ALS data is the better penetration of vegetation as also stated in (Mandlbürger et al., 2015c). This results in a higher point density on the ground in

vegetated areas. For ALB, sporadically even in bushes or trees remain in the DTM – for example on the railroad embankment (D2). Possibly, also an explanation for the smoother appearance of grassland (D3) in the ALS DTM can be found in the better ability to penetrate through hassocks on the ground.

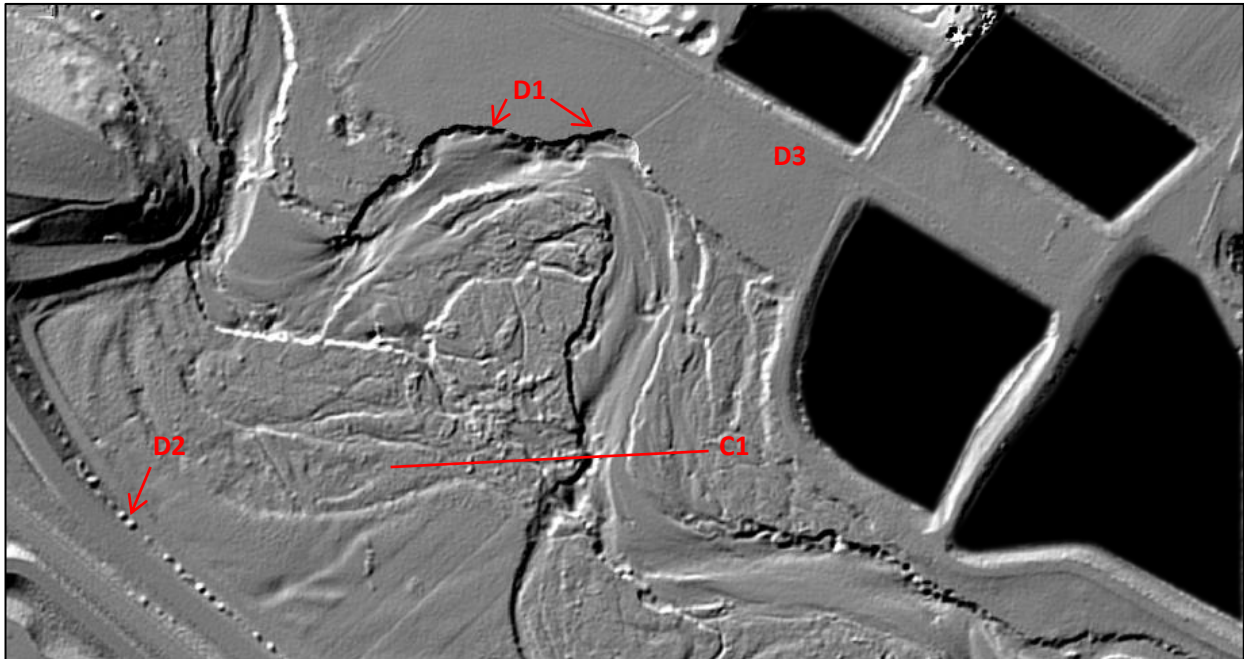


Figure 24: DTM of Sector East derived from ALB data. The main differences to the combined DTM are marked as details D1 – D3 and are described in the text.

Nevertheless, it also has to be mentioned that changing leaf conditions between the ALS data acquisition at the end of February and the ALB flight in April could have had an effect on the penetration properties. Overall, the deficits of ALB terrain representation w.r.t. ALS are rather small in this case study. There usually remain enough ground echoes to enable good terrain representation under vegetation as well as under water. This is emphasized by the cross section C1 visualized in Figure 25.

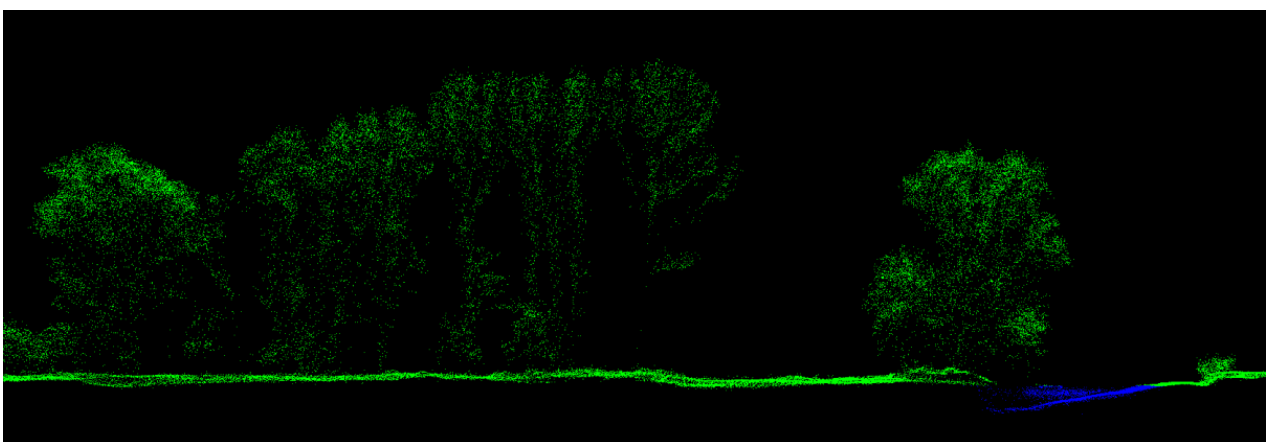


Figure 25: Cross Section C1 through the ALB point cloud. Green points represent “dry” objects, water points including surface, volume and ground echoes are blue. Even though the terrain point density decreases under the dense tree on the left, there remain enough points for terrain modeling with hierarchical robust interpolation.

Much clearer differences than between ALB and ALS can be identified for the photogrammetric DEMs (Figures 27 & 28). Whereas active laser sensors operating on the time-of-flight principle usually allow capturing multiple echoes (i.e. individual targets like vegetation, water surface, river bed) for a single laser the reflections from different targets are combined to undifferentiated mixed pixels in images. As soon as vegetation is dense enough to avoid clear sight to the ground, no terrain points can be reconstructed any more. Figure 26 shows an exemplary detail of a SURE point cloud as a cross section and in 3D. In contrast to the ALB point cloud it is clearly visible that only very few terrain points are present under the group of bushes.

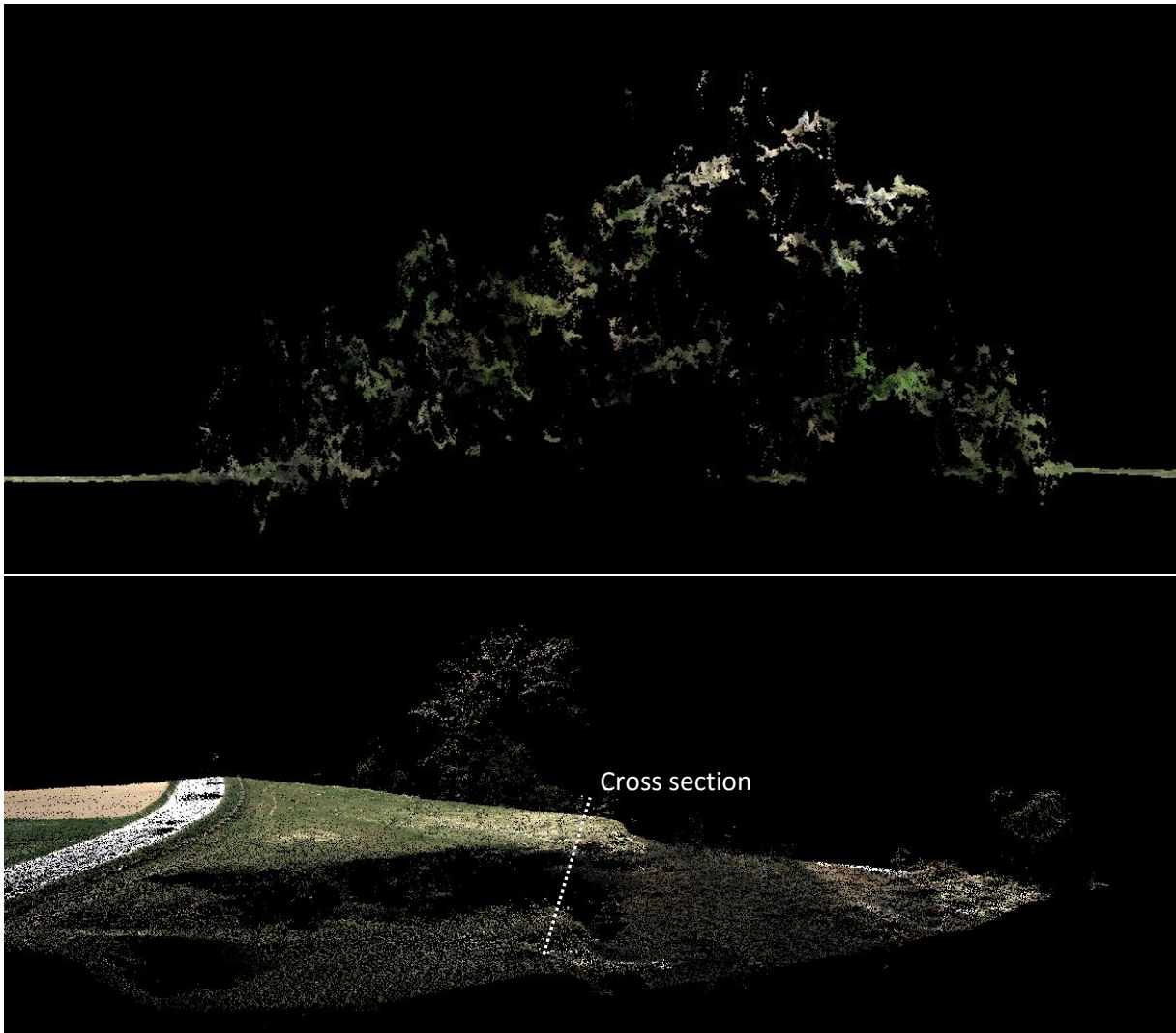


Figure 26: Visualization of a point cloud resulting from SURE image matching. The cross section above as well as the 3D view of the same group of trees and bushes show that there are hardly any points representing terrain under the vegetation.

Overcoming this problem by robust hierarchical interpolation is hindered by the fact that outliers in photogrammetry are not mostly above terrain but also below – especially for the water course (c.f. cross sections in Figures 12 & 26). This causes large-scale interpolation errors in vegetated areas and notably also in the river bed due to the stronger weighting of possibly erroneously low points. Therefore, the height model derived from SURE image matching (Figure 27) more has the

characteristics of a DSM than of a DTM. Most of the objects standing on the ground are still present, especially large parts of vegetation cover.

Another obvious peculiarity of *cost-based matching (CBM)* has already been mentioned in Section 5.5 for *Match-T*. It is the representation of smooth, slightly tilted terrain like it appears north of the river and between the ponds in the East. Instead of a continuous surface, the height model rather gives the impression of terraces (Figure 27).

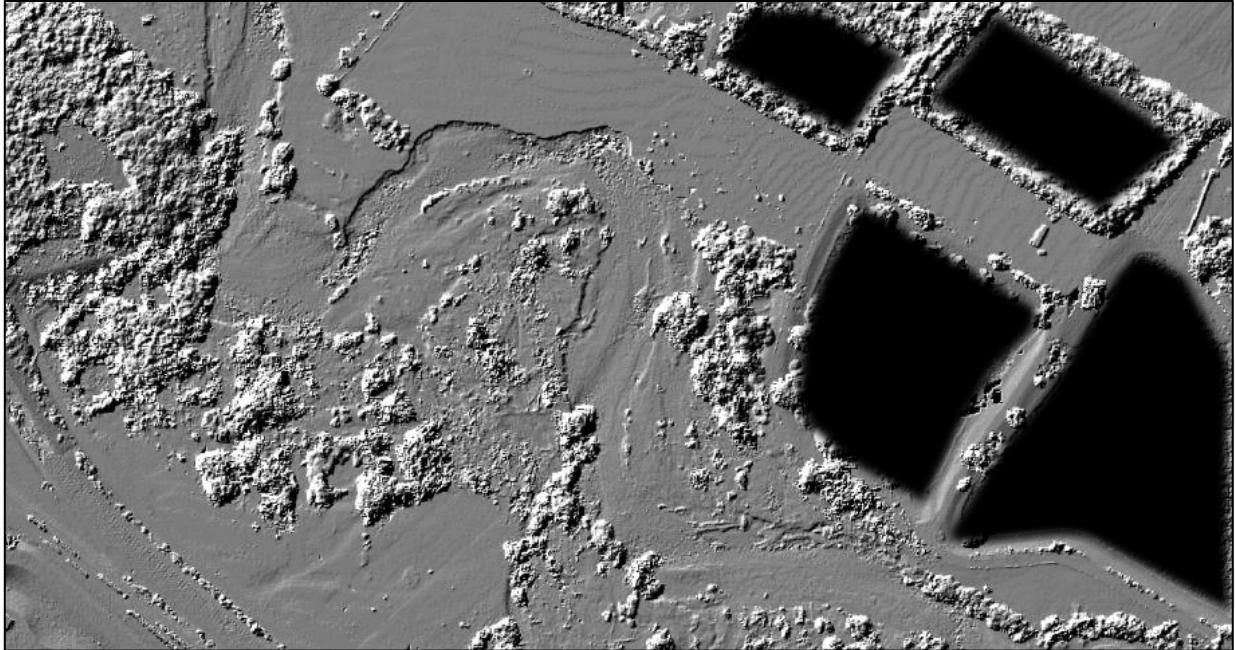


Figure 27: Height model from SURE image matching.

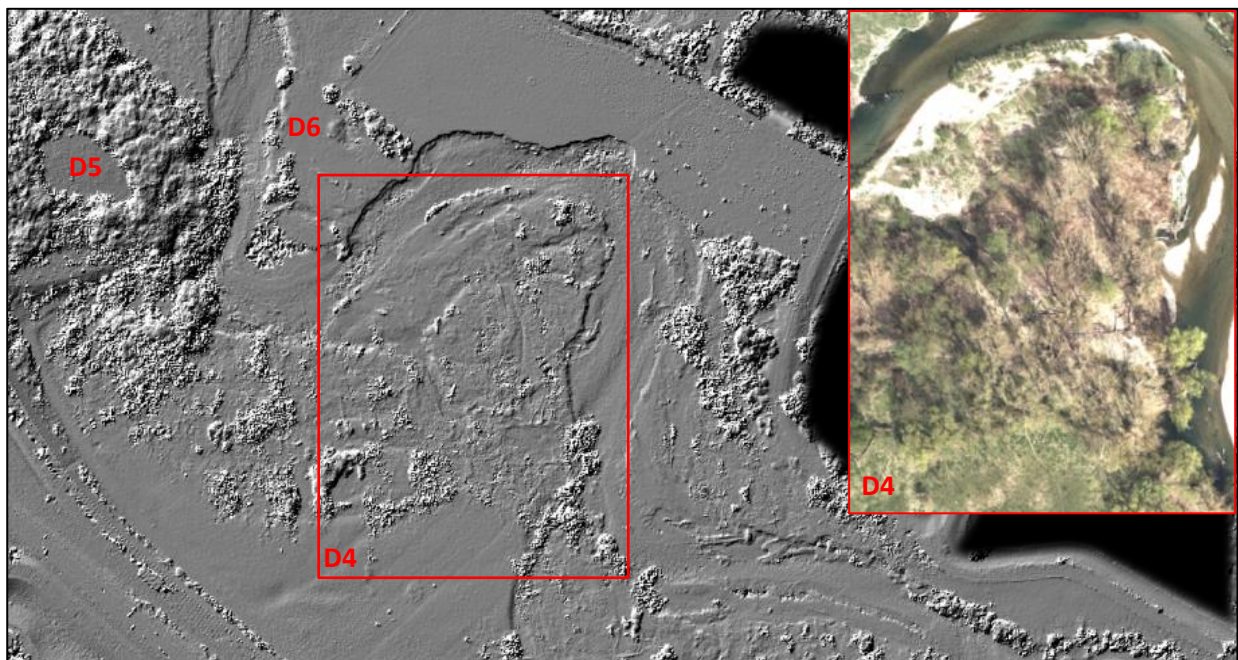


Figure 28: Height model from Match-T image matching compared to an aerial image of the respective area.

A certain improvement of the described deviations from a DTM can be observed in the height model derived from *Match-T* image matching (Figure 28). In area *D4*, where predominantly rather bald single trees are present with smaller areal extents, terrain is modeled very well albeit not all relief

features are as distinct as in the Laser Scanning DTMs. The most likely explanation for these better results is in the combination of *CBM* with *FBM* which detects predominantly terrain points. However, the extensive dense vegetation around *D5* can't be eliminated either since even *FBM* only detects canopy points there (c.f. Figure 21).

Another advantage of the *Match-T* height model is the nearly complete elimination of the fringes on plain surfaces – a noteworthy drawback is the handling of overexposed gravel banks (*D6*) which will be discussed in section 6.5.

6.2 Water Surface Model (DWM)

In the absence of independent water surface measurements (e.g. from terrestrial survey or from ALS) a quantitative accuracy assessment is not possible. The reader is therefore referred to the respective literature (Mandlbürger et al., 2015b; Mandlbürger et al., 2015c). However, the quality of the refraction correction can also be an indicator for DWM quality (c.f. sections 6.3 & 6.5).

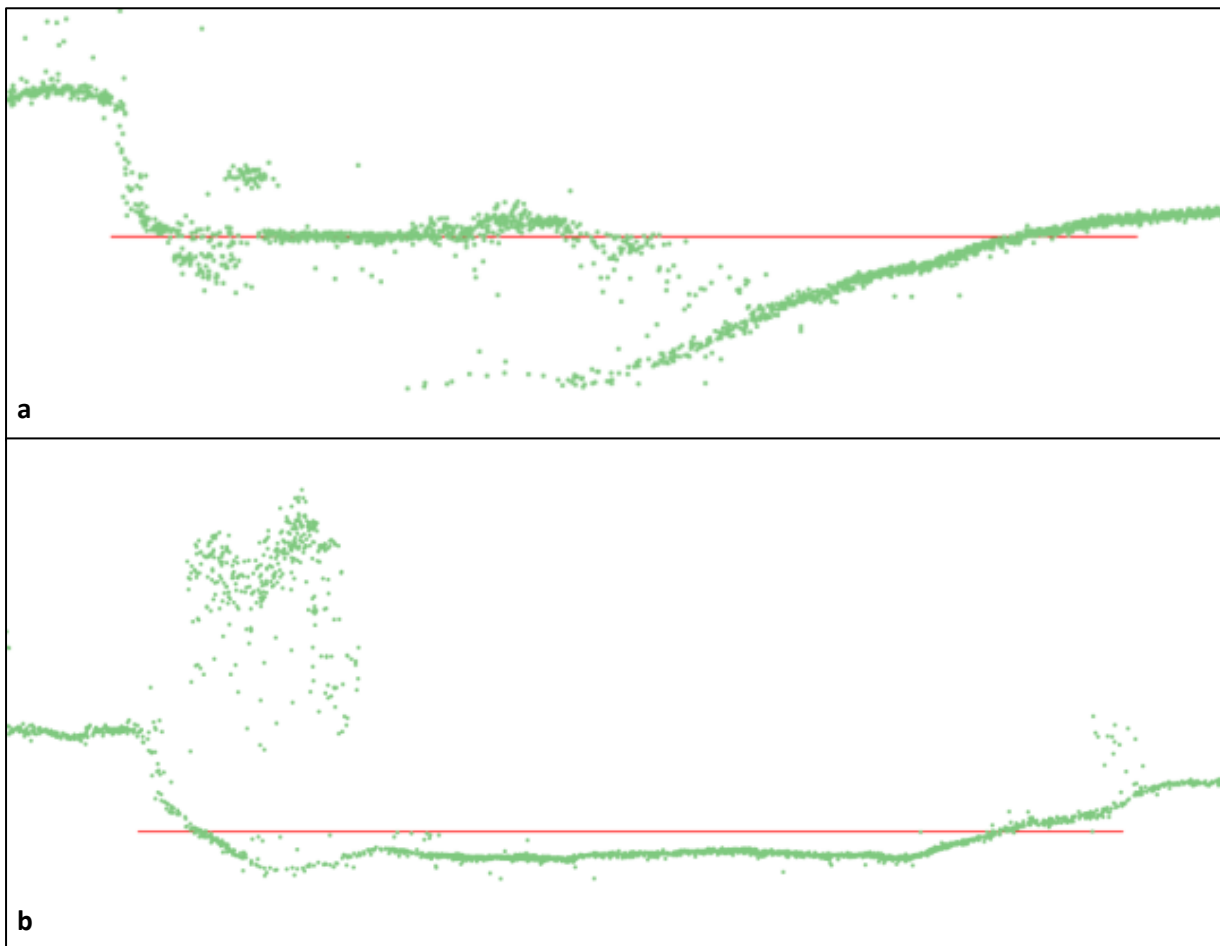


Figure 29: Two challenging cross sections in terms of water surface determination. Wood floating on the surface yields echoes slightly higher than the water surface (a). Though it is obvious in this case, smaller reflecting objects which cannot be distinguished from water echoes can introduce errors to the DWM. Shallow water typically exhibits few echoes from the water body (b).

Analyzing the general feasibility, Figure 8 is an example where it seems very likely that a good water surface estimation has been found. Experience shows that this is very often the case for deeper

water leading to many echoes from volume scattering also near the surface. For very shallow river runs (Figure 29 b), the water level estimation becomes considerably more difficult with very few echoes from the water body. Especially very shallow water often makes it necessary to interpolate over large measurement gaps. Another potential difficulty comes from objects like driftwood grounded in the sediment and protruding above the water line (Figure 29 a). There, the highest reflecting points eventually are above water.

One crucial assumption for the utilized method was the horizontal shape of the water surface perpendicular to the river axis. The specular water surface reflections obtained in Sector West offer the possibility to inspect the validity of this assumption.

As described in section 4.4, the final DWM was determined in two steps there. First, the semi-automatic procedure relying on cross section measurements was applied. Based on the resulting first model herein called DWM_{approx} , the point cloud was filtered to eliminate all points not belonging to the water surface. This is valid since there appears hardly any volume scattering under near nadir specular surface reflections (Figure 30).

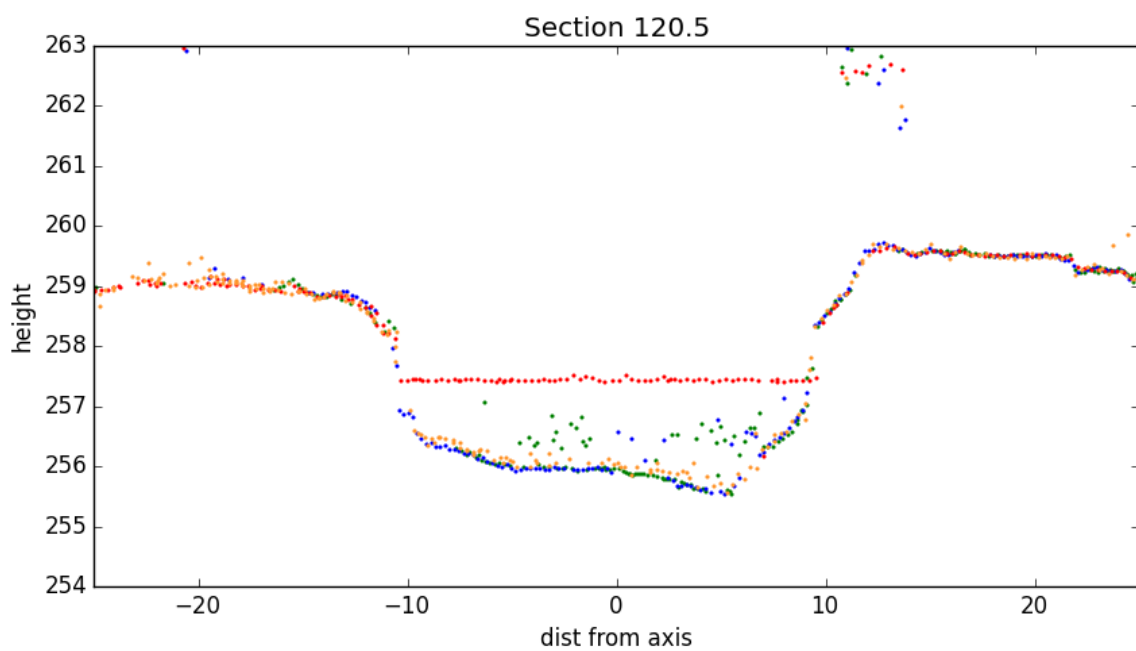


Figure 30: Cross section in Sector West. The forward-looking echoes of the descending strip (red) show a dense representation of the water surface but hardly any points in the submerged area. On the other hand, the backward-looking echoes of the same strip (yellow) as well as the points of a regular flight strip (blue, green) contain information about the river bed but lack echoes from the surface or slightly below.

From the filtered point cloud, the water surface is then interpolated again giving another estimation which is free from the constraint of horizontal cross sections. Comparing the interpolated DWM_{final} to DWM_{approx} gives insights to what extent the basic assumptions hold in practice. A difference of these two models is shown in Figure 31a.

First of all, the difference map shows nearly exclusively negative differences (i.e. DWM_{approx} is higher than DWM_{final}). The reason for this bias is very likely related to wrong assumptions during manual measurements. The usual predominance of volume scattering over surface scattering gives reason

for a tendency to be geared to the highest points which are likely to be water echoes. In the special case of specular reflections nearly exclusive coming directly from the water surface, this strategy leads to an overestimation of the DWM height.

Another theoretically more relevant finding concerns the assumptions of horizontal water surface perpendicular to the river axis. For most cross sections, the deviation is small at the order of few centimeters reaching up to >5 cm in some places. For example, the Section enlarged in Figure 31 b-d shows a very clear gradient between the right and the left bank of the river which of course could not be adequately represented by DWM_{approx} . The different lateral extents of DWM_{approx} and DWM_{final} appear due to the fact that cross section measurements are conducted in a way that the DWM slightly 'cuts' into the river bank, whereas the interpolation of actual surface echoes only extends as far as those surface echoes exist.

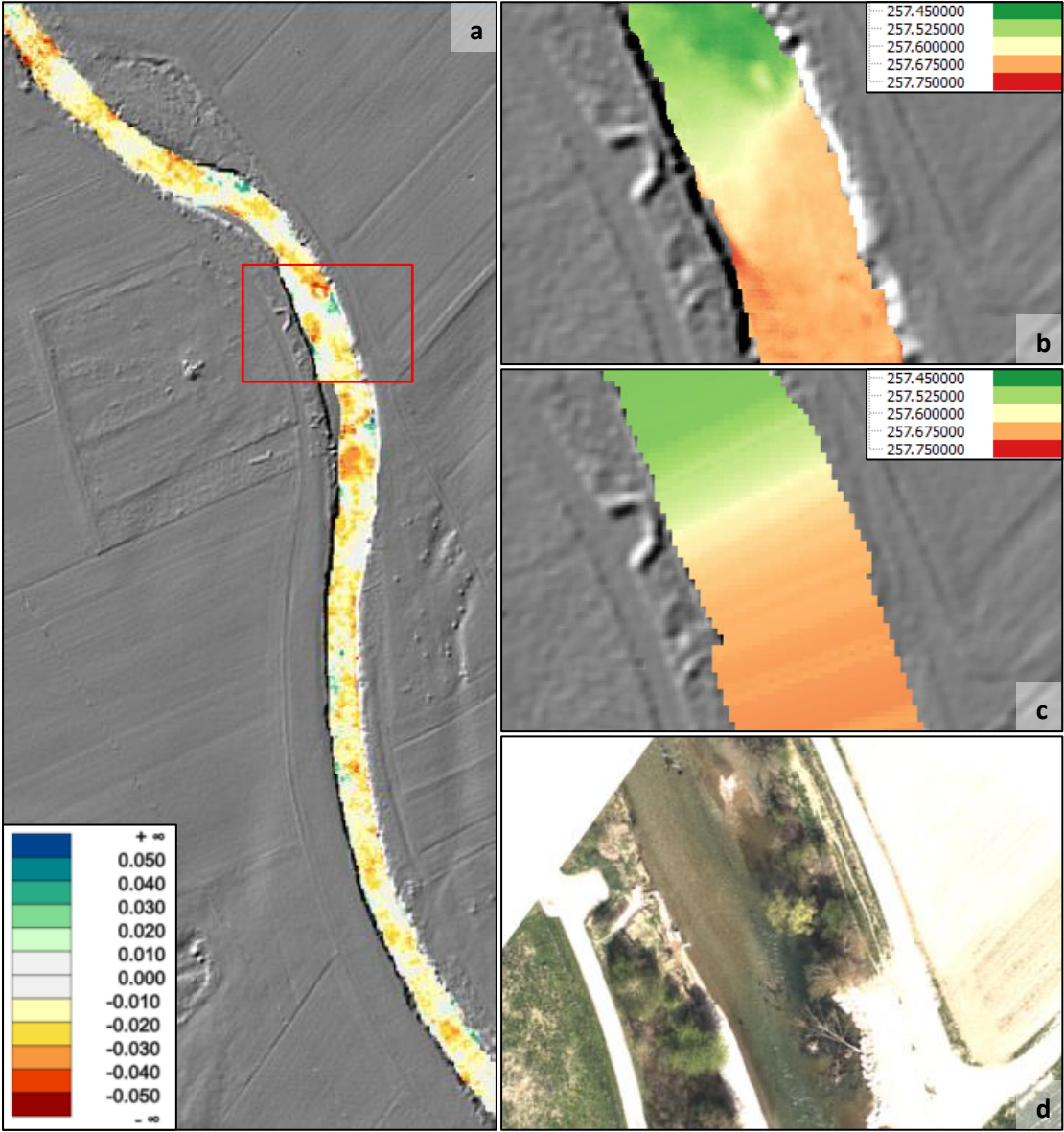


Figure 31: Difference $DWM_{final} - DWM_{approx}$ in Sector East (a), Z-Coding of a smaller section for both, DWM_{final} interpolated from surface echoes (b) and DWM_{approx} clearly showing the cross-sectional structure (c). (d) shows the aerial image of the respective section.

Keeping in mind that the bias introduced to the refraction correction procedure by DWM errors amounts to approximately 1/3 of this error, the impact of ignoring differences in water surface height within one perpendicular cross section can be expected to remain mostly below the laser ranging accuracy of 25 mm.

Despite the revealed advantages for water surface determination, near nadir laser bathymetry is of course not possible. As illustrated in Figure 30, the specular surface reflections come at the cost of hardly any information on the river bed.

6.3 Refraction correction

Photogrammetry and ALB rely on two basically different measurement principles. Hence, the respective refraction correction procedures have dissimilar characteristics as well. As already anticipated in Sections 4.5 and 5.4, even the vertical directions of these corrections are diametrical.

Whereas the dependence on light velocity causes uncorrected ALB models to overestimate depth, Photogrammetric mapping yields systematically too shallow river beds. In other words, the difference “corrected depth” minus “uncorrected depth” is negative for ALB and positive for Photogrammetry or vice versa for the respective height model (Figures 32 & 37).

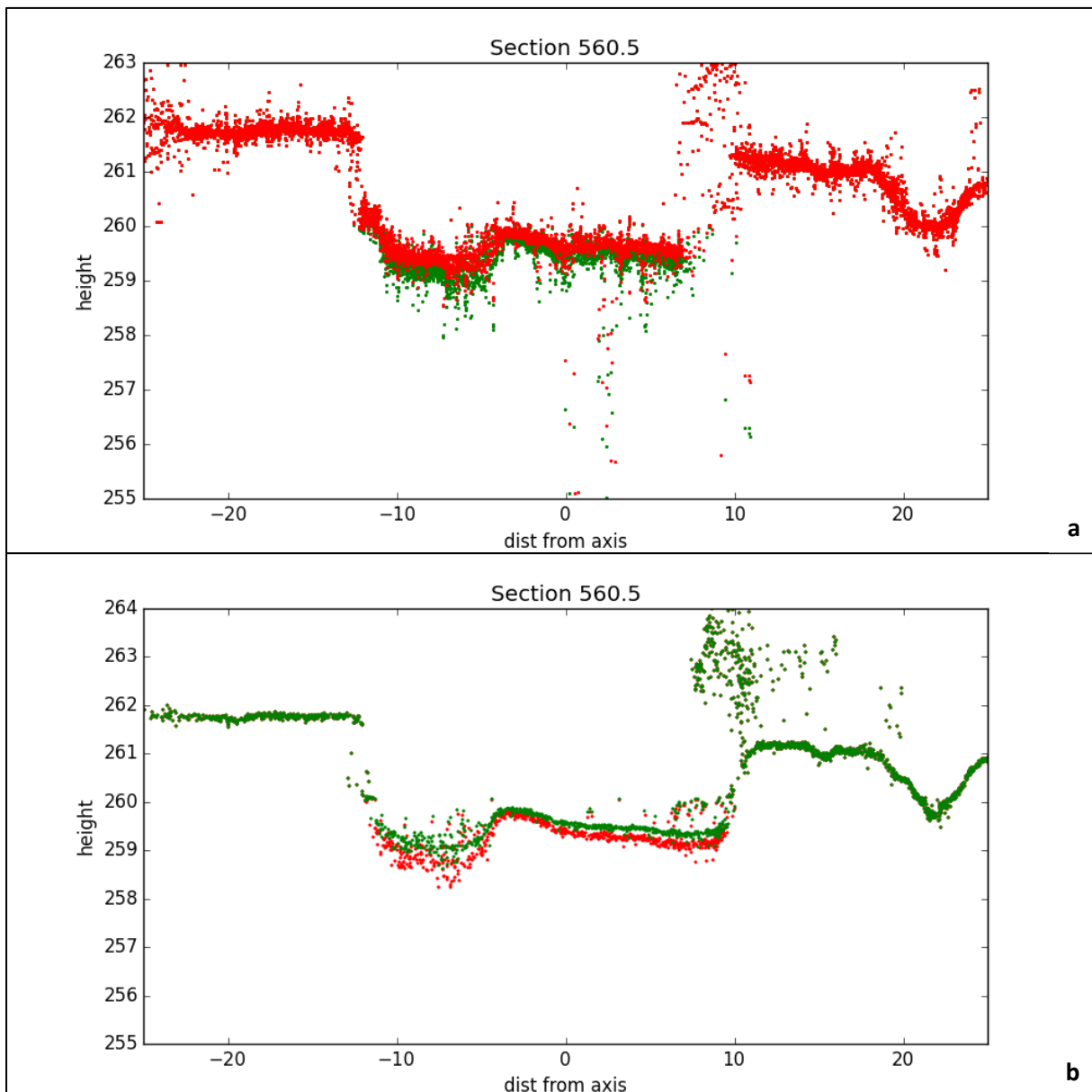


Figure 32: Uncorrected (red) and corrected (green) point cloud of a river cross section. For the photogrammetric point cloud from Match-T (a), the corrected river bed is deeper than the uncorrected one in contrast to the ALB point cloud (b). Remark: The coloring of (a) with the red points in front was chosen for reasons of perceptivity and has no further meaning.

6.4 Water Depth Model

6.4.1 Sector East

In the height models compared in Section 6.1, the final *Digital Terrain Model of the Watercourse (DTM-W)* was already included without detailed comment. For the further qualitative and quantitative discussion, a water depth model is derived by subtracting the DTM-W from the water surface model. The resulting depth map facilitates visual comparison between the different presented methods. In the following figures 33-36, the *DTM-W* overlaid with a depth model is presented and compared for *ALB*, *SURE* and *Match-T*; discussion of the results follows in Section 6.5.

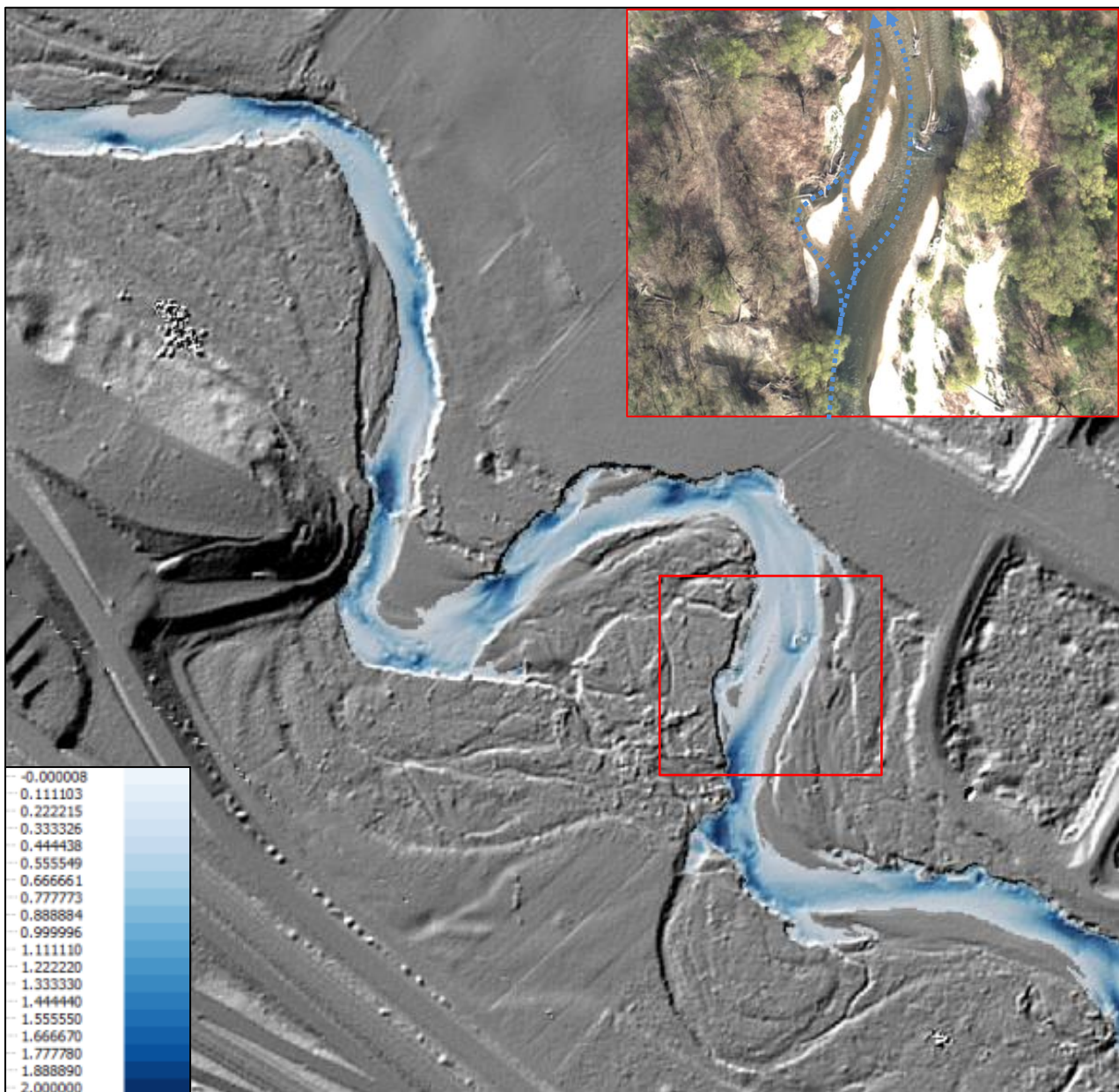


Figure 33: DTM and Water depth model for Sector East derived from ALB data compared to an aerial image of a rather critical section (red rectangle).

The ALB water depth model (Figure 33) has a very plausible appearance. In particular, when compared to the image overview in Figure 4 it can be stated that the aerial extent of the submerged river bed is very well represented with one exception marked in Figure 33: In this section, the river is very shallow and splits up to various channels of different slopes. However, when measuring the water surface for one cross section through the whole bed, a certain error is introduced. And even though the impact on refraction correction is rather small, cutting the “wrong” water surface with the smooth terrain results in significant differences concerning water body extent. Or in other words: The effects of a wrong water surface on the depth model extent are larger than on the depth values.

For Photogrammetric depth models, the deviations from reality are more obvious. Like already described in Section 6.1, overhanging trees hamper complete mapping of the river bed (Figure 34).

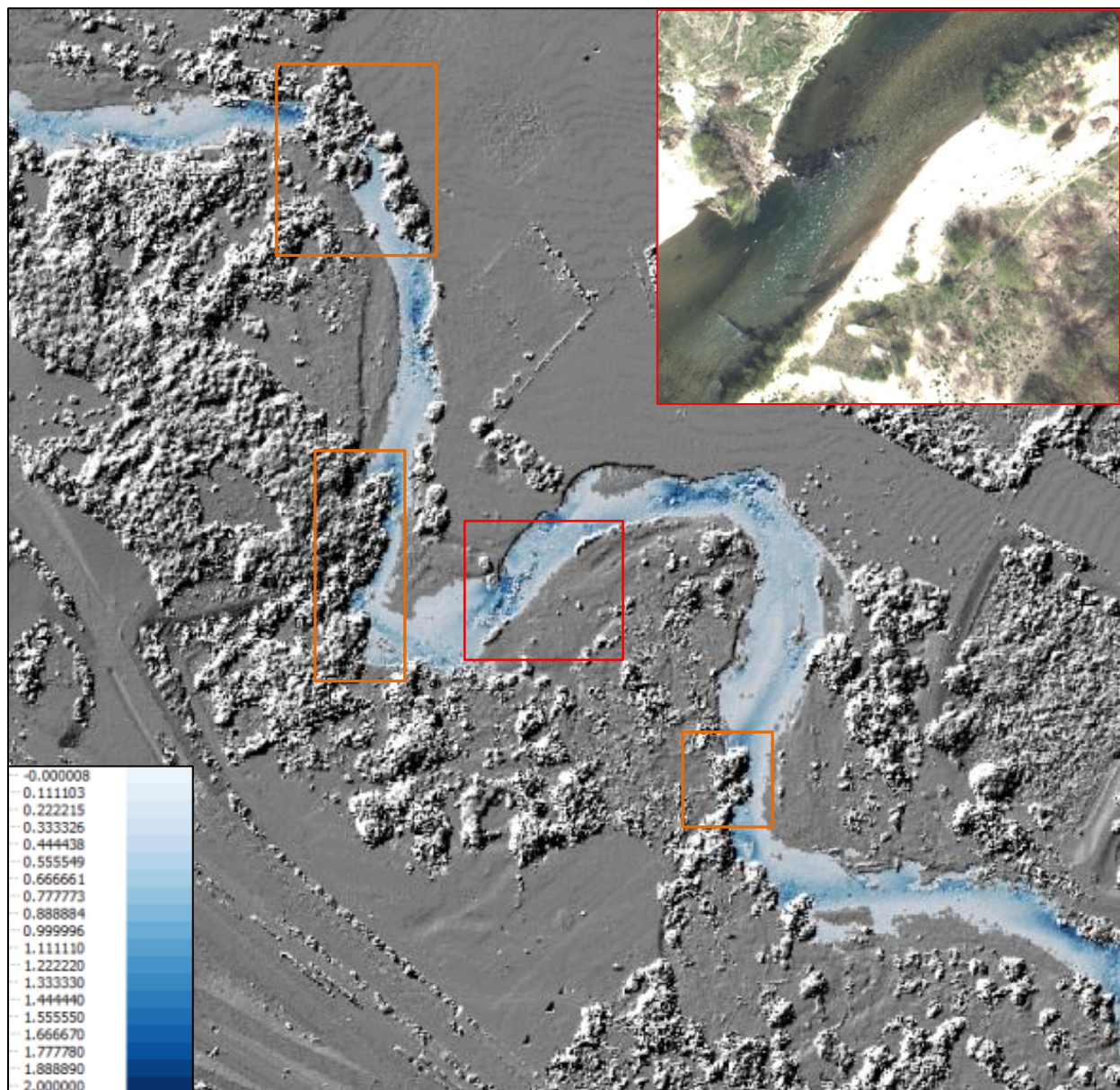


Figure 34: Height and water depth model derived from SURE image matching. Especially in the western part, overhanging trees cause gaps in the water depth model (c.f. the orange rectangles). The red marked section and the aerial image show the effects of sun glint obscuring information especially for deep, low-contrast river bed.

Apart from that, the main differences can be found in deeper pools with dark substrate and in areas of strong sun glint on the water surface where photogrammetry is partly incapable of determining meaningful correspondences. Unfortunately, most pools are overhung by trees disabling more universal analysis on the behavior of photogrammetry in deeper water. For the few available unobstructed pools, SURE data show a very noisy appearance where water the depth exceeds 1 m.

Compared to that, Match-T (Figure 35) shows a better ability of mapping pools and therefore also better correspondences with the *ALB* model. Nevertheless, the problem of overhanging trees remains unsolved.

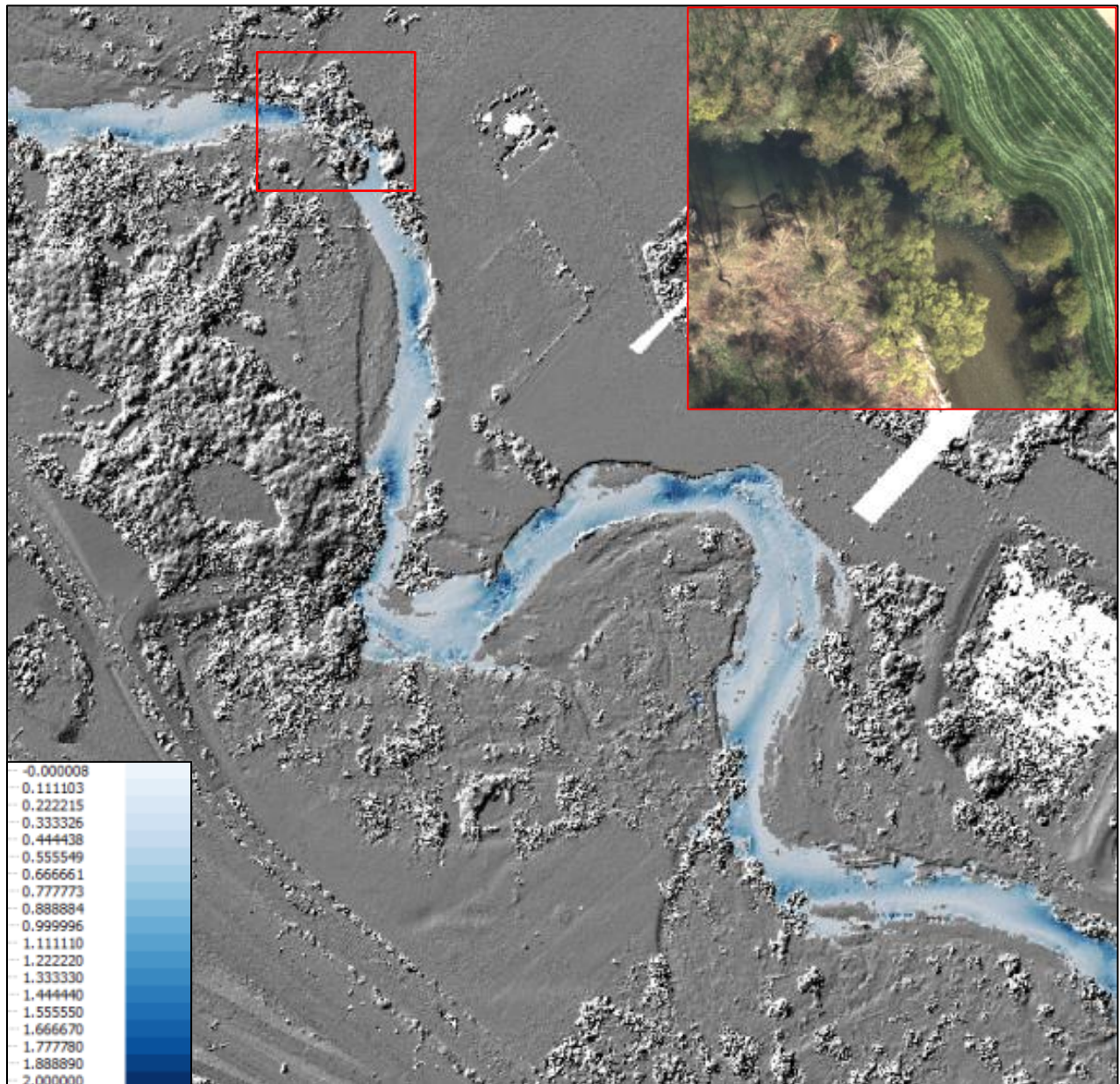


Figure 35: Match-T height and water depth model with an aerial image pointing out the impenetrability of vegetation when working with passive methods. Additionally, even though water is visible between the trees on the two river banks, the shadows avoid water depth reconstruction as well resulting in a complete gap within the water surface model.

6.4.2 Sector West

Coming to Sector West, the restrictions associated with photogrammetric water depth estimation become more obvious. Whereas ALB is still capable of providing a complete DTM-W, the numerous trees on the river banks hide the river bed and their shadows create artifacts in the depth model (detail D7 in Figure 36). Similar effects can also be observed due to a tree trunk lying in the river bed, as illustrated by detail D8.

However, it also has to be stated that, disregarding the shortcomings of the photogrammetric model in this sector, the areas of unimpeded sight on a constantly illuminated river bed show good correspondences between the two techniques. Nevertheless, the quantitative comparison of river bathymetric techniques in the next section will mainly focus on Sector East, where larger areas without large obvious discrepancies are given.

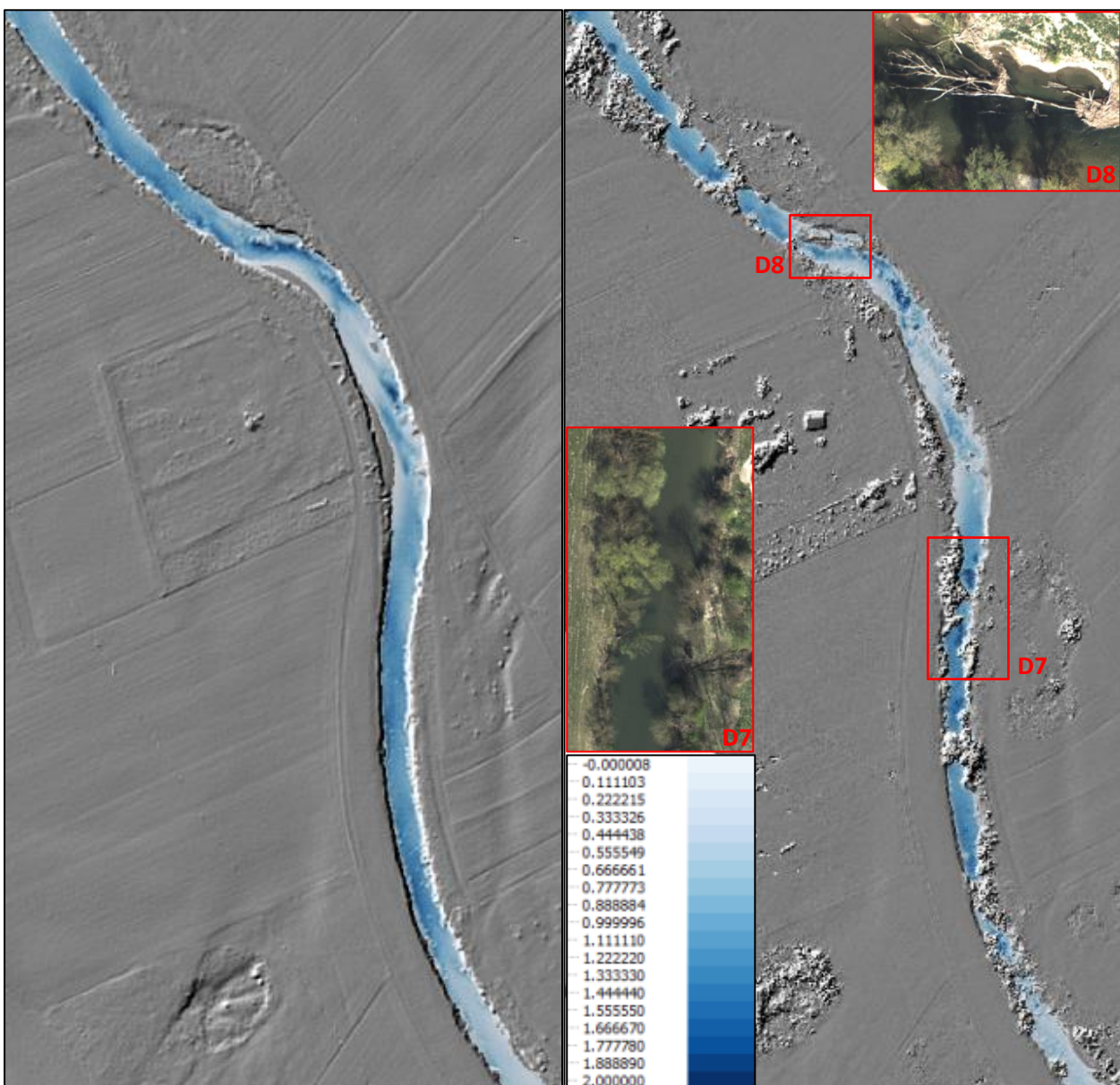


Figure 36: Water depth models from ALB (left) and from Match-T image matching (right). The problems in the latter associated with overhanging objects and shadowing is demonstrated in two detailed images.

6.5 Evaluation and direct comparison

Up to this point, the water depth models and other results have mainly been investigated qualitatively. In the light of the different characteristics of ALB and Photogrammetric data, emphasis thereby was on visual analysis of obvious large deviations. In this section, evaluation will go towards quantitative comparison in areas where no obvious grave deviations are present. The aim is to show whether or not the models from different techniques are consistent and in which order of magnitude the residuals lie.

As a matter of fact, this comparison is limited to the use of the presented models since no other independent reference data were obtained during the time of acquisition. Yet, there is a certain informative value in these comparisons due to the fact that the respective refraction correction for ALB and photogrammetry go in different directions (Section 6.3, Figure 37) making it unlikely to obtain coincidental agreement despite model errors. Furthermore, due to the high accuracy specified in (Mandlbürger et al., 2015b) and [V], ALB models can be regarded as a reference for photogrammetric ones.

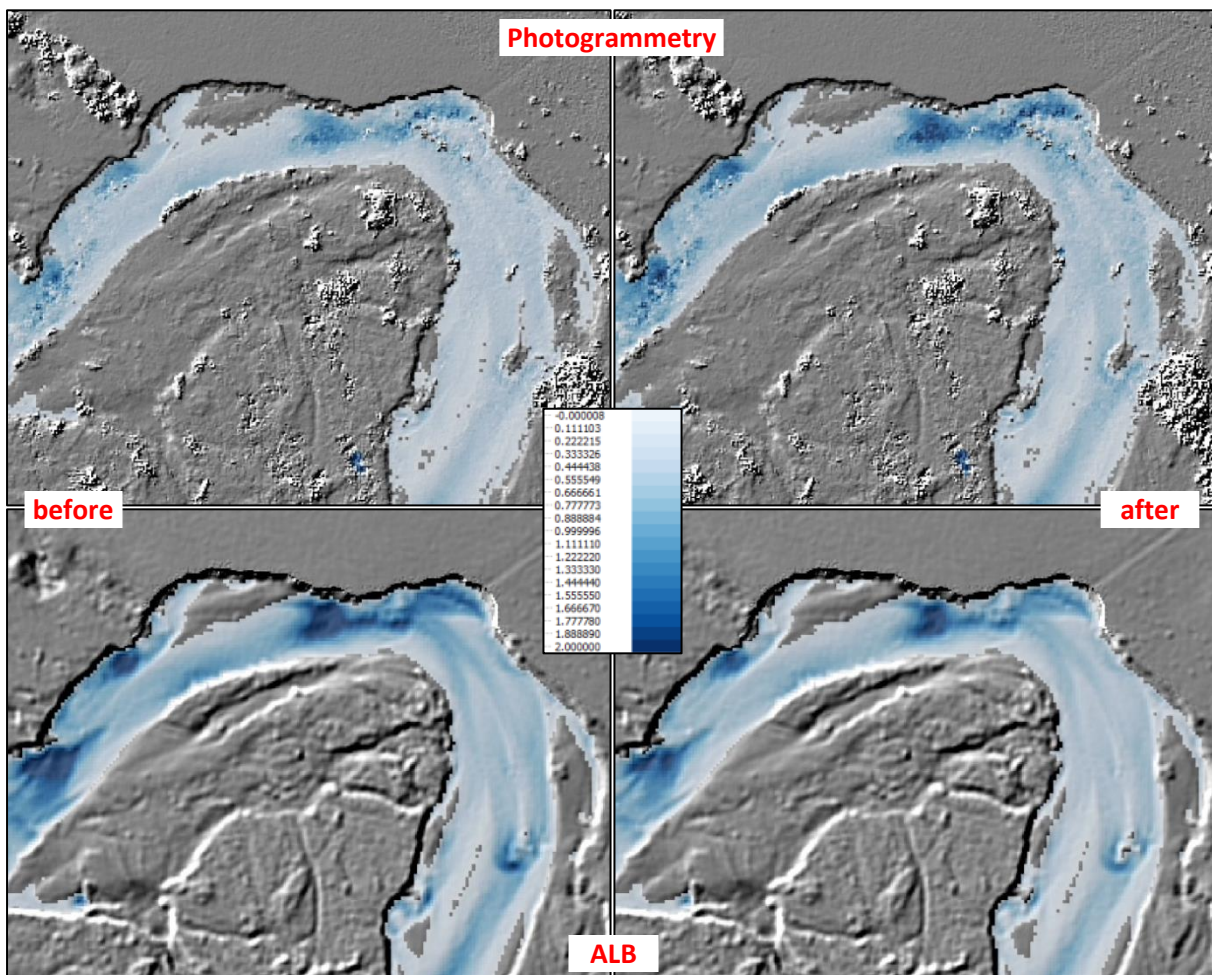


Figure 37: Direct comparison of both techniques before (left) and after (right) refraction correction. Even though some similar morphological characteristics can already be identified in the two uncorrected models (left), the different orders of magnitude can be clearly noticed. In contrast, the corrected models (right) differ mainly in their appearance with a very grainy photogrammetric model. A systematic bias is at least not observable with the naked eye.

In order to go towards a quantitative evaluation of the results, difference models are calculated between the height models of the watercourse. Figure 38 compares ALB to SURE.

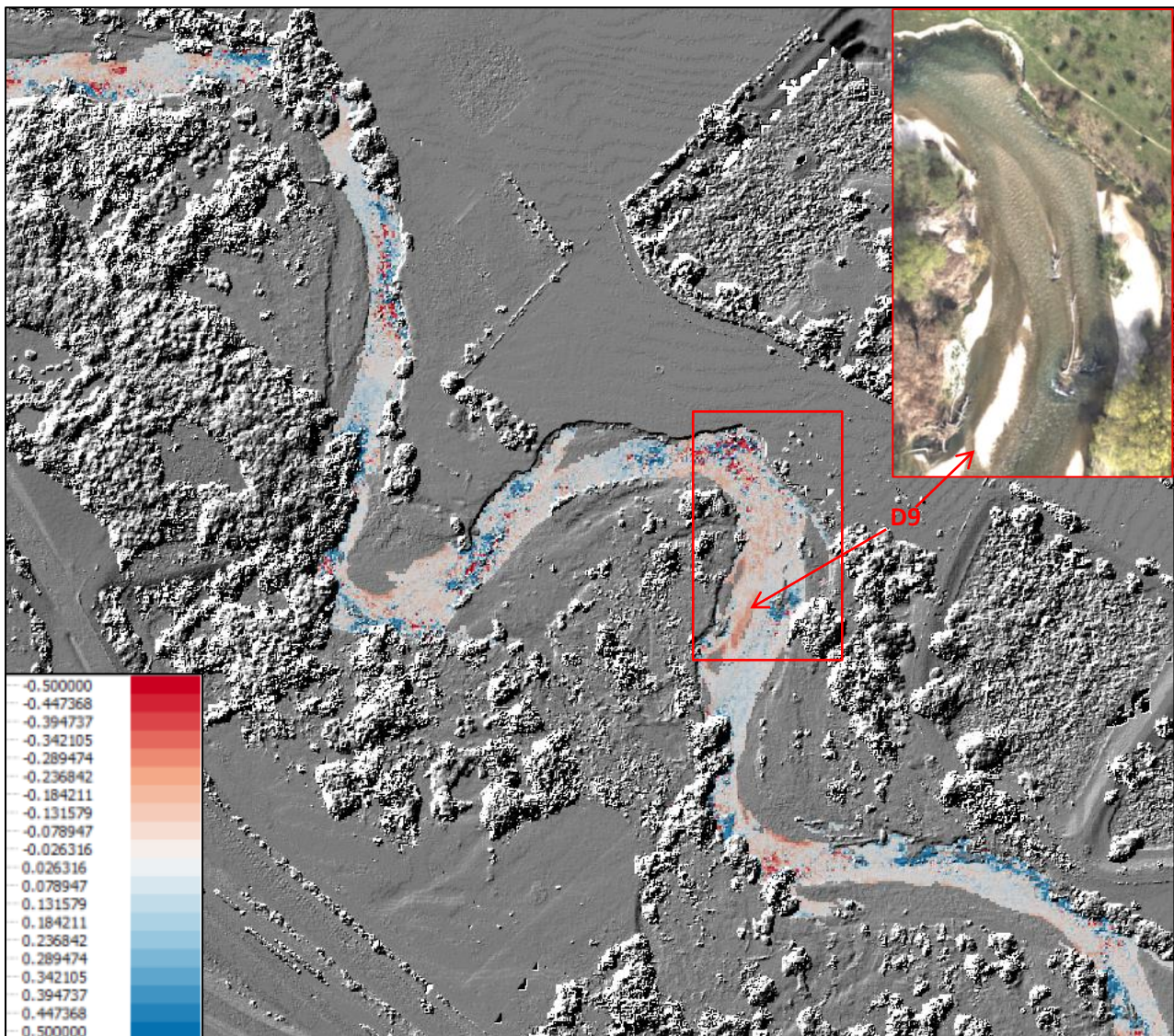


Figure 38: Difference of the photogrammetric river bed model (SURE) minus the ALB DTM. Ignoring the grave errors associated with vegetation, only the areas which are submerged according to both techniques are considered. Red tones corresponding to negative differences stand for areas where Photogrammetry suggests deeper water than ALB; blue tones identify a deeper ALB model.

Most of the revealed larger differences have already been anticipated during visual comparison of the water depth models in Section 6.2. A majority of the blue areas representing a too shallow photogrammetric model are situated in the close vicinity to vegetation on the river banks. Hence, they can be attributed to interpolation effects close to the canopy overtopping the river bed at the order of several meters.

Another obvious effect is the presence of positive and negative deviations in the deepest parts of the river. In fact, given the extremely noisy image matching in the river bed (c.f. Figure 12), such an effect is not surprising. However, to large extents it is compensated very well by taking the Median. In deeper water, the limited texture visibility possibly shifts the ratio of suitable point matchings and

noise to a degree which makes river bed reconstruction impossible. Additionally, the concerned sections are affected by sun glint which further increases this disproportion of signal and noise.

The remaining differences are below 10-20 cm to a large extent and reveal no clear systematic, with one exception: The wide, shallow river bed marked in Figure 38 is estimated significantly deeper by photogrammetry over a large area. Due to the perfectly visible riverbed texture, dominating wrong matches due to sun glint are out of question. Another explanation could be the effect of present water surface waves, though this poses the question why the deviation goes exclusively in negative direction lowering the river bed.

Therefore, the most likely explanation is an error through wrong water surface measurements. Due to a lack of water echoes in the shallow water, only few measurements could be made in this area. In combination with a steeper riverbed further upstream, the interpolation results in a systematically too high water surface. Accordingly, the refraction correction is too strong making ALB points higher and Photogrammetric points deeper. An additional indicator for a wrong water surface is the fact that the better part of the gravel bank (*D9*) is denoted as submerged by both techniques whereas the aerial image shows a large dry bank.

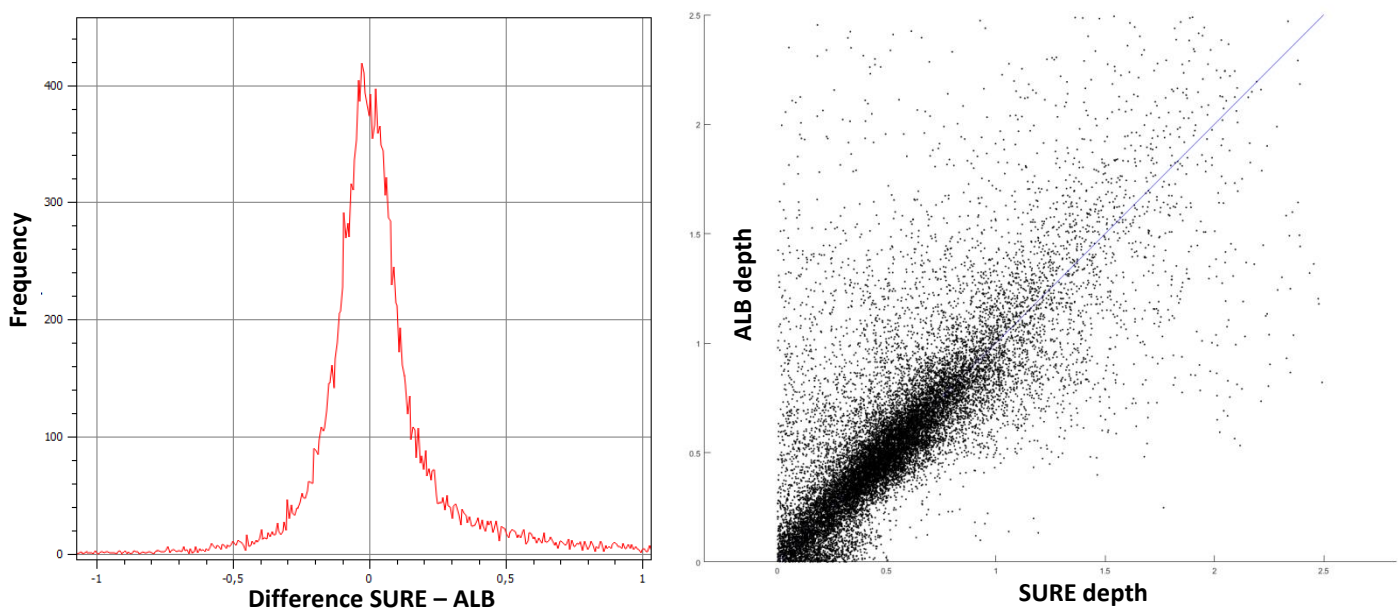


Figure 39: Histogram of the differences SURE minus ALB and a scatterplot of the complete depth models from SURE image matching and ALB. Blue is the line of perfect agreement.

The histogram of differences in Figure 39 affirms the described observations. The maximum slightly below zero is likely to come from overestimation of the water surface; a large part of the differences is smaller than 20 cm in magnitude. Errors larger than that are notably more frequent on the positive side corresponding to a higher photogrammetric model – a potential reason was already discussed in the context of vegetation on the river banks.

The lower left corner of the scatterplot confirms the predominance of negative errors with small magnitude as well. On the other hand, the higher density in the upper right part has to do with the multitude of larger positive errors. Apart from that, the scatter plot shows a good global agreement

of the two depth models indicating that neither refraction correction models nor the water surface are inherently biased. But this accordance with the blue line of perfect agreement disappears for depths larger than 1 m. As mentioned before, the reason for this is presumably the inability of SURE image matching to obtain reliable geometric information from water deeper than that.

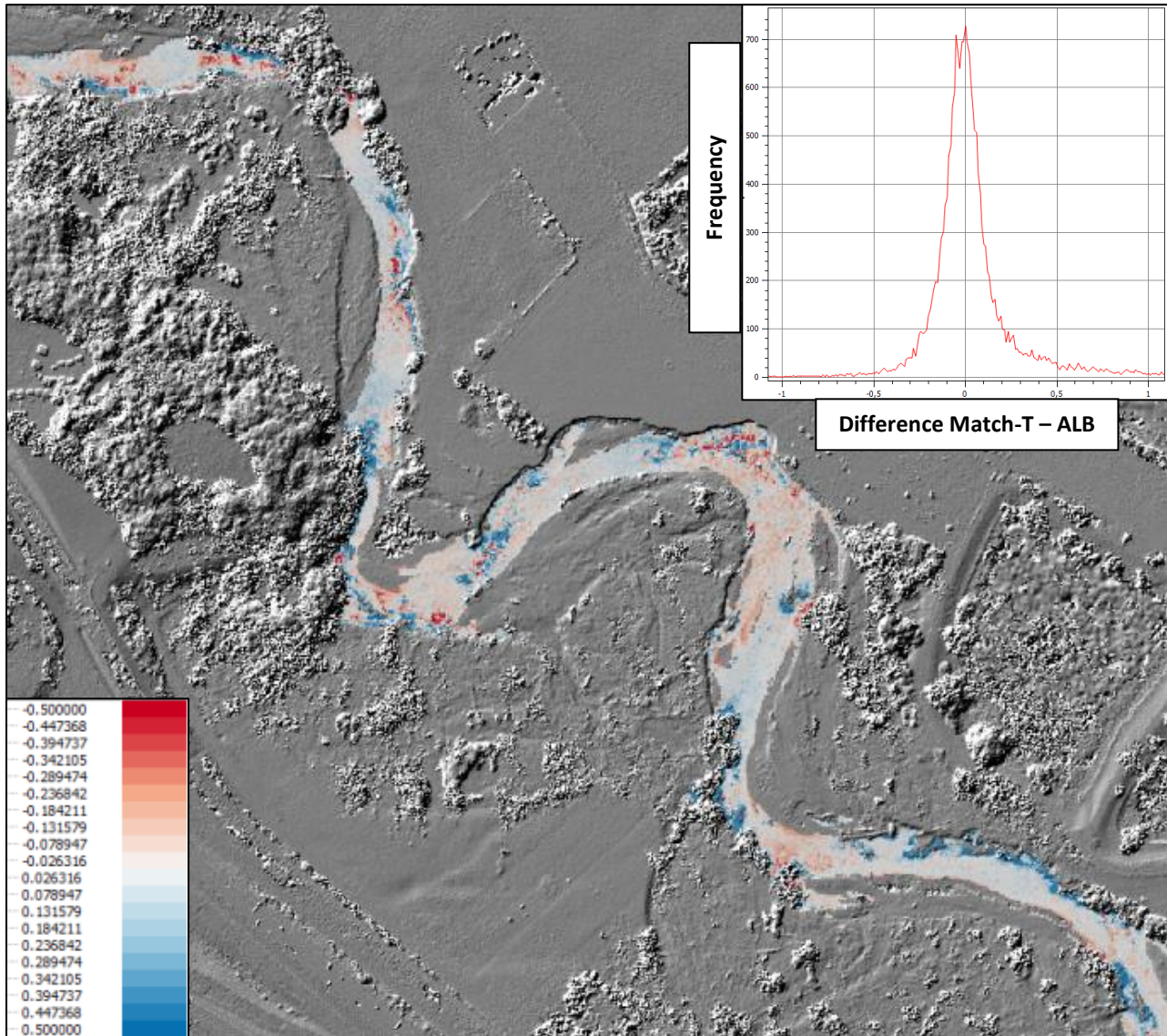


Figure 40: Difference of the photogrammetric height model from Match-T minus the ALB DTM. The coloring corresponds to that of the SURE-ALB differences. In the upper right corner, a histogram of differences is provided.

The characteristics described for SURE data are largely also present for Match-T. However, the supposition made during qualitative inspection that Match-T brings better results can only be partly confirmed here. Despite the better visual appearance of the difference model, the mean absolute difference is only 1 cm smaller than for SURE (0.152 vs. 0.164 m), the standard deviation of 0.237 is nearly equal to SURE (c.f. Table 1). But in contrast to SURE, the histogram has a maximum at zero, though there is a second local maximum again about 5 cm below. This parallel between the two image matching procedures affirms the theory of an independent error source like the water surface

model. While the errors near overhanging vegetation remain similar to SURE, especially deep pools are handled better by Match-T.

Accordingly, the scatterplot (Figure 41 right) of Match-T depths and ALB depths has a longer identifiable range of good agreement going clearly beyond depths of 1 m.

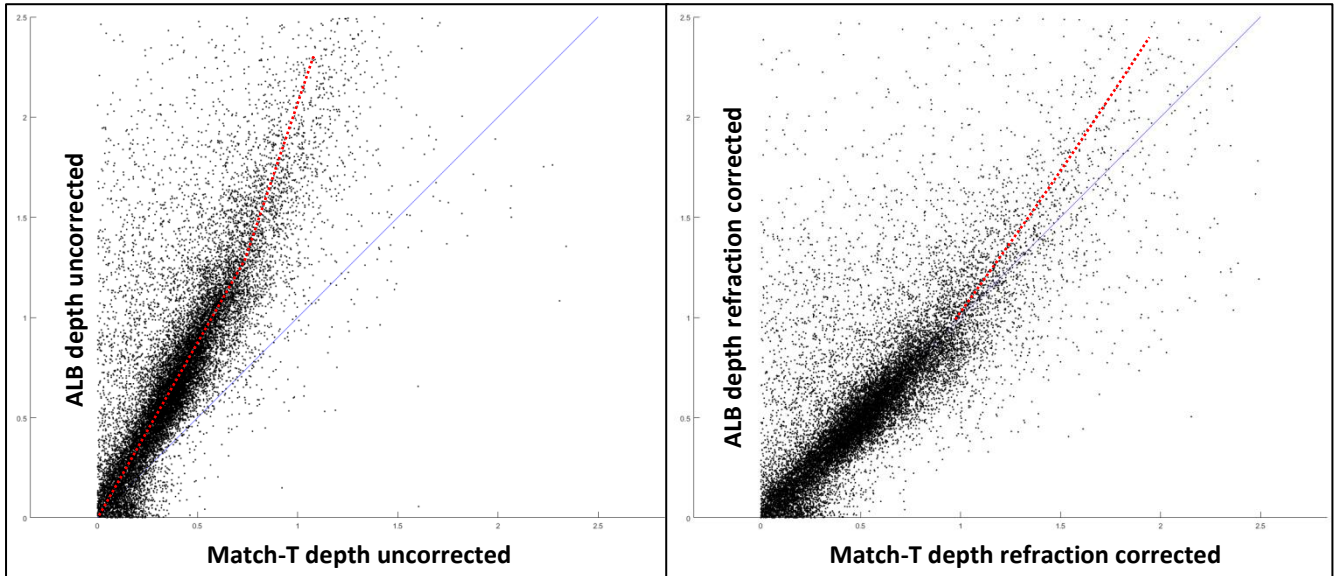


Figure 41: Scatterplot comparing Match-T and ALB depths before (left) and after (right) refraction correction.

Despite the better ability of Match-T to map deep water, there the results are not unbiased any more. The trend of underestimating depth w.r.t. ALB is even clearer than for SURE (c.f. the dashed red line in Figure 41 right). In order to locate the source of this trend, a second scatterplot with the uncorrected depths is provided in Figure 41 left which also shows a kink. This implies that the systematic is not introduced during refraction correction but arises either during image matching or during ALB georeferencing. However, the former is more likely due to the different characteristics of this effect for Match-T and SURE respectively. The cross section in Figure 42 is an example where the image matching points (blue) show a certain accordance with ALB points (green) in shallow water but don't go below a certain depth in the pool left of the river axis.

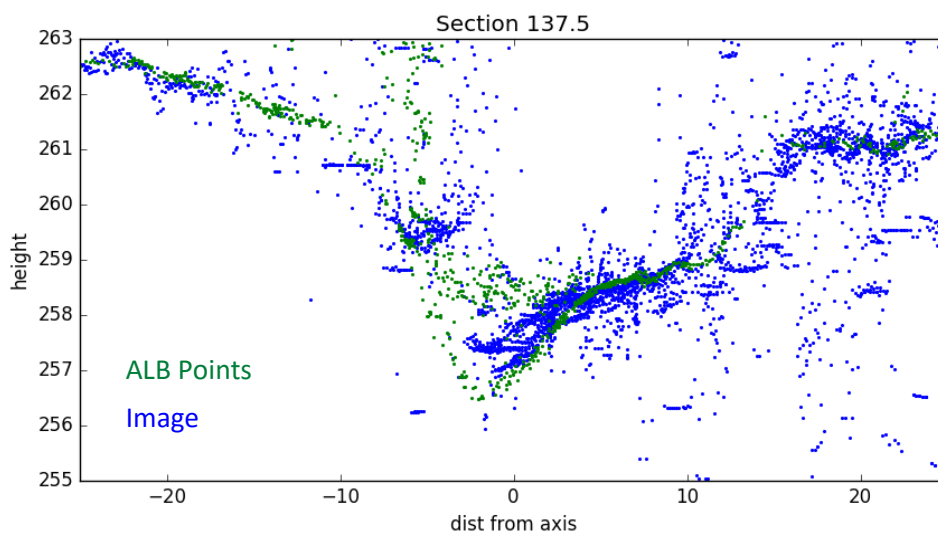


Figure 42: Cross section comparing refraction corrected ALB (green) and Match-T (blue) points.

After the assessment of possible bathymetry specific error sources, a further difference model is provided, again between Match-T and ALB. This time, it also includes terrain around the river channel (Figure 43). The aim is to determine, if the remaining deviations in the river bed which have not been assigned to a specific error source so far, can be classified as discrepancies due to orientation etc. or as bias related to uncorrected refraction effects.

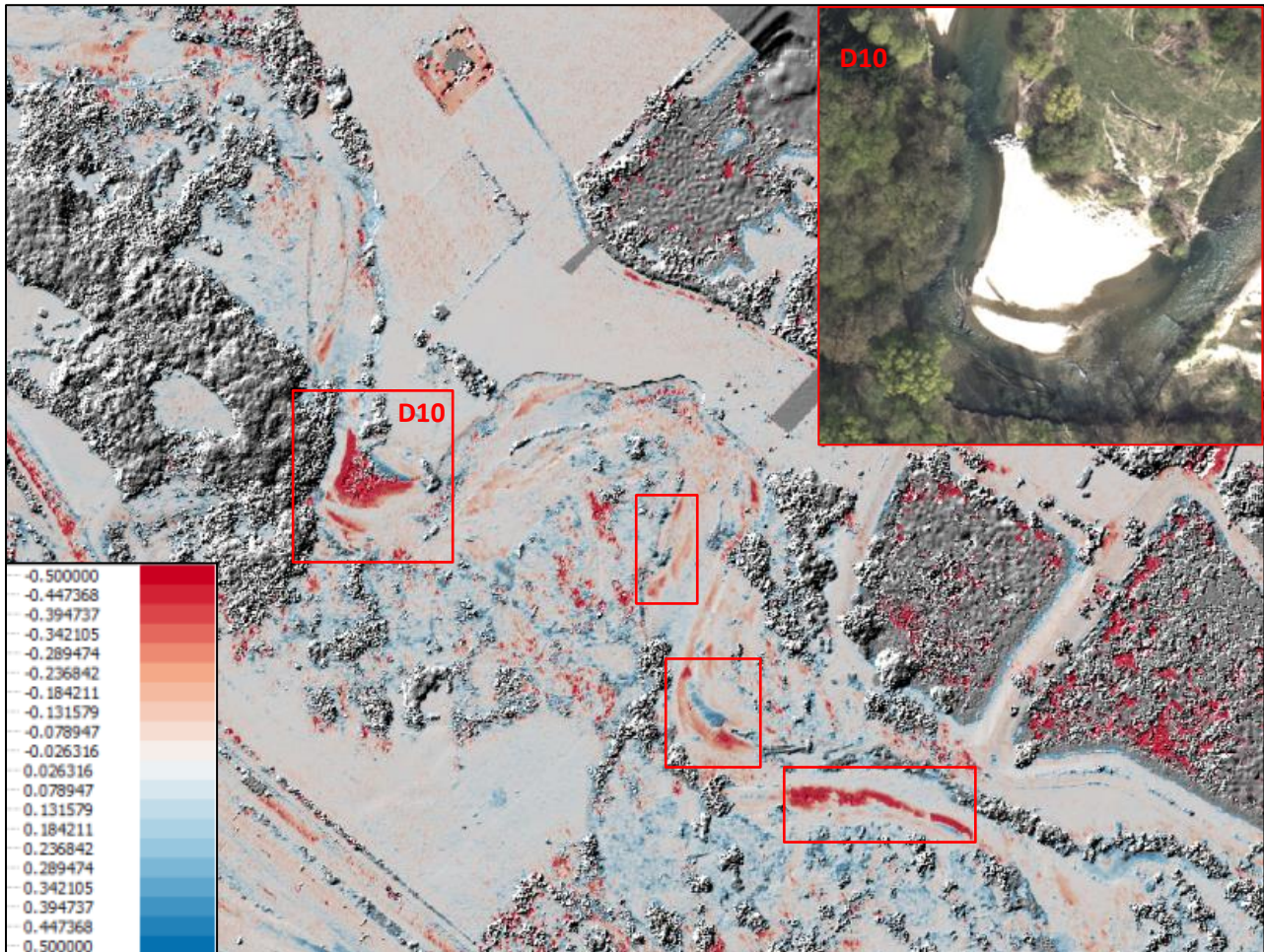


Figure 43: Difference of the Match-T model minus ALB. The whole area covered by both techniques is taken into account. In order to ensure comparability, vegetation was excluded using a roughness filter. The problem of overexposed gravel banks in aerial images is marked by red rectangles and also illustrated by one cutout of an aerial image (D10).

It appears that similar differences are present in both, the unproblematic areas of the river bed and dry terrain around. Unproblematic in this case means (i) shallow water in the range of 20 cm to approximately 1 m and (ii) areas not affected by overhanging vegetation. Statistical values are compared in lines 2 and 3 of Table 1. The largest remaining differences are the deep red areas directly besides or within the river. Those errors are easily explained and avoided in future campaigns: Due to overexposure of the images the riverbanks are completely saturated, i.e. they appear constantly in bright white disabling meaningful image matching.

To sum up the comparisons of all investigated techniques for Sector East, Table 1 presents statistical values of the differences between various models. Figure 44 shows an exemplary cross section with good agreement between the corrected point clouds from image matching and ALB.

Table 1: Statistics of height model differences for the river bed. The difference is always calculated by subtracting the first minus the second model. The attributes 'corr.' and 'uncorr.' refer to whether or not the models have been refraction corrected. The row 'Match-T vs ALB total' takes into account the whole smooth terrain including the river bed in Sector East. The first line has the purpose to visualize the effect of refraction correction which reduces the bias expressed by the Mean difference from 35 cm (first line) to 4 cm (second line).

Models	Mean diff. [m]	Mean abs. diff. [m]	$\sigma_{ diff }$ [m]	Figures
Match-T vs ALB uncorr.	-0.352	0.357	0.377	41 left
Match-T vs ALB corr.	-0.042	0.152	0.237	40, 41 right
Match-T vs ALB total	-0.044	0.140	0.366	43
SURE vs ALB corr.	-0.037	0.164	0.239	38,39
SURE vs Match-T corr.	-0.007	0.131	0.228	-

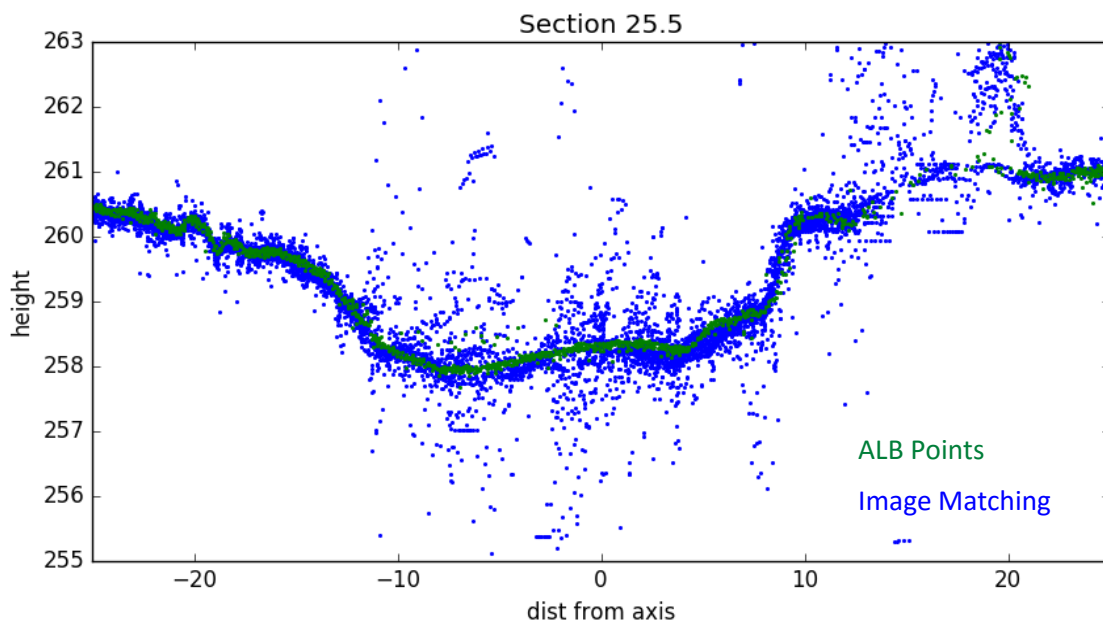


Figure 44: River cross section with a good agreement between refraction corrected ALB (green points) and Match-T Image Matching (blue) despite the large deviations of image matching points in both directions.

7 Conclusions

In this thesis a procedure for depth estimation based on two-media photogrammetry was presented and the results were compared against simultaneously captured ALB data as a reference. The procedure is characterized by the use of cost-based image matching (eventually in combination with FBM) in order to ensure high spatial resolution. The effect of light refraction on the results of image matching was theoretically assessed and a practical pointwise correction procedure was implemented. Furthermore, the photogrammetric workflow was adapted in order to adequately involve the processing steps dealing with the two-media problem.

To provide a reference for evaluation and a model of the water surface, ALB data covering the same study area were processed. The ALB workflow relies on software developed at TU Wien and has already been applied yielding satisfactory results concerning accuracy (Mandlbürger et al., 2015b). The main deviations from the standard ALS workflow are the semi-automatic water surface determination and the refraction correction procedure. Positive features of this active technique are the capability to penetrate through various obstacles like overhanging trees or objects floating in the water and the insensitivity to the effect of sun glint. Although the mapping quality of dry terrain isn't completely equivalent with infrared topographic laser scanners (Section 6.1), the demonstrated ability of ALB to provide terrain models of river beds and surrounding floodplains from one single data set is remarkable. Only dense vegetation posed problems to the green laser due to the weaker penetration capability.

Two-media photogrammetry exhibited a basic ability of mapping water depth as well, though it requires the fulfillment of certain prerequisites. The very limited capability to penetrate through vegetation caused deviations from a DTM and gaps in the water depth model where obstacles like overhanging trees are present. But also unobstructed visible water bodies do not necessarily lead to meaningful results. For example, dark substrate or sun glint on the water surface can make image matching somewhat arbitrary and prevent the extraction of meaningful results. Furthermore, the maximum measurable depth of photogrammetry in this case study was between 1 and 1.5 meters and therefore clearly smaller than for ALB.

Notwithstanding these shortcomings, one must not lose sight of the possibilities photogrammetry offers: Adequately considering the two media problem, it is a second technique besides ALB which by itself enables height model derivation for complete riverine landscapes. Under favorable conditions and with careful flight planning, tasks like for example morphological change monitoring could likely be fulfilled with photogrammetric methods. The equipment therefore is rather simple consisting of an aerial camera like used for other surveys.

Vegetated landscapes like the study area do not offer ideal conditions for passive methods, but for example shallow braided rivers like used for many of the studies on spectral regression (Section 2.1) do. Generally, as long as enough image overlaps are given, two-media photogrammetry can be a valuable alternative to these approaches. It relies on the same raw data but has the advantage of

being geometrically justified and not depending on spatially variable empirical relations. Therefore, no tedious measurements of training data on the ground are necessary.

8 Outlook

In contrast to the rapidly evolving field of ALB which is already used in various areas of application, two-media photogrammetry is rather rarely employed. The main reason for this, besides limitations of this technique described in the last chapter, is the comparably small amount of relevant studies during the era of digital photogrammetry and dense image matching. Even though the general feasibility has been shown in this thesis, the lack of commonly available processing software for the two-media case prevents broader common utilization of this technique. More research in several fields is needed in order to improve the presented workflow and enhance the attractiveness of photogrammetric water depth estimation.

But also ALB keeps posing new challenges. Especially the application for high resolution shallow water bathymetry is a rather new facet. Shifting priorities towards accuracy and high measurement rates, the demands on data processing undergo substantial changes as well. Although most of the processing steps are already implemented in *OPALS* and other software packages, noteworthy manual interaction is still needed when it comes to semi-automatic water surface determination. Despite of the measurement tool providing a good environment for this work, it remains laborious and time-intensive. Therefore, most of all extensive projects in branching river systems would benefit enormously from further automatization. However, Experience with the green laser dataset at hand has shown that reliable capturing of the water surface is not possible for the entire dataset (e.g. smooth areas) without operator interaction. A common workaround is the usage of an infrared laser for the water surface and the terrain. Maybe a future perspective could be to transmit a small part of the green beam in vertical direction. Detecting specular reflections near nadir has shown the capability of providing high water surface point densities given that the flight strip passes exactly above the water.

In contrast to these optimization problems, the water surface determination poses much more essential challenges to the photogrammetric workflow. During this study, the DWM from ALB was adopted to assure optimal comparability between the two techniques. In case of stand-alone photogrammetric bathymetry, another solution has to be found. For example, (Westaway et al., 2001) propose to interpolate the heights along the water-land boundary which of course depends on the visibility of that boundary. However, there are usually no static objects floating on the water surface to enable image matching and therefore the shoreline is the only available information on water surface height. Further research could thus adopt the DWM only as an approximation and include an accurate estimation in a least-squares adjustment along with the refraction correction.

Besides this essential task, there are numerous other potential enhancements, most notably:

- ➔ Use of imaging systems with an additional NIR channel for the elimination of sun glint (e.g. Hochberg et al., 2003; Hedley et al., 2005).
- ➔ Elimination of errors associated with a tilted water surface as a result of water surface waves – this is especially relevant for low flying heights due to the small ground sampling distance.
- ➔ Inclusion of two media characteristics already in the dense image matching procedure.

Practical work in this thesis has confirmed the general applicability of two-media photogrammetry for high resolution mapping of water depth. Yet it is unlikely that already the full potential of this method has been exploited and therefore continuative work in this field is explicitly motivated. Being aware of the inherent limitations passive optical imagery exhibited in this case study, matching ALB data in terms of water depth mapping quality is rather improbable. Nevertheless, further improvements potentially increase the attractiveness of two-media photogrammetry as an alternative to other optical techniques in suitable fields of application.

List of abbreviations

ALB.....	<i>Airborne Laser Bathymetry</i>
ALS.....	<i>(Topographic) Airborne Laser Scanning</i>
AT.....	<i>Aerotriangulation</i>
CBM.....	<i>Cost Based (Image) Matching</i>
CSV.....	<i>Comma-Separated Values text file format</i>
DEM.....	<i>Digital Elevation Model</i>
DSM.....	<i>Digital Surface Model</i>
DTM.....	<i>Digital Terrain Model</i>
DTM-W.....	<i>Digital Terrain model of the Watercourse</i>
DWM.....	<i>Digital Water Surface Model</i>
FBM.....	<i>Feature Based (Image) Matching</i>
FFH.....	<i>EU Flora Fauna Habitats Directive</i>
LAS.....	<i>LiDAR data exchange file format</i>
LiDAR.....	<i>Light detection and ranging</i>
NIR.....	<i>Near Infrared</i>
OPALS.....	<i>Orientation and Processing of Airborne Laser Scanning data (program system)</i>
TIF.....	<i>Tagged Image File format (raster)</i>
WFD.....	<i>EU Water Framework Directive</i>

References

- Briese, C., Pfeifer, N., Dorninger, P., 2002. *Applications of the robust interpolation for DTM interpolation*. International Archives of Photogrammetry, Remote Sensing and Spatial Information Sciences 34 (2002), 55-61.
- Carbonneau, P.E., Lane, S.N., Bergeron, N., 2006. *Feature based image processing methods applied to bathymetric measurements from airborne remote sensing in fluvial environments*. Earth Surface Processes and Landforms 31 (2006), 1413-1423.
- Delai, F., Moretto, J., Picco, L., Rigon, E., Ravazzolo, D., Lenzi, M.A., 2014. *Analysis of Morphological Processes in a Disturbed Gravel-Bed River (Piave River): Integration of LiDAR Data and Colour Bathymetry*. Journal of Civil Engineering and Architecture, Volume 8, No. 5 (2014), 639-648.
- Doneus, M., Doneus, N., Briese, C., Pregesbauer, M., Mandlbürger, G., Verhoen, G., 2012. *Airborne laser bathymetry – detecting and recording submerged archaeological sites from the air*. Journal of Archaeological Science 40 (2013), 2136-2151.
- EU, 1992. *Council Directive 92/43/EEC of 21 May 1992 on the conservation of natural of natural habitats and of wild fauna and flora*. Official Journal of the European Communities, L 206/7-50.
- EU, 2000a. *Directive 2000/60/EC of the European Parliament and of the Council of 23 October 2000 establishing a framework for Community action in the field of water policy*. Official Journal of the European Communities, L 327/1-72.
- EU, 2000b. *Factsheet: The EU Water Framework Directive*. EU Publications Office.
- EU, 2007. *Directive 2007/60/EC of the European Parliament and of the Council of 23 October 2007 on the assessment and management of flood risks*. Official Journal of the European Union, L288/27-34.
- Feurer, D., Bailly, J.S., Puech, C., Le Coarer, Y., Viau, A., 2008. *Very-high-resolution mapping of river-immersed topography by remote sensing*. Progress in Physical Geography, SAGE Publications (UK and US) 32 (2008), 403-419.
- Fryer, J.G., 1983. *A simple system for Photogrammetric mapping in shallow water*. Photogrammetric Record 11 (1983), 203-208.
- Fryer, J.G., Kniest, H.T., 1985. *Errors in depth determination caused by waves in Trough-Water Photogrammetry*. Photogrammetric Record 66 (1985), 745-753.
- Glira, P., Pfeifer, N., Briese, C., Ressel, C., 2015a. *Rigorous strip adjustment of airborne laser scanning data based on the ICP algorithm*. ISPRS Geospatial Week 2015, 28 September - 03 October 2015, La Grande Motte, France.
- Glira, P., Pfeifer, N., Briese, C., Ressel, C., 2015b. *A Correspondence Framework for ALS Strip Adjustments based on Variants of the ICP Algorithm*. Photogrammetrie-Fernerkundung-Geoinformation (PFG) 2015/4, 275-289.

Guenther, G.C., Cunningham, A.G., LaRocque, P.E., Reid, D.J., 2000. *Meeting the accuracy challenge in airborne LiDAR Bathymetry*. Proceedings of EARSeL-SIG-Workshop LIDAR, June 16-17, 2000, Dresden, Germany.

Hedley, J.D., Harborne, A.R., Mumby, P.J., 2005. *Simple and robust removal of sun glint for mapping shallow-water benthos*. International Journal of Remote Sensing, Vol 26, No 10 (2005), 2107-2112.

Hilldale, R.C., Raff, D., 2007. *Assessing the ability of airborne LiDAR to map River Bathymetry*. Earth Surface Processes and Landforms 33 (2007), 773.

Hirschmüller, H., 2005. *Accurate and Efficient Stereo Processing by Semi-Global Matching and Mutual Information*. IEEE Conference on Computer Vision and Pattern Recognition (CVPR), San Diego, USA, June 20-26, 2005.

Hirschmüller, H., 2011. *Semi-Global Matching – Motivation, Developments and Applications*.

Hochberg, E.J., Andréfouet, S., Tyler, M.R., 2003. *Sea surface correction of high spatial resolution Ikonos images to improve bottom mapping in near-shore environments*. IEEE Transactions in Geoscience and Remote Sensing 41 (2003), 1724-1729.

Hollaus, M., Mandlbürger, G., Pfeifer, N., Mücke, W., 2010. *Land Cover dependent derivation of Digital Surface Models from Airborne Laser Scanning data*. IAPRS, Vol 28, Part 3A, 221-226.

Kager, H., Waldhäusl, P., 1989. *ORIENT: A universal photogrammetric adjustment system*. Optical 3-D Measurement Techniques, Wichmann Verlag, Karlsruhe, 447-455.

Kinzel, P.J., Nelson, J.M., Wright, W., 2006. *Monitoring Changes in the Platte River Riparian Corridor with Serial LiDAR Surveys*. U.S. Department of the Interior, U.S. Geological Survey, Fact Sheet 2006-3063.

Kinzel, P.J., Wright, C.W., Nelson, J.M., Burman, A.R., 2007. *Evaluation of an Experimental LiDAR for Surveying a Shallow, Braided, Sand-Bedded River*. USGS Staff – Published Research, Paper 77.

Lane, S.N., Widdison, P.E., Thomas, R.E., Ashworth, P.J., Best, J.L., Lunt, I.A., Sambrook Smith, G.H., Simpson, C.J., 2010. *Quantification of braided river channel change using archival digital image analysis*. Earth Surface Processes and Landforms (2010).

Legleiter, C.J., Roberts, D.A, Lawrence, R.J., 2009. *Spectrally based remote sensing of river bathymetry*. Earth Surface Processes and Landforms 34 (2009), 1039-1059.

Legleiter, C.J., 2012. *Remote measurement of river morphology via fusion of LiDAR topography and spectrally based bathymetry*. Earth Surface Processes and Landforms 37 (2012), 499-518.

Legleiter, C.J., 2013. *Mapping river depth from publicly available aerial images*. River Research and Applications 29 (2013), 760-780.

Legleiter, C.J., Goodchild, M.F., 2014. *Alternative Representations of In-Stream Habitat: Classification using Remote Sensing, Hydraulic Modelling, and Fuzzy Logic*. International Journal of Geographical Information Science.

- Mandlbürger, G., Pfennigbauer, M., Steinbacher, F., Pfeifer, N., 2011. *Airborne Hydrographic LiDAR Mapping – Potential of a new technique for capturing shallow water bodies*. 19th International Congress on Modelling and Simulation, Perth, Australia, 12-16 December 2011.
- Mandlbürger, G., Otepka, J., Miller, P., Steinbacher, F., Pfennigbauer, M., Pfeifer, N., 2012. *Vermessung von Fließgewässern mittels Airborne Laser Bathymetry*.
- Mandlbürger, G., Pfennigbauer, M., Pfeifer, N., 2013a. *Analyzing near water surface penetration in Laser Bathymetry – a case study at the Pielach River*. ISPRS Annals of Photogrammetry, Remote Sensing and Spatial Information Sciences, Volume II-5/W2, 2013. ISPRS Workshop Laser Scanning 2013, 11-13 November 2013, Antalya, Turkey.
- Mandlbürger, G., Hauer, C., Wieser, M., 2013b. *Monitoring of instream habitats with focus on morphological dynamics based on Airborne Laser Bathymetry*.
- Mandlbürger, G., Wieser, M., Otepka, J., Pfeifer, N., 2015a. *Dokumentation von Hochwasser bedingten Veränderungen von Flussläufen mittels Laser Bathymetrie am Beispiel der Pielach*. 18. Internationale Geodätische Woche 2015, Obergurgl, Austria.
- Mandlbürger, G., Hauer, C., Wieser, M., Pfeifer, N., 2015b. *Topo-bathymetric LiDAR for monitoring river morphodynamics and instream habitats – A case study at the Pielach River*. Remote Sensing 7, No 5 (2015), 6160-6195.
- Mandlbürger, G., Pfennigbauer, M., Riegl, U., Haring, A., Wieser, M., Glira, P., Winiwarter, L., 2015c. *Complementing airborne laser bathymetry with UAV-based lidar for capturing alluvial landscapes*. SPIE Remote Sensing, 21-24 September 2015, Toulouse, France.
- Marcus, W.A., Legleiter, C.J., Aspinall, R.J., Boardman, J.W., Crabtree, R.L., 2003. *High spatial resolution hyperspectral mapping of in-stream habitats, depths, and woody debris in mountain streams*. Geomorphology 55 (2003), 363-380.
- Marcus, W.A., Fonstad, M.A., 2008. *Optical remote mapping of rivers at sub-meter resolutions and watershed extents*. Earth Surface Processes and Landforms 33 (2008), 4-24.
- McKean, J., Nagel, D., Tonina, D., Bailey, P., Wright, C.W., Bohn, C., Nayegandhi, A., 2009. *Remote Sensing of Channels and Riparian Zones with a Narrow-Beam Aquatic-Terrestrial LIDAR*. Remote Sensing 9 (2009), 1065-1096.
- Moretto, J., Rigon, E., Mao, L., Delai, F., Picco, L., Lenzi, M.A., 2014. *Short-term geomorphic analysis in a disturbed fluvial environment by fusion of LiDAR, color bathymetry and dGPS surveys*. Catena 122 (2014), 180-195.
- Murase, T., Tanaka, M., Tani, T., Miyashita, Y., Ohkawa, N., Ishiguro, S., Suzuki, Y., Kayanne, H., Yamano, H., 2008. *A Photogrammetric Correction Procedure for Light Refraction Effects at a Two-Medium Boundary*. Photogrammetric Engineering & Remote Sensing, Vol 74, No 9 (2008), 1129-1136.

- Nayegandhi, A., Wright, C.W., Brock, J.C., 2009. *EAARL: An Airborne LiDAR System for Mapping Coastal and Riverine Environments*. In: *Remote Sensing Applications for Aquatic Resource Monitoring*, PNAMP Special Publication, USA (2009), 3-5.
- Parsons, D.R., Best, J.L., Orfeo, O., Hardy, R.J., Kostachuk, R., Lane, S.N., 2005. *Morphology and flow fields of three-dimensional dunes, Rio Paranà, Argentina: Results from simultaneous multibeam echo sounding and acoustic Doppler current profiling*. *Journal of Geophysical Research: Earth Surface*, Vol 110 (2005).
- Passalacqua, P., Trung, T. D., Fofoula-Georgiou, E., Sapiro, G., Dietrich, W.E., 2010. A geometric framework for channel network extraction from lidar: Nonlinear diffusion and geodesic paths. *Journal of Geophysical Research*, Vol 115 (2010).
- Pfeifer, N., Stadler, P., Briese, C., 2001. *Derivation of digital terrain models in the SCOP++ environment*. Proceedings of OEEPE Workshop on Airborne Laserscanning and Interferometric SAR for Detailed Digital Terrain Models, Stockholm, Sweden.
- Pfeifer, N., Mandlburger, G., Otepka, J., Karel, W., 2014. OPALS – A framework for airborne laser scanning data analysis. *Computers, Environment and Urban Systems* 45 (2014), 125-136.
- Pfennigbauer, M., Steinbacher, F., Ullrich, A., Aufleger, M., 2010. A Novel Approach to Laser-Based Hydrographic Data Acquisition. *European LiDAR Mapping Forum*, Salzburg, Austria.
- Pyle, C.J., Richards, K.S., Chandler, J.H., 1997. *Digital photogrammetric monitoring of river bank erosion*. *The Photogrammetric Record* 89 (1997), 753-764.
- Renard, V., Allenou, J.-P., 1979. *Sea beam, multi-beam Echo-Sounding in "Jean Charcot": Description, evaluation and results*. *International Hydrographic Review*, Monaco, LVI (1979).
- Ressl, C., Kager, H., Mandlburger, G., 2008. *Quality checking of ALS projects using statistics of strip differences*. *International Archives of the Photogrammetry, Remote Sensing and Spatial Information Sciences* 37 (2008), 253-260.
- Ressl, C., Mandlburger, G., Pfeifer, N., 2009. *Investigation adjustment of Airborne Laser Scanning Strips without usage of GNSS/IMU trajectory data*. *Laser Scanning, IAPRS*, Vol. 28 – 1-2 September 2009, Paris, France.
- Rinner, K., 1969. *Problems of two-media photogrammetry*. *Photogrammetric Engineering* 35 (1969), 275-282.
- Steinbacher, F., Pfennigbauer, M., Ullrich, A., Aufleger, M., 2010. *Airborne Hydromapping area-wide surveying of shallow water areas*. Proceedings of 38th ISPRS Congress.
- Stumpf, R.P., Holderied, K., Sinclair, M., 2003. *Determination of water depth with high-resolution satellite imagery over variable bottom types*. *Limnology and Oceanography* 48 (2003), 647-556.
- Tewinkel, G.C., 1963. *Water depths from aerial photographs*. *Photogrammetric Engineering* 29 (1963), 1037-1042.

Wenzel, K., Rothermel, M., Fritsch, D., 2013. *SURE – The ifp software for dense image matching*. Photogrammetric Week 13 (2013).

Westaway, R.M., Lane, S.N., Hicks, D.M., 2000. *The development of an automated Correction Procedure for Digital Photogrammetry for the Study of wide, shallow, gravel-bed Rivers*. Earth Surface Processes and Landforms 25 (2000), 209-226.

Westaway, R.M., Lane, S.N., Hicks, D.M., 2001. *Remote Sensing of Clear-Water, Shallow, Grave-Bed Rivers Using Digital Photogrammetry*. Photogrammetric Engineering & Remote Sensing, Vol. 67, No. 11, November 2001, 1271-1281.

Williams, R.D., Brasington, J. Vericat, D., Hicks D.M., 2013. *Hyperscale terrain modelling of braided rivers: fusing mobile terrestrial laser scanning and optical bathymetric mapping*. Earth Surface Processes and Landforms (2013).

Web References

[I] European Commission information site on the Habitats Directive:

http://ec.europa.eu/environment/nature/legislation/habitatsdirective/index_en.htm (06.05.2016)

[II] European Commission information site on the Water Framework directive:

http://ec.europa.eu/environment/water/water-framework/info/intro_en.htm (06.05.2016)

[III] European Commission information site on the Floods Directive:

http://ec.europa.eu/environment/water/flood_risk/index.htm (06.05.2016)

[IV] Article (German) and map about protection areas in Lower Austria:

<http://www.noen.at/nachrichten/noe/politik-bildung/Naturschutz-Wie-viel-vertraegt-das-Land;art79519,427334> (06.05.2016)

[V] Riegl VQ-880-G data sheet: http://www.riegl.com/uploads/tx_pxpriegldownloads/DataSheet_VQ-880-G_2015-10-06_PRELIM_INARY.pdf (06.05.2016)

[VI] Allied Vision information site about the Prosilica GT 6600 Camera:

<https://www.alliedvision.com/de/produkte/kameras/kameradetails/Prosilica%20GT/6600.html> (06.05.2016)

[VII] ESRI Webhelp article providing a good explanation of World Files:

http://webhelp.esri.com/arcims/9.3/General/topics/author_world_files.htm (06.05.2016)

[VIII] Trimble info site about the Inpho software: <http://www.trimble.com/imaging/inpho.aspx> (06.05.2016)

[IX] Trimble info sheet about the Match-T DSM Image Matching application:

http://trl.trimble.com/docushare/dsweb/Get/Document-789928/022516-018B_Inpho_MATCH-T_DSM_TS_A4_0915_LR.pdf (06.05.2016)

[X] LAS File reader/writer provided in Matlab File exchange:

<http://www.mathworks.com/matlabcentral/fileexchange/48073-las-file-reader-writer> (06.05.2016)

[XI] OPALS software information and documentation: <http://geo.tuwien.ac.at/opals/html/index.html>
(06.05.2016)

[XII] Optech SHOALS 1000 System Specification: <http://www.fugro-pelagos.com/lidar/lib/brochures/SHOALS-1000Tspecs.pdf> (06.05.2016)

[XIII] Fugro LADS Mk3 datasheet: <http://www.fugrolads.com/download/datasheets/Fugro-LADS-Mk3>
(06.05.2016)

[XIV] Leica AHAB HawkEye III information and system specification:
<http://www.airbornehydro.com/sites/default/files/Leica%20AHAB%20HawkEye%20III.pdf>
(06.05.2016)

[XV] Riegl VQ-820-G data sheet:
http://www.riegl.com/uploads/tx_pxpriegldownloads/DataSheet_VQ-820-G_2015-03-24.pdf
(06.05.2016)

[XVI] LiDAR Magazine article of the year 2013 comparing state-of-the-art bathymetric sensors:
http://www.lidarmag.com/PDF/LiDARMagazine_Quadros-BathymetricLiDARSensors_Vol3No6.pdf
(06.05.2016)

[XVII] SCOP++ software manual: <https://photo.geo.tuwien.ac.at/software/scop/> (06.05.2016)

[XIX] Riegl LMS- Q1560 datasheet: http://www.riegl.com/uploads/tx_pxpriegldownloads/LMS-Q1560_at_a_glance_2015-08-24.pdf (06.05.2016)

[XX] Article about the spectral absorption properties of water:
http://www1.lsbu.ac.uk/water/water_vibrational_spectrum.html (06.05.2016)

[XXI] <http://de.mathworks.com/products/matlab/?requestedDomain=www.mathworks.com>